UNIVERSITY *of the*
WESTERN CAPE

EVALUATION OF GROUNDWATER FLOW THEORIES AND AQUIFER PARAMETERS ESTIMATION

Dissertation submitted to the University of the Western Cape in the fulfilment of the degree of Doctor of Philosophy

by

Liang Xiao

Department of Earth Sciences
Faculty of Natural Sciences, University of the Western Cape

Supervisor
Professor *Yongxin Xu*

Co-supervisor
Dr *Lixiang Lin*

November 2014
Cape Town, South Africa

DECLEARATION

I declare that **EVALUATION OF GROUNDWATER FLOW THEORIES AND AQUIFER PARAMETERS ESTIMATION** is my own work, and that has not been submitted for any degree or examination in any other university, and that all the sources I have used or quoted have been indicated and acknowledged by complete references.

Full name: Liang Xiao Date: November 2014

Signed.....

ABSTRACT

Evaluation of Groundwater Flow Theories and Aquifer Parameters Estimation

Liang Xiao
PhD Thesis
Department of Earth Sciences
University of the Western Cape, South Africa

Keywords: Deterministic mathematical models, analytical solutions, Theis problem, transient confined-unconfined flow, change of hydraulic properties, drawdown derivative analysis, dlg*s*/dlg*t*, box models, ^{14}C age of groundwater, dolomite aquifer

This thesis deals with some fundamental aspects of groundwater models. Deterministic mathematical models of groundwater are usually used to simulate flow and transport processes in aquifer systems by means of partial differential equations. Analytical solutions for the deterministic mathematical models of the Theis problem and the transient confined-unconfined flow in a confined aquifer are investigated in the thesis. The Theis equation is a most commonly applied solution for the deterministic mathematical model of the Theis problem. In the thesis, a most simplified similarity transformation method for derivation of the Theis equation is proposed by using the Boltzmann transform.

To investigate the transient confined-unconfined flow towards a fully penetrating well in a confined aquifer, a new analytical solution for the deterministic mathematical models of interest is proposed in the thesis. The proposed analytical solution considers a change of hydraulic properties (transmissivity and storativity) during the confined-unconfined conversion. Based on the proposed analytical solution, a practical method to determine distance of the conversion interface from pumping well and diffusivity of the unconfined region is developed by using a constant rate test. Applicability of the proposed analytical solution is demonstrated by a comparison

with previous solutions, namely the MP and the Chen models. The results show that the proposed analytical solution can be used to assess the effect of the change of diffusivity on the transient confined-unconfined flow. The MP model is only accepted if the transmissivity during the confined-unconfined conversion is constant. The Chen model, given as a special case of the proposed analytical solution, is limited to the analysis of the transient confined-unconfined flow with a fixed diffusivity.

An important application of groundwater models is to estimate parameters, such as hydraulic properties and flow dynamics, of groundwater systems by assessing and analysing field data. For instance, the pumping and the hydrochemistry and environmental tracer tests are two effective ways to obtain such data. To evaluate hydraulic properties of aquifer systems by derivative interpretation of drawdown data from pumping tests, a new diagnostic analysis method is proposed based on a lg-lg drawdown derivative, dlg*s*/dlg*t*, and the differentiation algorithm namely Lagrange Interpolation Regression (LIR) in the thesis. Use of a combined plot of dlg*s*/dlg*t* and a semi-lg drawdown derivative (d*s*/dlg*t*) is made to identify various flow segments during variable discharge tests with infinite conditions, constant rate tests in bounded aquifers and tests involving double-porosity behaviours. These can be applied to further characterize pumped aquifers. Compared to traditional diagnostic analysis method using plot of d*s*/dlg*t* alone, the combined drawdown derivative plot possesses certain advantages identified as: (1) the plot of dlg*s*/dlg*t* is strikingly sensitive for use in unveiling differences between pumping and its following recovery periods in intermittent variable discharge tests; (2) storativity (*S*) of pumped aquifers can be evaluated by using the combined plot; and (3) quantitative assessments of double-porosity behaviours can also be achieved. Based on two case studies, advantages and disadvantages of uses of the LIR and other existing differentiation methods in calculations of numerical drawdown derivative are demonstrated in practice. The results suggest that the LIR is a preferred method for numerical differentiation of drawdown data as it can be used to effectively minimise noisy effects. The proposed derivative approach provides hydrologists with an additional tool for characterizing pumped aquifers.

Use of hydrochemistry and environmental tracer tests to assess flow dynamics of groundwater systems is demonstrated via a case study in the dolomite aquifer of South Africa. An emphasis is on determining mean residence times (MRTs) of the dolomite aquifer by means of an appropriate box model with time series of ^{14}C values of dissolved inorganic carbon (^{14}C-DIC) and initial ^{14}C activities of spring samples during 1970s and 2010s. To obtain the calibrated ^{14}C MRTs, ^{13}C values of dissolved inorganic carbon ($\delta^{13}C$-DIC) of the spring samples are applied to estimate mineral dissolution in the dolomite aquifer and calculate the initial ^{14}C activities. The results indicate that the spring samples have about 50%-80% initial ^{14}C activities. By using the appropriate box model, the calibrated ^{14}C MRTs of the spring system are given within a range from $\leq$ 10 to 50 years. Additionally, the flow dynamics, including the recharge source and area, the effect of climate change on the temporal trend of the groundwater MRTs and the groundwater flow circulation, of the dolomitic spring system are also discussed for further possible management interventions in the dolomite aquifer.

ACKNOWLEDGE

This thesis would not have been possible without the assistance and cooperation of many individuals and institutions. I would like to acknowledge my debt and wish to record my sincere thanks to the following,

- My supervisor Professor Yongxin Xu from Earth Sciences Department at University of the Western Cape for his thorough and thoughtful coaching.
- Dr. S.A. Talma from Council of Scientific and Industrial Research (CSIR) for granting the author permission to access data collected by his CSIR project.
- Dr. D.B. Bredenkamp for his helpful discussions, advices and support of data collection.
- My friend Joey from University of Cape Town for his assistance and support during my study and research in South Africa.
- My colleagues namely Xiaobin Sun, Iris Wu and Xiaoming Liu from University of the Western Cape for their assistance and cooperation.
- Mrs. Caroline Barnard and Mrs. Mandy Naidoo from University of the Western Cape for all their hard work and care for assisting the author to complete the research.
- Dr. Lixiang Lin from Council of Geoscience for data collection.
- Finally, to my parents, a special thanks to you for your immense support during my study.

Content

List of Figures

List of Tables

Chapter 1

Introduction

1.1 Background

Groundwater is the water stored in porous media, such as soil pore spaces or factures of rock formations, beneath the earth's surface. Groundwater flow is the movement of the water that travels and seeps in the porous media underground. An aquifer is defined as a geologic formation or a stratum which contains groundwater and allows significant amounts of groundwater to move through it under ordinary field conditions. During the process of groundwater movement through an aquifer system, groundwater behaviours are governed by characteristics of the water itself and the medium where it flows. To understand groundwater behaviour, groundwater models, such as deterministic mathematical models and black box models, are most commonly applied methods to describe the flow processes in groundwater systems.

1.1.1 Deterministic Mathematical Models

Deterministic mathematical models generally use partial differential equations to simulate the flow and transport processes in groundwater systems (Bear, 1972; Anderson and Woessner, 1992; Konikow, 2001). Assuming the groundwater flow is a time dependent problem, complete descriptions of the deterministic mathematical models comprise statements of governing equations, boundary and initial conditions. The deterministic mathematical models can be solved analytically or numerically. However, the analytical solutions require that the parameters and boundaries be highly idealised and detailed.

The governing equations are mathematical relationships describing approximations of groundwater movements through aquifer systems. They can be derived for different conceptual views of groundwater systems by mathematically combining water mass balance with Darcy's law (Darcy, 1856). There are two different conceptual views of groundwater systems: (1) aquifer viewpoint and (2) flow system viewpoint. The aquifer viewpoint is based

on concepts of confined and unconfined aquifers (Anderson and Woessner, 1992). For a confined aquifer, a general form of the governing equation is

$$\frac{\partial}{\partial x}\left(T_x \frac{\partial h}{\partial x}\right) + \frac{\partial}{\partial y}\left(T_y \frac{\partial h}{\partial y}\right) = S\frac{\partial h}{\partial t} - R + L \tag{1.1}$$

where h is the hydraulic head. T_x and T_y are the horizontal components of transmissivity. S is the storage coefficient. R is a sink/source term which is defined to be intrinsically positive to represent recharge. L is the leakage through a confined bed (Anderson and Woessner, 1992).

For an unconfined aquifer, it is practically assumed that the components of transmissivity, T_x and T_y, in Eq. (1.1) are replaced by $T_x = K_x h$ and $T_y = K_y h$, respectively, and the component of L in Eq. (1.1) is equal to zero. It produces a nonlinear governing equation, also called Boussinesq equation (Bear, 1972; Anderson and Woessner, 1992), for an unconfined flow as,

$$\frac{\partial}{\partial x}\left(K_x h \frac{\partial h}{\partial x}\right) + \frac{\partial}{\partial y}\left(K_y h \frac{\partial h}{\partial y}\right) = S_y \frac{\partial h}{\partial t} - R \tag{1.2}$$

where h is the saturated thickness in an unconfined aquifer. K_x and K_y are the horizontal components of conductivity tensor. S_y is the specific yield of an unconfined aquifer.

The flow system viewpoint refers to three-dimensional distribution of heads, hydraulic conductivities and storage properties in groundwater systems. It allows analyses of both vertical and horizontal flow components and thus permits assessments of two-dimensional or three-dimensional groundwater flow. A general form of the governing equation for the flow system viewpoint is

$$\frac{\partial}{\partial x}\left(K_x \frac{\partial h}{\partial x}\right) + \frac{\partial}{\partial y}\left(K_y \frac{\partial h}{\partial y}\right) + \frac{\partial}{\partial z}\left(K_z \frac{\partial h}{\partial z}\right) = S_s \frac{\partial h}{\partial t} - R^* \tag{1.3}$$

where K_z is the vertical component of conductivity tensor. S_s is the specific storage. R^* is a sink/source term which is defined as the volume of inflow to the system per unit volume of aquifer per unit of time (Anderson and Woessner, 1992).

Being general descriptions of groundwater flow motions, the governing equations do not contain any information on characterizations of special groundwater flow cases. To obtain solutions for special cases, boundary and initial conditions must also be specified along with the governing equations of interest. The boundary conditions are mathematical statements

specifying dependent variable or derivative of the dependent variable at the boundaries of the groundwater flow problems (Anderson and Woessner, 1992). Generally, hydrogeological boundary conditions can be mathematically classified as three types as follows: (1) Specified head boundaries (Dirichlet conditions) (Anderson and Woessner, 1992; Cassiani, 1999; Chang and Chen, 2003), (2) Specified flow boundaries (Neuman conditions) (Numan, 1972; Anderson and Woessner, 1992; Chang and Chen, 2003) and (3) Head-dependent flow boundaries (Cauchy or mixed boundary conditions) (Anderson and Woessner, 1992; Chang and Chen 2003). The initial conditions, also called boundary conditions in time, are statements describing the initial head distribution in groundwater systems (Anderson and Woessner, 1992). A correct selection of the boundary and the initial conditions is critical for the construction of deterministic mathematical models for the groundwater flow problems.

1.1.2 Black Box Models

Compared to deterministic mathematical models, black box models generally ignore spatial variations of parameters and describe groundwater flow by means of linear systems approaches with adjusted parameters (Zuber, 1986a, b). The box models, also called lumped-parameter models, are useful methods to interpret radioisotope (e.g. ^{3}H or ^{14}C) processes of passing through groundwater systems (Maloszewski and Zuber, 1993, 1996, 1998; Stewart, 2012) before appearing in outflow. In the lumped-parameter models, it is assumed that groundwater systems are continuous, flow patterns are in steady state, and variations of flow rate through groundwater systems are negligible (Zuber, 1986a, b; Zuber and Maloszewski, 2000). A convolution integral of the lumped-parameter models is given as,

$$C_{out}(t) = \int_0^{\infty} C_{in}(t-\tau)h(\tau)\exp(-\lambda\tau)\mathrm{d}\tau \qquad (1.4)$$

where C_{in} and C_{out} are the input and the output concentrations of a radioisotope. τ is the entry time of groundwater and $t-\tau$ is the groundwater residence time. $h(\tau)$ is the response function of hydrological system of interest. λ is the radioactive decay constant, expressing as $\lambda = \ln 2/T_{1/2}$. $T_{1/2}$ is the half-life of a radioisotope.

The response functions, $h(\tau)$, are used to depict the output distribution of an isotope injected instantaneously at the inlet in different flow patterns (Zuber and Maloszewski, 2000),

Based on different response functions, the lumped-parameter models are divided into four components as Piston flow model, Exponential flow model, Dispersion flow model and Exponential-piston flow model (Zuber and Maloszewski, 2000; Maloszewski et al., 2004). In the Piston flow model, the flow pattern is assumed to have a same transit time, and the hydrodynamic dispersion and diffusion can be negligible (Maloszewski and Zuber, 2000). The transit time (t_t) is the only variable parameter. The response function is expressed as

$$h(\tau) = \delta(\tau - t_t) \tag{1.5}$$

In the Exponential flow model, the flow pattern is assumed to have an exponential distribution of transit time, and there is no exchange among the flow lines (Maloszewski and Zuber, 1996). The transit time (t_t) is the only variable parameter. The response function is given as

$$h(\tau) = (t_t)^{-1} \exp\left(-\frac{\tau}{t_t}\right) \tag{1.6}$$

In the Dispersion model, it is assumed that there are exchanges among the flow lines (Maloszewski and Zuber, 1996). Two variable parameters of the Dispersion model are the tracer transit time (t_t) and the dispersion coefficient (P_D). The response function is given by the one-dimensional solution to the dispersion equation for a semi-infinite medium as follows,

$$h(\tau) = \left(\frac{4\pi P_D \tau}{t_t}\right)^{-\frac{1}{2}} \tau^{-1} \exp\left[-\frac{t_t\left(1-\frac{\tau}{t_t}\right)^2}{4P_D\tau}\right] \tag{1.7}$$

In Exponential-piston flow model, the groundwater flow is assumed to include two flow patterns in line (Maloszewski and Zuber, 1996). They are piston flow pattern at the early time and exponential flow pattern at the later time. Two variable parameters involved are the tracer transit time (t_t) and the ratio of the exponential volume to the total volume (f). The response functions are obtained as

$$h(\tau) = 0 \text{ for } \tau < t_t(1-f) \tag{1.8a}$$

$$h(\tau) = (f t_t)^{-1} \exp\left[-\left(\frac{\tau}{f t_t}\right) + \left(\frac{1}{f}\right) - 1\right] \text{ for } \tau > t_t(1-f) \tag{1.8b}$$

where f is the ratio of the exponential volume to the total volume. P_D is the dispersion parameter. t_t is the transit time.

1.1.3 Aquifer Parameters Estimation

An important application of groundwater models is to estimate parameters, such as hydraulic properties and flow dynamics, of groundwater systems by assessing and analysing field data. For instance, the pumping and the hydrochemistry and environmental tracer tests are two effective ways to obtain such data.

A pumping test is a field experiment in which an aquifer is discharged in a pumped well at a controlled rate and water-level response (drawdown) is measured in surrounding observation wells or the pumped well itself. An aim of the pumping test is to estimate hydraulic properties, such as transmissivity, conductivity and storativity, of the pumped aquifer. The pumping test is also used to identify aquifer boundaries. Type-curve matching methods are commonly applied methods to interpret drawdown data, which are generally developed based on different mathematical models for transient groundwater flows induced by the pumping (e.g. Theis, 1935; Ferris et al., 1962; Warren and Root, 1963; Kruseman and Ridder, 1991). Additionally, drawdown derivative plots are other useful methods for diagnostic and quantitative analysis of the pumping test. In the drawdown derivative plots, important flow segments are easy to be identified as different curve patterns (Bourdet et al., 1983, 1989; Beauheim and Pickens, 1986; Ehlig-Economides, 1988; Horn, 1990; Spane and Wurstner, 1993; Goode, 1997; Renard, 2005; Samani et al., 2006). Based on accurate identification of each flow segment, the drawdown derivative plots can also be applied to estimate the hydraulic properties of the pumped aquifer.

Hydrochemistry and environmental tracer tests are widely used to investigate chemical processes of groundwater flow, which can be utilized to further assess flow dynamics of groundwater systems (Mook, 2000). The assessment of the flow dynamics of groundwater systems includes understanding of recharge areas and sources, groundwater ages and its temporal trend, effects of climate change and flow circulation. To gain such understanding, hydrochemical parameters and environmental isotopes, such as tritium (^{3}H), oxygen-18 ($\delta^{18}O$), hydrogen (δD), carbon isotopes (δ^{13}C-DIC and ^{14}C-DIC) and strontium isotopes (Sr), of groundwater samples are usually collected in field work or laboratory analyses. Generally, recharge areas can be identified by interpretation of hydrogeochemical types of groundwater samples, whilst recharge sources can be suggested by using

concentrations of sodium (Na^{1+}) and chloride (Cl^{1-}) ions or δD and $\delta^{18}O$ measurements of groundwater samples. Groundwater age can be evaluated by use of time series of ^{3}H or ^{14}C measurements of groundwater samples and appropriate groundwater models (e.g. Maloszewski and Zuber, 1993, 1996, 1998; Stewart, 2012).

1.2 Research Objectives

The Theis (1935) equation is one of the fundamental solutions for the deterministic mathematical models of groundwater flow. Derivation approaches of the Theis equation are investigated in the thesis. So far, the Theis equation have been obtained by various methods (Lo áciga, 2009), including (1) analogies to solutions of heat conduction problems, (2) methods based on initial guesses, (3) the Laplace transform, (4) a hybrid method of separation of variables and (5) similarity transform methods.

With increasing demand of groundwater around the world, many confined aquifers have been reported to be pumped intensively (Wang and Zhan, 2009). A conversion from artesian (confined) to unconfined conditions occurs when a pumping rate or time is sufficiently large. The kind of groundwater flow conversion is investigated in the thesis. According to deterministic mathematical models of interest, new analytical solutions for the transient confined-unconfined flow driven by a fully penetrating well in a confined aquifer will be proposed.

Traditional drawdown derivative plot, d*s*/dlg*t*, have been used for the diagnostic analysis of pumping tests for many years. However, disadvantages of its use were identified in practice (Xiao and Xu, 2014). In the thesis, a new drawdown derivative pattern, dlg*s*/dlg*t*, is proposed to facilitate the diagnostic analysis of pumping tests. Comparison of the plot of dlg*s*/dlg*t* with the plot of d*s*/dlg*t* is to be made to unveil advantages and disadvantages of each derivative pattern. Meanwhile, an alternative differentiation algorithm for drawdown derivative calculations will also be introduced.

A hydrochemistry and environmental tracer method is adopted and used to assess the flow dynamics of spring system in the dolomite aquifer of South Africa. The aim is to determine ^{14}C age of the dolomite spring system and reveal its temporal trend by a lumped-parameter model. The recharge sources and areas, the effect of climate change and the flow circulation

in the dolomite spring system will also be discussed. Hence, the research objectives of the thesis are expected as follows:

1. Derivation of the Theis equation by a method of simplified similarity transformation.
2. Development of a new analytical solution for the transient confined-unconfined flow towards a fully penetrating pumping well. Statement of advantages of the new analytical solution over previous ones.
3. Discussion of a possibility of use of derivative pattern, dlg*s*/dlg*t*, for diagnostic analysis of aquifer tests. Clarification of differences of various differentiation algorithms of use in numerical derivative calculation.
4. Investigation of ^{14}C age of the dolomite spring system in South Africa by a hydrogeochemistry and environmental isotope method. Discussion of flow dynamics of the dolomite spring system.

Chapter 2

Literature Review

The previous researches on each groundwater issue of interest in the thesis are reviewed in the following section.

2.1 Derivation of the Theis (1935) Equation

The Theis (1935) equation is derived based on a governing equation with related initial and boundary conditions for a two-dimensional radial flow to a point source in an infinite, homogeneous and confined aquifer. It is considered as one of the fundamental analytical solutions for the deterministic mathematical models of groundwater flow. C.V. Theis (1935) realized that the Darcy's law was analogous to a law of heat flow conducting in solids and used a solution of temperature distribution due to an instantaneous line heat source to first derive his equation. After that, Li (1972) reported a derivation process of the Theis equation based on an initial guess of drawdown gradient developed by Jacob (1940). Verruift (1982) presented the solution of the Theis problem by means of the Laplace transform. Hermance (1999) obtained the Theis equation by using a hybrid method of separation of variables and the Hankel transform. A summary of these derivation methods for the Theis equation was given by Lo áciga (2009).

Similarity transformation method of solving a differential equation was first introduced by Boltzmann in 1894 (Debnath, 2004). Birkhoff (1950) recognized that the Boltzmann's method was built based on algebraic symmetry of a partial differential equation (Debnath, 2004), and a similarity solution of the partial differential equation could be gained by solving a related ordinary differential equation. Perina (2010) used a guessed priori as $u = Sr^2/4tT$ to replace independent variable in for two-dimensional radial flow, and put forward the first similarity transformation method to derive the Theis equation. Masoodi and Ghanbari (2012) used a suitable variable, depicted as $\eta = Cr^A t^B$, in place of an independent variable to convert a partial differential equation to an ordinary differential equation, and gained a general form of the similarity transformation method for derivation of the Theis equation.

However, the unknown parameters of C, A and B of the suitable variable leaded the derivation was complex and loose. In this thesis, a most simplified form of similarity solution is presented to derive Theis equation by using Boltzmann transform.

2.2 Solutions of Transient Confined-unconfined Flow

A conversion from artesian to unconfined conditions have been reported to occur in many large aquifers all around the world (Walton, 1964; Stoner, 1981; Springer and Bair, 1992), because of heavy pumping rates and times or small aquifer transmissivity. Researches on numerical and analytical solutions of the transient confined-unconfined flow were carried out in the last five decades. For the numerical solutions, Rushton and Wedderburn (1971) employed a resistance-capacitance electrical analogue to analyse the confined-unconfined conversion behaviour in aquifers. A specific yield for the unconfined region was used to replace the storativity of the confined aquifer in the numerical solution. Elango and Swaminathan (1980) put forward a finite-element numerical solution for the transient confined-unconfined flow. Based on the Dupuit's assumptions, the numerical solution was given by a finite-element method with four-sided mixed-curved isoperimetric elements; however, it was limited to analysing a steady-state flow. Wang and Zhan (2009) presented a semi-numerical solution for the transient confined-unconfined flow. The solution considered the change of both transmissivity and storativity during the confined-unconfined conversion and solved the nonlinearity of unconfined flow by the Runge-Kutta method.

For the analytical solutions, Moench and Prickett (1972) proposed a mathematical solution (MP model) for the transient confined-unconfined flow by using a constant transmissivity in the unconfined region. The MP model was obtained based on the analogous case of heat flow in cylindrical symmetry where freezing or melting takes place. Hu and Chen (2008) described an approximate solution (Chen model) for the transient confined-unconfined flow according to the Girinskii's potential function. The Girinskii's potential was defined as a potential of a steady-state groundwater flow in a horizontal-layered porous medium and utilized to depict a variable transmissivity of the unconfined region in the Chen model. The development of the MP and the Chen models has facilitated the understanding of the transient

confined-unconfined flow in a confined aquifer. However, limitations of the use of the two analytical solutions in practice are noticed as follows:

1. The two models do not fully consider the change of hydraulic properties during the confined-unconfined conversion. For example, the variability of transmissivity is neglected in the MP model; the change of diffusivity is neglected in the Chen model.
2. Due to the use of a constant transmissivity in the unconfined region, the MP model is only accepted as the unsaturated zone thickness in the unconfined zone is considerably smaller than the thickness of the confined aquifer (Bear, 1972).
3. The Chen model is given only for a steady-state flow because of the application of the Girinskii's potential function.

2.3 Derivative Analysis of Pumping Tests

Derivative interpretations of pressure data recorded during aquifer tests have been used to characterize pumped aquifers for many years. The traditional derivative analysis method using a semi-lg drawdown derivative ($ds/d\lg t$) is described by conceptual methodologies and computerized methods. Two types of applications of the derivative analysis were highlighted as (1) model identifications and (2) parameter determinations (Van Tonder et al., 2000; Renard, 2005; Renard et al., 2009). The model identifications were facilitated by the diagnostic plot of drawdown derivative which was proved to be highly sensitive to changes of drawdown behaviours. The derivative plot of $ds/d\lg t$ was first introduced as an aid for interpreting dynamic drawdown data from an artesian aquifer by Chow (1952). But the Chow's method was limited to interpretation of drawdown data with the Theis' solution. Even since that, much useful research has been done, particularly in petroleum industry. This research usually employed the pressure derivative plot to describe different hydrogeological formations, including inner boundaries (wellbore storage), outer boundaries (inflow and no-flow) and various flow regimes (radial flow), during constant rate and its following recovery tests (Djebbar and Kumar, 1980; Bourdet et al., 1983, 1989; Beauheim and Pickens, 1986; Ehlig-Economides, 1988; Horn, 1990; McConnell, 1993; Spane and Wurstner, 1993; Goode, 1997; Renard, 2005; Samani et al., 2006). The parameter determinations were specialized analyses of hydraulic properties of pumped aquifers during special flow regimes.

The derivative plots of d*s*/dlg*t* could be used in place of the traditional semi-lg drawdown plots to determine aquifer transmissivity (Chow, 1952; Bourdet et al., 1989; Spane and Wurstner, 1993) based on accurate identification of radial flows in constant rate tests.

An important aspect of performing derivative analysis is a selection of an appropriate method to eliminate negative effects of "noise" during numerical differentiation of drawdown data (Bourdet et al., 1983, 1989; Spane and Wurstner, 1993; Bourdet, 2002). Bourdet et al. (1989) introduced a simple three-point formula to calculate numeric drawdown derivative. It was followed by an alternative method presented by Spane and Wurstner (1993) for computing derivatives. As well as the Bourdet method, the Spane method also used a logarithmic differentiation interval. However, instead of using three points in the Bourdet method, the Spane method calculated the left and the right derivatives by applying linear regression to all of the points falling within the differentiation interval. Bourdet (2002) recommended an adjacent points (nearest neighbours) method for use in numerical differentiation of drawdown data. To remove noisy effects, the nearest neighbours method applied the data points separated by a certain distance measured in logarithmic time. Generally, the separation or the differentiation interval ranges between 0.1 and 0.5 of a logarithm cycle. Based on these differentiation algorithms, the software named *AQTESOLV* (Duffield, 2007) could be used to perform simultaneous matching of any type-curve solution to both drawdown and its derivative data.

The development of the pressure derivative method has noticeably improved the diagnostic and quantitative analysis of constant rate and slug tests (e.g. Karasaki et al., 1988; Ostrowski and Kloska, 1989; Spane and Wurstner, 1993) in confined aquifers. However, limitations of the use of the plot of d*s*/dlg*t* and the existing differentiation algorithms for calculations of numerical drawdown derivative are identified in practice as follows:

1. Pumping and its following recovery periods in intermittent variable discharge tests cannot be distinguished in the plot of d*s*/dlg*t*.
2. Storativity of pumped aquifers cannot be evaluated by using the plot of d*s*/dlg*t* alone.
3. Quantitative assessments of double-porosity behaviours cannot be achieved by the plot of d*s*/dlg*t* alone.

4. Noise effects cannot be avoided in the derivative calculation process by using the existing differentiation algorithms.

2.4 Isotopic Methods for Groundwater Dating

Groundwater age, also called residence turnover time, is defined as the time elapsed since the water parcel had its last contact with atmosphere (Bethke and Johnson, 2008; Kazemi et al., 2008). Actually, groundwater can be replenished by different recharge events, resulting in an variable distribution of groundwater ages in time and space. Mean Residence Time (MRT) is used to describe such groundwater age distribution (Mook, 2000), which can often be determined by means of ^{14}C dating approaches.

2.4.1 ^{14}C Dating

Radiocarbon (^{14}C) dating is an approach for determining age of an object by using the properties of radiocarbon. The ^{14}C dating of groundwater systems was first introduced by Muennich (1957, 1968). After that, ^{14}C dating has been widely used by hydrologists around the world and has proved to be one of the most successful and common methods to date groundwater (e.g. Le Gal La Salle et al., 2001; Douglas et al., 2007; Mokrik et al., 2008; Coetsiers and Walraevens, 2009; Hoque and Burgess, 2012; Stewart, 2012).

In general, the ^{14}C dating of groundwater is based on the difference between ^{14}C concentrations of dissolved inorganic carbon (^{14}C-DIC) of groundwater samples and its initial concentrations at the time of recharge. However, this approach usually encounters two major problems namely: (1) appropriate model for depicting the relation between ^{14}C-DIC and initial ^{14}C activities and (2) calibration of the initial ^{14}C activities.

2.4.1.1 Models for ^{14}C Dating of Groundwater

The water in subsurface can be considered as having mobile and immobile parts, depending on pore size distribution in an aquifer. For a mobile system, the groundwater MRT can be identified as the radioisotope (e.g. ^{3}H or ^{14}C) MRT (Zuber and Maloszewski, 2000) if there are no stagnant zones in the system, and the radioisotope is injected and measured in flux. In such case, the lumped-parameter models are simplest and most useful approaches for

groundwater dating. In the lumped-parameter models, initial ^{14}C activities and ^{14}C-DIC of the groundwater samples are used as input and output data, C_{in} and C_{out} , of Eq. (1.4), and the groundwater MRT can be obtained by solving the inverse problem (Zuber and Maloszewski, 2000; Maloszewski et al., 2004).

An important aspect of performing ^{14}C dating in a mobile groundwater system is a selection of an appropriate lumped-parameter model for the groundwater system of interest (Figure 2-1). The former researches (Maloszewski and Zuber, 1993, 1996, 1998; Zuber and Maloszewski, 2000; Maloszewski et al., 2004) suggested that the Piston flow (PM) and the Dispersion (DM) models are preferred methods to date the groundwater sample collected in a confined or partially confined aquifer, whilst the Exponential (EM) and the Exponential-piston flow (EPM) models are recommended for the groundwater dating for an unconfined aquifer or the discharge area.

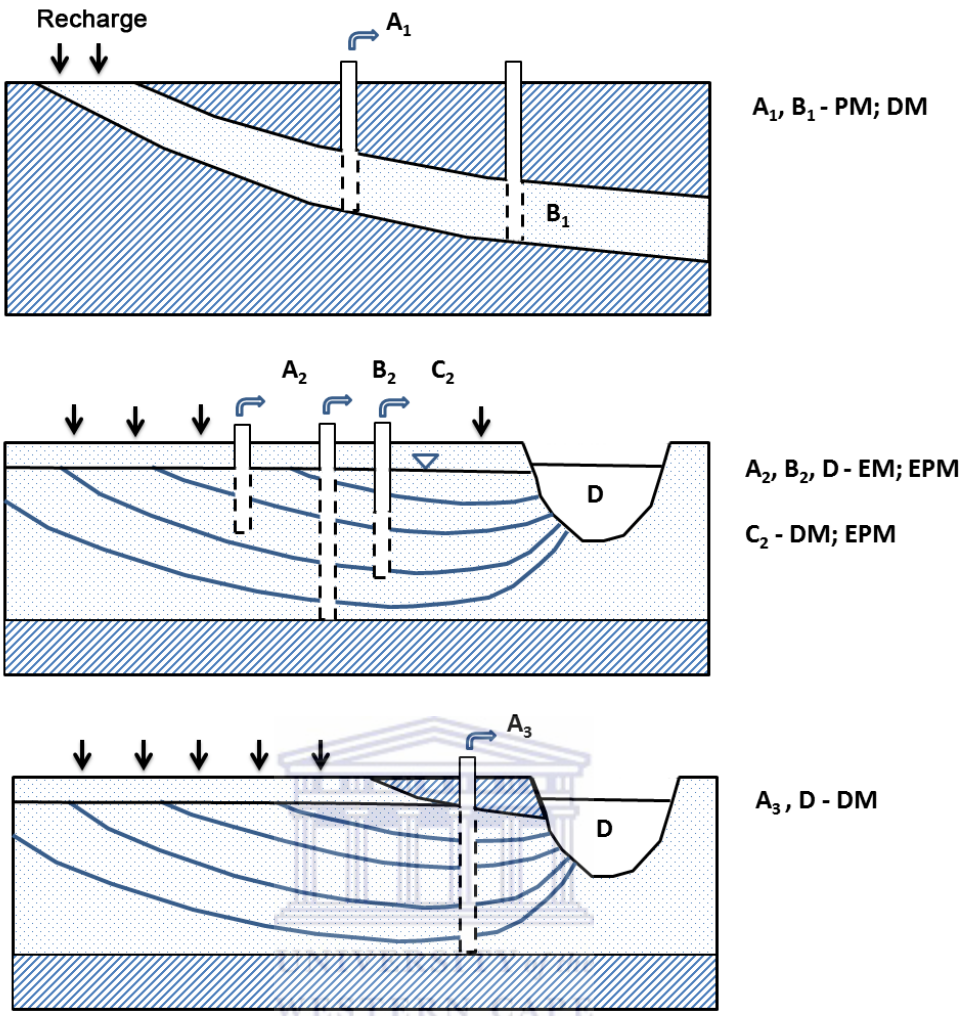

Figure 2-1 Schematic cases showing the possible applicability of different lumped-parameter models. Cases A, B, C and D represent the different sampling methods in different aquifer conditions (Maloszewski et al., 2004).

For an immobile groundwater system, the groundwater is assumed to be surrounded by the rock with low permeability, and the groundwater age is usually understood as the time span since the system has been separated from atmosphere (Zuber and Maloszewski, 2000). Assuming that decrease of ^{14}C concentration is mainly induced by ^{14}C decay, the groundwater age can be identified as the radiometric age of ^{14}C. In such case, the ^{14}C age of groundwater can be obtained by solving the following inverse problem,

$$\frac{C(t_t)}{C(0)} = \exp(\lambda t_t) \tag{2.1}$$

where t_t is the ^{14}C age. $C(t_t)$ and $C(0)$ are the actual and the initial ^{14}C concentrations, respectively. λ is the ^{14}C decay coefficient.

2.4.1.2 Calibration of Initial ^{14}C Activities

The application of ^{14}C dating often faces considerable problems that lead to overestimations of the groundwater MRTs due to dilution effects on initial ^{14}C activities. The dilution effects are mainly from (1) mineral, such as carbonate or dolomite, dissolution by carbon dioxide (CO_2) (Pearson and Hanshaw, 1970； Tamers, 1975) and (2) ion exchange reaction in a mineral-water system (Cartwright et al., 2007; Cartwright, 2010). In addition, diffusion of carbon from low porosity layers can also impact the ^{14}C activities. Generally, the two dilution processes can be examined by independent environment tracers. For example, carbon-13 values of dissolved inorganic carbon ($\delta^{13}C$-DIC) are usually used to evaluate the mineral dissolution; strontium isotopes (Sr) (Cartwright et al., 2007; Cartwright, 2010) can be applied to assess the isotopic exchange reaction in a mineral-water system.

Approaches to calibrate dilution effect of mineral dissolution on initial ^{14}C activities are based on an isotopic mixing model or a chemical mixing model (Pearson and Hanshaw, 1970； Tamers, 1975). It is assumed that (1) ^{14}C has same chemical behaviours as ^{13}C; (2) dissolved CO_2 in groundwater samples is derived from soil root zone; and (3) mineral dissolution by CO_2 or the isotopic exchange reaction takes place under open system conditions. Based on these assumptions, $\delta^{13}C$-DIC or compositions of CO_2 and bicarbonates (HCO_3^{1-}) can be utilized to account for dilution effect from mineral dissolution on initial ^{14}C activities in groundwater systems.

In a saturated zone, dissolved inorganic carbon can undergo isotopic exchange with mineral in dolomite aquifers. During these processes, ^{14}C activity of groundwater may be changed, however, the amount of dissolved carbon in groundwater remains stable. Strontium isotopes ($^{87}Sr/^{86}Sr$), produced by decay of the radioactive alkali metal rubidium (^{87}Rb), are generally recommended to assess such dilution effect from isotopic exchange on initial ^{14}C activities (Cartwright et al., 2007; Cartwright, 2010). The approach is built based on the facts that (1) mineral dissolution or isotopic exchange reaction change the $^{87}Sr/^{86}Sr$ ratios in the mineral-water system; (2) mineral precipitation does not separate $^{87}Sr/^{86}Sr$ ratios from the mineral-water system; and (3) the long half-life of ^{87}Rb means that the change of $^{87}Sr/^{86}Sr$ ratios is not due to the decay of ^{87}Rb in groundwater.

2.4.2 Previous Work on Isotope Study in the Dolomite Aquifer, South Africa

Studies on measurements and interpretations of isotope components in the dolomite aquifer of South Africa were carried out since 1970. Bredenkamp and Vogel (1970) published the first measurements from this aquifer and pointed out possibilities of use of isotope methods to determine recharge into the dolomite aquifer by studying flow patterns and flow rates. This was followed by assessments of recharge through the soils using tritium (^{3}H) (Bredenkamp et al., 1974). A study by Verhagen et al. (1979) also added information to some springs. Kronfeld et al. (1994) published a study on use of uranium isotopes and their decay products in the dolomite aquifer. Talma and Bredenkamp (1985) interpreted ^{14}C data from the springs in terms of phreatic flow models. Bredenkamp et al. (1992) described ^{14}C, tritium data and flow patterns of the Kuruman springs in terms of recharge from two separate environments contributing to the spring flow. Partridge (1985) related rainfall to runoff of the Thaba Sikwe spring to estimate growth rates of tufa deposits at Taung. A recharge manual given by Bredenkamp et al. (1995) for elaborating on these concepts was then further developed in a report on interpretation of monitoring data of spring samples (Bredenkamp, 2000). Talma and Vogel (2001) employed piston and exponential models to explain the variation of ^{14}C time series and obtained uncalibrated MRTs of the spring samples with about 50-100 years. It was followed by calibrations of the initial ^{14}C activities by use of tritium (^{3}H) (Bredenkamp, 2007; Bredenkamp et al., 2007) with an exponential mixing model. The results showed that most of the sample points had about 50%-100% initial ^{14}C activities and the calibrated groundwater MRTs were much younger than the uncalibrated ones obtained previously.

Chapter 3

A Simplified Similarity Transformation Method for Derivation of the Theis Equation

In this chapter, a most simplified similarity transformation method for derivation of the Theis equation is proposed by using the Boltzmann transform.

3.1 Mathematical Model

A governing equation for two-dimensional radial flow to a point source in an infinite, homogeneous and non-leaky confined aquifer is given in terms of groundwater drawdown (Bear, 1972) as

$$\frac{\partial^2 s}{\partial r^2} + \frac{1}{r}\frac{\partial s}{\partial r} = \frac{S}{T}\frac{\partial s}{\partial t} \tag{3.1}$$

The boundary conditions are

$$s(r \to \infty, t) = 0 \tag{3.2a}$$

$$\lim_{r\to 0} 2\pi T \frac{\partial s}{\partial r} = -Q \tag{3.2b}$$

And the initial condition is

$$s(r, 0) = 0 \tag{3.3}$$

where Q is the pumping rate. r is the distance from the pumping to the observed wells. s is the drawdown. S is the storage coefficient of the pumping aquifer. t is the pumping time. T is the transmissivity of the pumping aquifer.

3.2 Derivation of the Theis Equation by the Boltzmann Transform

To transform the partial differential equation (Eq. (3.1)) to an ordinary differential equation, a series of similarity items is directly introduced based on the principles of similarity solutions of linear differential equation (as Eqs. 8.11.12ab in Dehath (2004)) as follows,

$$v(\eta) = st^{-\frac{\gamma}{\beta}} \tag{3.4a}$$

$$\eta = rt^{-\frac{\alpha}{\beta}} \tag{3.4b}$$

where $v(\eta)$ is the similarity item of s and t. η is the similarity item of r and t. α, β and γ are the fixed constants. Using Eqs. (3.4a) and (3.4b), the three terms in Eq. (3.1) are rewritten by use of the similarity variable η as follows,

$$\frac{\partial s}{\partial r} = t^{\left(\frac{\gamma}{\beta}-\frac{1}{2}\right)}\frac{\partial v}{\partial \eta} \tag{3.5a}$$

$$\frac{\partial^2 s}{\partial r^2} = t^{\left(\frac{\gamma}{\beta}-1\right)}\frac{\partial^2 v}{\partial \eta^2} \tag{3.5b}$$

$$\frac{\partial s}{\partial t} = -\frac{\alpha}{\beta} rt^{\left(\frac{\gamma}{\beta}-\frac{\alpha}{\beta}-1\right)}\frac{\partial v}{\partial \eta} + \frac{\gamma}{\beta} v(\eta) t^{\left(\frac{\gamma}{\beta}-1\right)} \tag{3.5c}$$

It can be assumed that $\beta = 2\alpha$ and $\gamma = 0$ according to the Boltzmann transform (Debnath, 2004). Eq. (3.1) is regenerated as

$$\frac{\partial^2 v}{\partial \eta^2} + \left(\frac{1}{\eta} + \frac{S}{2T}\eta\right)\frac{\partial v}{\partial \eta} = 0 \tag{3.6}$$

Similarly, the boundary conditions (Eqs. (3.2a) and (3.2b)) and initial condition (Eq. (3.3)) are gained as

$$v(\eta \to \infty) = 0 \tag{3.7a}$$

$$\lim_{\eta \to 0} \eta \frac{\partial v}{\partial \eta} = -\frac{Q}{2\pi T} \tag{3.7b}$$

$$v(0) = 0 \tag{3.7c}$$

After separating variables and integrating Eq. (3.6), an expression of $\frac{\partial v}{\partial \eta}$ is given as

$$\frac{\partial v}{\partial \eta} = \frac{D}{\eta}\exp\left(-\frac{S\eta^2}{4T}\right) \tag{3.8}$$

where D is the integration constant. Applying Eq. (3.7b) to Eq. (3.8), D is found as $-\frac{Q}{2\pi T}$. Hence, Eq. (3.8) is gained as

$$\frac{\partial v}{\partial \eta} = -\frac{Q}{2\pi T\eta}\exp\left(-\frac{S\eta^2}{4T}\right) \tag{3.9}$$

Integrating Eq. (3.9) produces that

$$v(\eta) = -\int_0^\eta \frac{Q}{2\pi Tk}\exp\left(-\frac{Sk^2}{4T}\right)\mathrm{d}k + B \tag{3.10}$$

where k is the variable of integration, B is the integration constant. Considering the boundary condition as Eq. (3.7a) to Eq. (3.10), B is expressed as

$$B = \int_0^{\infty} \frac{Q}{2\pi T k} \exp(-\frac{Sk^2}{4T})\, \mathrm{d}k \tag{3.11}$$

Combining Eqs. (3.10) and (3.11), $v(\eta)$ is obtained as

$$v(\eta) = \int_{\eta}^{\infty} \frac{Q}{2\pi T k} \exp(-\frac{Sk^2}{4T})\, \mathrm{d}k \tag{3.12}$$

Letting $U = \frac{Sk^2}{4T}$, Eq. (3.12) is replaced as

$$v(\eta) = \frac{Q}{4\pi T} \int_{\frac{S\eta^2}{4T}}^{\infty} \frac{\exp(-U)}{U}\, \mathrm{d}U \tag{3.13}$$

Considering Eqs. (3.4a), (3.4b) and (3.13), the final function of drawdown, s, is given as

$$s = \frac{Q}{4\pi T} \int_{\frac{Sr^2}{4Tt}}^{\infty} \frac{\exp(-U)}{U}\, \mathrm{d}U \tag{3.14}$$

3.3 Summary

In this chapter, the Theis equation is obtained based on a governing equation in terms of drawdown with initial and boundary conditions. The Boltzmann transform is used to transfer the differential equation to the ordinary equation. The resultant solution is absolutely identical to the Theis equation (Theis, 1935). The approach adapted proves to be the most simplified similarity transformation method.

Nomenclature

Q	constant pumping rate, [L^3/t]
r	distance of observation well from pumping well, [L];
s	drawdown.[L];
S	storage coefficient of confined aquifer, dimensionless;
t	time, [t];
T	transmissivity of the aquifer, [L/t];

Chapter 4

New Analytical Solution for Transient Confined-unconfined Flow towards a Fully Penetrating Well in a Confined Aquifer

In this chapter, a new analytical solution for the transient confined-unconfined flow induced by a fully penetrating well in a confined aquifer is proposed. The proposed analytical solution considers a change of hydraulic properties during the confined-unconfined conversion. A comparison of the proposed analytical solution with previous solutions, namely the MP and the Chen models, is made to theoretically demonstrate advantages and disadvantages of each model.

4.1 Conceptual Model

Consider a non-leaky confined aquifer that extends horizontally and has a horizontal initial piezometric head (Figure 4-1). The confined aquifer is homogeneous but anisotropic and is fully penetrated by pumping and observation wells of infinitesimal diameters and discharged at a constant rate in the pumping well. The piezometric surface drops with time and an unconfined region occurs when the piezometric surface is below the upper surface of the confined aquifer. A conversion interface between the confined and the unconfined regions gradually moves away from the pumping well as the pumping continues.

The transient confined-unconfined flow can be depicted by following mathematical models. In the unconfined region ($0 \leq h_1(r,t) \leq b$, $0 < r \leq R$), a governing equation of the transient flow is obtained as

$$K_r \frac{\partial}{\partial x}\left(h_1 \frac{\partial h_1}{\partial x}\right) + K_r \frac{\partial}{\partial y}\left(h_1 \frac{\partial h_1}{\partial y}\right) = S_y \frac{\partial h_1}{\partial t} \tag{4.1a}$$

The boundary condition representing the fully penetrating well extension is

$$\lim_{r \to 0} 2\pi K_r h_1 r \frac{\partial h_1}{\partial r} = Q \tag{4.1b}$$

The boundary at the conversion interface is

$$h_1(R,t) = b \tag{4.1c}$$

Considering that the confined-unconfined conversion occurs as $h_1(r,t) \leq b$, a new initial boundary of the unconfined flow is introduced as

$$h_1(r,0) = b \tag{4.1d}$$

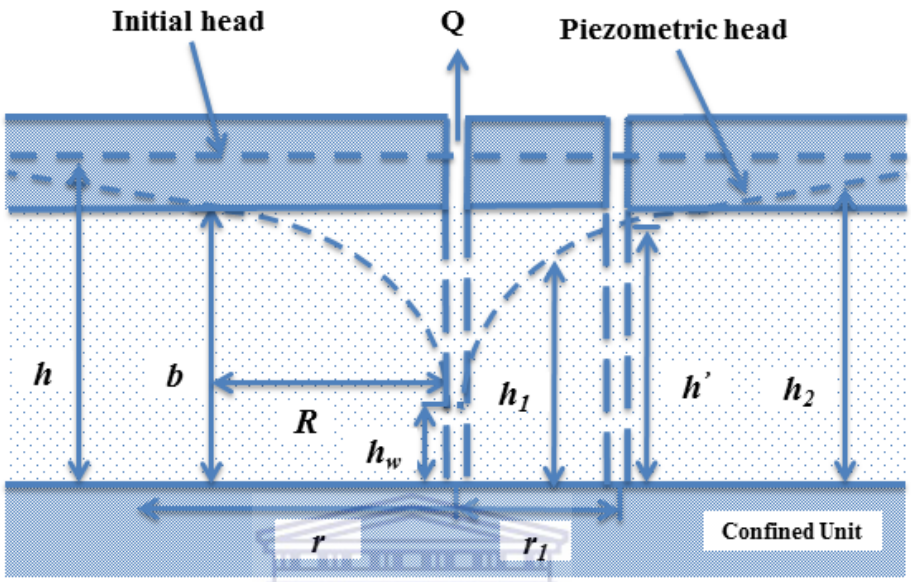

Figure 4-1 A schematic diagram of the transient confined-unconfined flow towards a fully penetrating well in a confined aquifer.

In the confined region ($b \leq h_2(r,t) \leq h,\ r \geq R$), the transient flow is depicted as

$$K_r b \frac{\partial}{\partial x}\left(\frac{\partial h_2}{\partial x}\right) + K_r b \frac{\partial}{\partial y}\left(\frac{\partial h_2}{\partial y}\right) = S \frac{\partial h_2}{\partial t} \tag{4.2a}$$

The far-field boundary condition is

$$h_2(r \to \infty, t) = h \tag{4.2b}$$

The boundary at the conversion interface is

$$h_2(R,t) = b \tag{4.2c}$$

A continuity of flow at the conversion interface is given as

$$\frac{\partial h_1(r,t)}{\partial r}\Big|_{r=R} = \frac{\partial h_2(r,t)}{\partial r}\Big|_{r=R} \tag{4.3}$$

where b is the thickness of the aquifer. h is the initial piezometric head. $h_1(r,t)$ and $h_2(r,t)$ are the elevations of the piezometric surface measured with respect to the aquifer base in the unconfined and the confined regions, respectively. K_r is the horizontal

conductivity of the aquifer. Q is the pumping rate. r is the radial distance from pumping well. R is the horizontal distance of the conversion interface between the confined and the unconfined regions from the pumping well. S_y is the special yield in the unconfined region. S is the storage coefficient of the confined aquifer. t is the pumping time.

4.2 Development of Analytical Solutions

The analytical solutions of the two flow cases are presented in the following.

4.2.1 Solution for Unconfined Flow

A common approach presented by Bear (1972) is utilized to linearize Eqs. (4.1a)-(4.1d) as follows,

$$\frac{\partial^2(h_1{}^2)}{\partial r^2}+\frac{1}{r}\frac{\partial(h_1{}^2)}{\partial r}=\frac{S_y}{K_r h_0}\frac{\partial(h_1{}^2)}{\partial t} \tag{4.4a}$$

$$\lim_{r\to 0}\pi K_r r\frac{\partial(h_1{}^2)}{\partial r}=Q \tag{4.4b}$$

$$h_1(R,t)=b \tag{4.4c}$$

$$h_1(r,0)=b \tag{4.4d}$$

where h_0 is the average water level in the unconfined region. Introducing a new item as $s_1'(r,t)=b^2-h_1(r,t)^2$, Eqs. (4.4a)-(4.4d) are rewritten as

$$\frac{\partial^2 s_1'}{\partial r^2}+\frac{1}{r}\frac{\partial s_1'}{\partial r}=\frac{S_y}{K_r h_0}\frac{\partial s_1'}{\partial t} \tag{4.5a}$$

$$\lim_{r\to o}\pi K_r r\frac{\partial s_1'}{\partial r}=-Q \tag{4.5b}$$

$$s_1'(R,t)=0 \tag{4.5c}$$

$$s_1'(r,0)=0 \tag{4.5d}$$

Derivation processes of the solution of the initial boundary-value problem given as Eqs. (4.5a)-(4.5d) are provided in Appendix A. The analytical solution is obtained as

$$h_1(r,t)^2=b^2-\frac{Q}{2\pi K_r}\left[W\left(\frac{S_y r^2}{4K_r h_0 t}\right)-W\left(\frac{S_y R^2}{4K_r h_0 t}\right)\right]=b^2-\frac{Q}{2\pi K_r}\left[W\left(\frac{S_y r^2}{4T' t}\right)-W\left(\frac{S_y R^2}{4T' t}\right)\right] \tag{4.6}$$

where $T'=K_r h_0$ is defined as the average transmissivity in the unconfined region. $W(u)$

is the Theis well function. It is worth noting that the average transmissivity, T', in the unconfined region is supposed to be variable due to the change of the average water level (h_0) with time.

4.2.2 Solution for Confined Flow

Introducing a new item as $s_2'(r,t) = h - h_2(r,t)$, Eqs. (4.2a)-(4.2c) are rewritten as

$$\frac{\partial^2 s_2'}{\partial r^2} + \frac{1}{r}\frac{\partial s_2'}{\partial r} = \frac{S}{K_r b}\frac{\partial s_2'}{\partial t} \tag{4.7a}$$

$$s_2'(r \to \infty, t) = 0 \tag{4.7b}$$

$$s_2'(R,t) = h - b \tag{4.7c}$$

Derivation processes of the solution of Eqs. (4.7a)-(4.7c) are provided in Appendix B. The analytical solution is captured as

$$h_2(r,t) = h - \frac{Q}{4\pi K_r b}\frac{\exp\left(-\frac{S_y R^2}{4K_r h_0 t}\right)}{\exp\left(-\frac{SR^2}{4K_r bt}\right)} W\left(\frac{Sr^2}{4K_r bt}\right) = h - \frac{Q}{4\pi T}\frac{\exp\left(-\frac{S_y R^2}{4T't}\right)}{\exp\left(-\frac{SR^2}{4Tt}\right)} W\left(\frac{Sr^2}{4Tt}\right) \tag{4.8}$$

where $T = K_r b$ is the constant transmissivity of the confined region.

4.3 Parameter Determinations

The analytical solutions for the transient confined-unconfined flow towards a fully penetrating well are obtained as Eqs. (4.6) and (4.8) for the unconfined and the confined flow patterns, respectively. It is suggested that the parameters, including the distance (R) of the conversion interface from the pumping well and the variable diffusivity (T'/S_y) in the unconfined region, should significantly influence the elevation of the piezometric surface during the confined-unconfined flow.

To assess such parameters concerned, a practical method is developed by using the proposed analytical solution and a constant rate test. It is assumed that the elevations of the piezometric surface in the pumping and the observation wells are measured as h_w and $h'(r_1,t)$, respectively, with respect to each time point of interest, t, during the pumping test (Figure 4-1). The distance between the observation and the pumping wells is r_1. The constant pumping rate (Q) and the hydraulic properties (S and T) of the pumped confined aquifer are

given parameters.

When $h_w \leq b$, the transient confined-unconfined flow occurs. The distance (R) of the conversion interface from the pumping well can be determined as follows. Expressions on the flow towards the conversion interface are given by subjecting Eq. (4.8) to the boundary condition (Eq. (4.2c)) as

$$b = h - \frac{Q}{4\pi T}\frac{\exp\left(-\frac{S_y R^2}{4T't}\right)}{\exp\left(-\frac{SR^2}{4Tt}\right)} W\left(\frac{SR^2}{4Tt}\right) \tag{4.9a}$$

$$\frac{S_y}{4T't} = -\ln\left[\frac{(h-b)4\pi T}{QW\left(\frac{SR^2}{4Tt}\right)}\right] \mathrm{X} \frac{1}{R^2} + \frac{S}{4Tt} \tag{4.9b}$$

In the early time as the conversion starts ($r_1 \geq R$), the flow towards the observation well is under confined condition, the solution of $h'(r_1, t)$ is gained by Eq. (4.8) as

$$h'(r_1, t) = h - \frac{Q}{4\pi T}\frac{\exp\left(-\frac{S_y R^2}{4T't}\right)}{\exp\left(-\frac{SR^2}{4Tt}\right)} W\left(\frac{S{r_1}^2}{4Tt}\right) \tag{4.10a}$$

An expression of R in the confined region is obtained by use of Eqs. (4.10a) and (4.9a) as

$$\frac{h-h'(r_1,t)}{h-b} = \frac{W\left(\frac{S{r_1}^2}{4Tt}\right)}{W\left(\frac{SR^2}{4Tt}\right)} \tag{4.10b}$$

The R value in the confined region is assumed to be a root of Eq. (4.10b). If $r_1 \leq R$, the flow towards the observation well is under unconfined condition. An expression of $h'(r_1, t)$ is given by Eq. (4.6) as

$$h'(r_1, t)^2 = b^2 - \frac{Q}{2\pi K_r}\left[W\left(\frac{S_y {r_1}^2}{4T't}\right) - W\left(\frac{S_y R^2}{4T't}\right)\right] \tag{4.11a}$$

Combining Eq. (4.11a) with Eq. (4.9b) yields

$$h'(r_1, t)^2 = b^2 - \frac{Q}{2\pi K_r}\left\{W\left\{-\ln\left[\frac{(h-b)4\pi T}{QW\left(\frac{SR^2}{4Tt}\right)}\right] \mathrm{X} \frac{{r_1}^2}{R^2} + \frac{S{r_1}^2}{4Tt}\right\} - W\left\{-\ln\left[\frac{(h-b)4\pi T}{QW\left(\frac{SR^2}{4Tt}\right)}\right] + \frac{SR^2}{4Tt}\right\}\right\} \tag{4.11b}$$

The R value in the unconfined region can be calculated by Eq. (4.11b) with respect to each time point of interest. Based on the accurate determination of R values by means of Eqs. (4.10b) or (4.11b) in the confined or the unconfined regions, the diffusivity of the unconfined

region (T'/S_y) can be expressed by Eq. (4.9b) as

$$\frac{S_y}{T'} = -\ln\left[\frac{(h-b)4\pi T}{QW\left(\frac{SR^2}{4Tt}\right)}\right] \mathrm{X} \frac{4t}{R^2} + \frac{S}{T} \tag{4.12}$$

The change of the hydraulic properties during the confined-unconfined conversion can be assessed by Eq. (4.12). It is indicated the diffusivity (T'/S_y) in the unconfined region is generally changed with the R value and the pumping time. Subjecting the relation $T' = K_r h_0$ to Eq. (4.12), the average water level (h_0) in the unconfined region can also be estimated.

As mentioned above, the distance (R) of the conversion interface from the pumping well and the diffusivity (T'/S_y) of the unconfined region can be determined by using the proposed analytical solution and a constant rate test. Based on the given parameters of the confined aquifer and the measurements of the elevation of the piezometric surface ($h'(r_1, t)$) in the observation well, the procedures of the parameter determinations are suggested as: (1) assess the R value in the confined or the unconfined regions by using Eqs. (4.10b) or (4.11b) with respect to the time point of interest, and then (2) estimate the value of diffusivity (T'/S_y) in the unconfined region by means of Eq. (4.12).

4.4 Discussion

A number of issues are deserved further discussion as follows.

4.4.1 Comparison with Previous Solutions

In the subsection, new derivation processes of the previous solutions, namely the MP (Moench and Prickett, 1972) and the Chen (Hu and Chen, 2008) models, are given. A comparison of the proposed alternative analytical solution to the MP and the Chen models is also made to demonstrate applicability of the proposed analytical solution and identify advantages and disadvantages of use of each solution.

4.4.1.1 Derivation of the MP Model

In the MP model, the governing equation (Moench and Prickett, 1972), which differs from Eq. (4.1a), for the unconfined flow is given as

$$K_r b \frac{\partial}{\partial x}\left(\frac{\partial h_1}{\partial x}\right) + K_r b \frac{\partial}{\partial y}\left(\frac{\partial h_1}{\partial y}\right) = S_y \frac{\partial h_1}{\partial t} \tag{4.13a}$$

The boundary conditions are

$$\lim_{r\to 0} 2\pi K_r b r \frac{\partial h_1}{\partial r} = Q \tag{4.13b}$$

$$h_1(R,t) = b \tag{4.13c}$$

Like Eq. (4.1d), the initial boundary of the unconfined flow pattern is

$$h_1(r,0) = b \tag{4.13d}$$

Detailed derivation of the analytical solution of Eqs. (4.13a)-(4.13d) is given in Appendix C. The solution is

$$h_1(r,t) = b - \frac{Q}{4\pi K_r b}\left[W\left(\frac{S_y r^2}{4Tt}\right) - W\left(\frac{S_y R^2}{4Tt}\right)\right] \tag{4.14}$$

In the confined region, the transient flow is described as

$$K_r b \frac{\partial}{\partial x}\left(\frac{\partial h_2}{\partial x}\right) + K_r b \frac{\partial}{\partial y}\left(\frac{\partial h_2}{\partial y}\right) = S \frac{\partial h_2}{\partial t} \tag{4.15a}$$

$$h_2(r \to \infty, t) = h \tag{4.15b}$$

$$h_2(R,t) = b \tag{4.15c}$$

A solution of $\frac{\partial h_1(r,t)}{\partial r}$ by Eq. (4.14) is

$$\frac{\partial h_1(r,t)}{\partial r} = \frac{Q}{2\pi K_r b r}\exp\left(-\frac{S_y r^2}{4Tt}\right) \tag{4.16}$$

Subjecting Eq. (4.16) to Eq. (4.3) produces the item of $\frac{\partial h_2(r,t)}{\partial r}|_{r=R}$ as

$$\frac{\partial h_2(r,t)}{\partial r}|_{r=R} = \frac{Q}{2\pi K_r b R}\exp\left(-\frac{S_y R^2}{4Tt}\right) \tag{4.17}$$

Involved math processes to derive the solution of Eqs.(4.15a)-(4.15c) and (4.17) are outlined in Appendix C. The analytical solution is given as

$$h_2(r,t) = h - \frac{Q}{4\pi K_r b}\frac{\exp\left(-\frac{S_y R^2}{4Tt}\right)}{\exp\left(-\frac{SR^2}{4Tt}\right)} W\left(\frac{Sr^2}{4Tt}\right) \tag{4.18}$$

Eqs. (4.14) and (4.18) for the unconfined and the confined flow pattern, respectively, are identical with those from the MP model, as seen Eqs. (14) and (15) in Moench and Prickett (1972).

Compared to the proposed analytical solution, the MP model is derived based on the assumption that the elevation of the piezometric surface (h_1) in the unconfined region is approximately equal to the thickness (b) of the confined aquifer, as shown in Eqs. (4.13a) and (4.13b). Hence, the MP model is only accepted as the unsaturated zone thickness in the unconfined region nearby the conversion interface is considerably smaller than the thickness of the confined aquifer. If the unsaturated zone thickness in the zone that far from the conversion interface is sufficiently large, the use of the MP model is expected to introduce significant errors. In such a case, the proposed analytical solution is better fitted for analyzing the unconfined flow pattern with a variable transmissivity of $T = K_r h_1$.

4.4.1.2 Derivation of the Chen Model

The Chen model (Hu and Chen, 2008) can be directly obtained by using the proposed analytical solution. It is assumed that the diffusivity during the confined-unconfined conversion is fixed ($T/S = T'/S_y$). The expression for the elevation of the piezometric surface in the confined region is given by Eq. (4.8) as

$$h_2(r,t) = h - \frac{Q}{4\pi T} W\left(\frac{Sr^2}{4Tt}\right) \tag{4.19}$$

According to Eq. (4.9a), the item of $W\left(\frac{SR^2}{4Tt}\right)$ is given as

$$W\left(\frac{SR^2}{4Tt}\right) = \frac{4\pi K_r b}{Q}(h - b) \tag{4.20}$$

Combining Eq. (4.20) with Eq. (4.6) leads to the expression for the elevation of the piezometric surface in the unconfined region as

$$h_1(r,t)^2 = 2bh - b^2 - \frac{Q}{2\pi K_r} W\left(\frac{Sr^2}{4Tt}\right) \tag{4.21}$$

Eqs. (4.21) and (4.19) are the same as the expressions for the elevation of the piezometric surface in the unconfined and the confined regions, respectively, from the Chen model (see Eqs. (12) and (11) in Hu and Chen (2008)). The Chen model is given as a special case of the

proposed analytical solution with a fixed diffusivity during the confined-unconfined conversion.

In general, the average water level (h_0) could be assumed to be smaller than the original head (b) of the unconfined flow (Bear, 1972). It leads that the specific yield (S_y) of the unconfined region could be smaller than the storage coefficient (S) of the confined aquifer according to the assumption of $Kb/S = Kh_0/S_y$ in the Chen model. However, practically, the S_y value of the unconfined region is often 100 times or much larger than the S value of the confined region. Hence, the use of the Chen model in practice is doubtful. In such case, the proposed analytical model is recommended for the analysis of the transient confined-unconfined flow with a variable diffusivity in the unconfined region.

4.3.2 Effect of Wellbore Storage and Unsaturated flow

The effect of the change of hydraulic properties on the transient confined-unconfined flow towards a fully penetrating well of infinitesimal diameter in a confined aquifer is investigated by using the proposed analytical solution in this chapter. However, there are two other issues that deserve further investigations. The first one is the effect of the well bore storage on the transient confined-unconfined flow. There are increasing evidences suggesting that the drawdown induced by a large-diameter pumping well is influenced by the wellbore storage (Mishra et al., 2013). In the study, the effect of the wellbore storage is negligible due to the use of an infinitesimal wellbore.

The second issue is the effect of the unsaturated zone above the saturated region on the transient confined-unconfined flow. Previous research (e.g. Neuman, 1972; Nwankwor et al., 1992; Mathia and Butler, 2006; Tartakovsky and Neuman, 2007; Moench, 2008; Mishra et al., 2013) has shown that the presence of the unsaturated zone can lead a delayed response of the water table in an unconfined aquifer. This kind of drawdown behaviour is often interpreted as a result of the change of phreatic storage coefficient with time. However, the sensibility of the effect of unsaturated flow on the transient confined-unconfined flow has remained uncertain so far.

4.5 Summary

A new analytical solution for the transient confined-unconfined flow towards a fully penetrating well in a confined aquifer is proposed. It can be used to investigate the effect of the change of hydraulic properties on the confined-unconfined conversion. A new initial boundary condition for the mathematical model of the unconfined flow is introduced as Eq. (4.1d). The transient confined and unconfined flow patterns can be depicted as Eqs. (4.6) and (4.8), respectively. It is indicated that the elevation of the piezometric surface during the confined-unconfined conversion should be affected by the distance of the conversion interface from the pumping well and the diffusivity in the unconfined region.

To assess such parameters concerned, a practical method is developed by use of the proposed analytical solution and a constant rate test. The results show that, if the flow towards the observation well is under confined condition, the distance of the conversion interface from the pumping well can be calculated by Eq. (4.10b). If the flow towards the observation well is under unconfined condition, Eq. (4.11b) can be employed to evaluate the distance of the conversion interface from the pumping well. Based on the accurate determination of the distance of the conversion interface from the pumping well, the diffusivity of the unconfined region can be estimated by using Eq. (4.12) which suggests that the diffusivity of the unconfined region is generally changed with the distance of the conversion interface from the pumping well and the pumping time.

The applicability of the proposed analytical solution is demonstrated by a comparison with the previous solutions, namely the MP and the Chen models. The results also unveil the disadvantages of the use of the two previous models. The MP model using a constant transmissivity during the confined-unconfined conversion is only accepted as the drawdown in the unconfined region nearby the conversion interface is considerably smaller than the thickness of the confined aquifer. The Chen model, given as a special case of the proposed model, is limited to the analysis of the transient confined-unconfined flow with a fixed diffusivity. Consequently, the proposed new analytical solution provides a comprehensive understanding of the transient confined-unconfined flow induced by a fully penetrating well.

Nomenclature

b	aquifer thickness, [L];
$h_1(r,t)$	elevation of piezometric surface in unconfined region, [L];
$h_2(r,t)$	elevation of piezometric surface in confined region, [L];
$h'(r_1,t)$	elevation of piezometric surface in observation well, [L];
h_w	elevation of piezometric surface in pumping well, [L];
h_0	average elevation of piezometric surface in unconfined region, [L];
Q	constant pumping rate, [L^3/t]
K_r	horizontal conductivity of the aquifer, [L/t];
r	radial distance, [L];
r_1	distance of observation well from pumping well, [L];
R	horizontal distance of conversion interface from pumping well, [L];
S_y	specific yield of unconfined region, [dimensionless];
S	storage coefficient of confined region, [dimensionless];
t	time, [t];
$T' = K_r h_0$	average transmissivity in the unconfined region, [L^2/t];
$T = K_r b$	transmissivity in the confined region, [L^2/t];
$W(u)$	Theis well function;

Chapter 5

Diagnostic Analysis of Pumping Tests Using Derivative of dlgs/dlg*t* with Case Studies

In this chapter, a lg-lg (lg stands for logarithm to the base 10) drawdown derivative, dlg*s*/dlg*t*, is proposed for diagnostic analysis of pumping tests including variable discharge tests with infinite conditions, constant rate tests in bounded aquifers and tests involving double-porosity behaviours. A new differentiation algorithm is introduced to prevent noisy data from being cumulative during numeric derivative calculation processes. Advantages and disadvantages of different derivative methods are also discussed.

5.1 Methodology

The drawdown derivative plots for variable discharge tests, constant rate tests in bounded aquifers and tests involving double-porosity behaviours are presented in following subsections.

5.1.1 Derivative Plot for Variable Discharge Test

Practically, aquifers are sometimes pumped at variable rates instead of a constant rate (Kruseman and Ridder, 1991). There are two general types of variable discharge tests: (1) uninterrupted variable discharge test and (2) intermittent variable discharge test. For an uninterrupted variable discharge test, an aquifer is continuously pumping at different discharge rates. For an intermittent variable discharge test, it involves a series of discharge and recovery phases. Adjusted time functions (t_e) based on deconvolution algorithms were introduced for drawdown expression of variable discharge tests by Birsoy and Summers (1980). The drawdown derivative is taken with respect to the logarithm of the adjusted time to the base 10, $\lg t_e$, in the chapter.

A wellbore storage effect, defined as physical water storage in a well or borehole deviating from an ideal line sink, appears at the early pumping time. This effect may last from a few seconds to many minutes, depending on the storage capacity of the well. According to an

analytical solution presented by Spane and Wurstner (1993), drawdown and its logarithmic expression during the wellbore storage period can be written as

$$s = \frac{Q_1 t_e}{\pi r_c^2} \tag{5.1}$$

$$\lg s = \lg t_e + \lg \frac{Q_1}{\pi r_c^2} \tag{5.2}$$

where s is the drawdown in the well, r_c is the stress well casing radius, t_e is the adjusted time defined by Birsoy and Summers (1980)

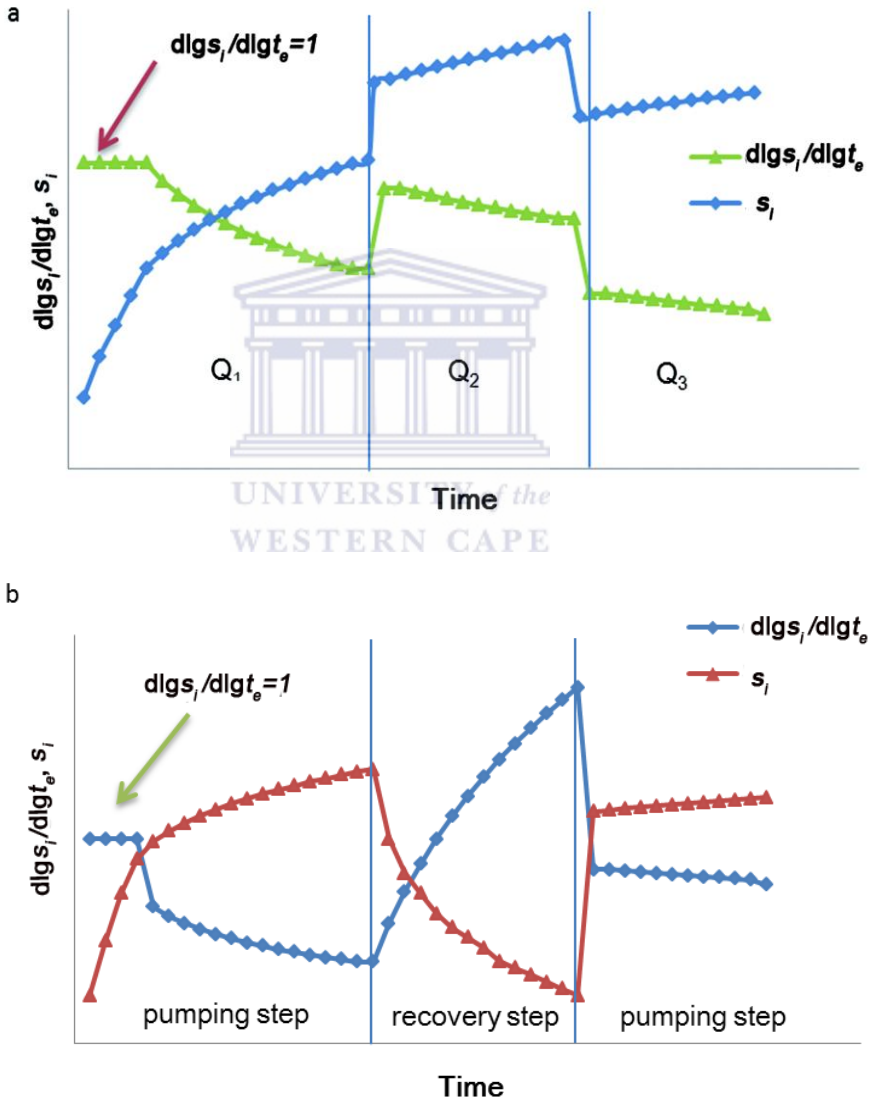

Figure 5-1 Conceptual plots of drawdown and dlgs$_i$/dlgt$_e$ in normal time scale for (a) uninterrupted variable discharge tests; (b) intermittent variable discharge tests.

A drawdown derivative of dlgs/dlgt_e during the storage effect stage is found as

$$\frac{\mathrm{dlg}s}{\mathrm{dlg}t_e} = 1 \tag{5.3}$$

After the wellbore storage effect is over, a radial flow will be expected for an ideal homogenous and isotropic aquifer. The drawdown expression proposed by Birsoy and Summers (1980) for the discharge and recovery period is as follows,

$$s_i = \frac{2.3Q_i}{4\pi T}\lg(ct_e) \tag{5.4}$$

where c is either $\frac{2.25T}{r^2S}$ for the discharge period or 1 for the recovery period (Cooper and Jacob, 1946), r is the distance from pumping well. Hence, logarithm of s_i with respect to logarithm of t_e is given as

$$\lg s_i = \lg\frac{2.3Q_i}{4\pi T} + \lg[\lg(ct_e)] \tag{5.5}$$

For a pumping period, the expressions of drawdown derivative, $\mathrm{d}s_i/\mathrm{dlg}t_e$ and $\mathrm{dlg}s_i/\mathrm{dlg}t_e$, for the radial flow can be gained as

$$\frac{\mathrm{d}s_i}{\mathrm{dlg}t_e} = \frac{2.3Q_i}{4\pi T} \tag{5.6}$$

$$\frac{\mathrm{dlg}s_\mathrm{i}}{\mathrm{dlg}t_e} = \frac{1}{\ln\left(\frac{2.25T}{r^2S}t_e\right)} \tag{5.7}$$

The traditional application of derivative analysis during the radial flow is to evaluate hydraulic properties, namely T (transmissivity) and S (storativity), of pumped aquifers. Based on Eqs. (5.6) and (5.7), T and S are calculated as

$$T = \frac{2.3Q_i}{4\pi\frac{\mathrm{d}s_i}{\mathrm{dlg}t_e}} \tag{5.8}$$

$$S = \frac{5.2Q_i t_e}{4\pi r^2\frac{\mathrm{d}s_i}{\mathrm{dlg}t_e}\times\exp\left(\frac{\mathrm{dlg}t_e}{\mathrm{dlg}s_i}\right)} \tag{5.9}$$

In each pumping period, there is a T value generated by using Eq. (5.8) based on a mean value of $\mathrm{d}s_i/\mathrm{dlg}t_e$ during a radial flow. An average value of the T series for all radial flows is defined to be the T value of a pumped aquifer. For S value determination, a series of S results by Eq. (5.9) is evaluated for points of interest during all radial flows based on values of $\mathrm{d}s_i/\mathrm{dlg}t_e$ and $\mathrm{dlg}s_i/\mathrm{dlg}t_e$. Similarly, a mean value of the S series is assumed to be the S value of a pumped aquifer.

For a recovery period, the derivative formulas of $\mathrm{d}s_i/\mathrm{dlg}t_e$ and $\mathrm{dlg}s_i/\mathrm{dlg}t_e$ can be obtained by

a similar approach as

$$\frac{\mathrm{d}s_i}{\mathrm{dlg}t_e} = \frac{2.3Q_i}{4\pi T} \tag{5.10}$$

$$\frac{\mathrm{dlg}s_\mathrm{i}}{\mathrm{dlg}t_e} = \frac{1}{\ln t_e} \tag{5.11}$$

Using Eq. (5.10), T value can also be estimated during the recovery period as

$$T = \frac{2.3Q_i}{4\pi \frac{\mathrm{d}s_i}{\mathrm{dlg}t_e}} \tag{5.12}$$

Figure 5-1(a) and (b) depicts the conceptual derivative plots of dlgs_i/dlgt_e for uninterrupted variable discharge and intermittent variable discharge tests, respectively. It is indicated that various characteristic behaviours can be identified in the plot of dlgs_i/dlgt_e. At the early time as pumping test starts, the wellbore storage effect is identified as a straight line with the value equal to 1 in the plot of dlgs_i/dlgt_e. When the radial flows are attained, the plots of dlgs_i/dlgt_e in pumping and its following recovery periods are described as Eqs. (5.7) and (5.11), respectively, whilst the values of ds_i/dlgt_e over pumping and its following recovery periods are found to lie along a same straight line as seen in Eqs. (5.6) and (5.10). It suggests that the plot of dlgs_i/dlgt_e is better fitted to distinguish pumping and its following recovery periods in intermittent variable discharge tests. The hydraulic properties (T and S) of pumped aquifers can be evaluated during the radial flow by using Eqs. (5.8) and (5.9). It is worth noting that constant rate and its following recovery tests can be assumed to be a special case of the intermittent variable discharge tests including single pumping and its following recovery steps. Hence, the proposed derivative analysis for intermittent variable discharge tests can also be used to analyze constant rate and its following recovery tests.

5.1.2 Derivative Plot for Aquifer Boundary

In addition to estimating aquifer parameters, another traditional application of drawdown derivative plots is to identify boundary conditions when pumping tests are conducted in bounded aquifers. The effects of boundary conditions may occur at the late time of the test as pumping proceeds. Stallman (Ferris et al., 1962) put forward a curve-fitting method of analyzing pumping tests in aquifers that has one or more straight boundaries. In general, the real bounded system can be assumed to be replaced by an imaginary system including a

pumping well, a piezometer and a series of image wells. Drawdown, *s*, in a piezometer can be expressed according to Stallman method (Ferris et al., 1962) as

$$s = \frac{2.3Q}{4\pi T}[W(u) \pm W(r_{r1}^2 u) \pm \cdots W(r_{rn}^2 u)] \tag{5.13}$$

where $s_d = 2.3QW(u)/(4\pi T)$ is the drawdown from discharging well ; $s_r = 2.3QW(r_{r1\to n}^2 u)/(4\pi T)$ is the drawdown from an image well; $r_{r1\to n}$ is the ratio equal to r_i/r; r is the distance between the piezometer and real discharging well; r_i is the distance between the piezometer and *i* th image well; $u = r^2 S/4Tt$.

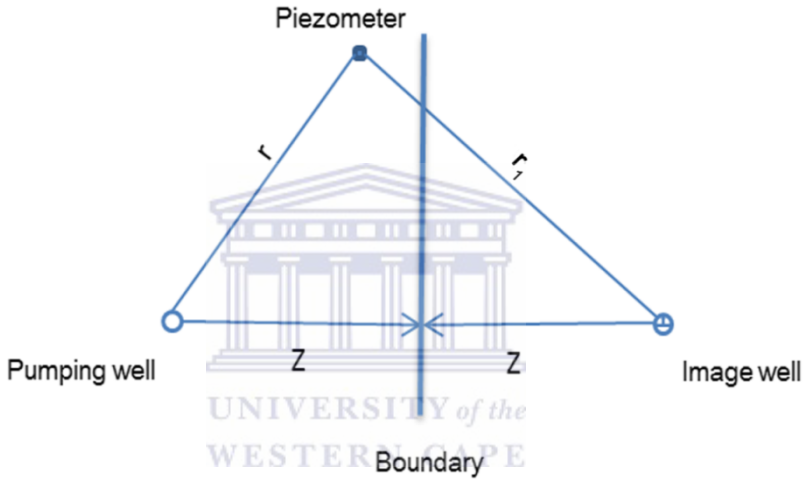

Figure 5-2 A conceptual image system under single boundary conditions (after Ferris et al., 1962). The drawdown in piezometer is the discharging results from both pumping and image wells.

Figure 5-2 shows a conceptual image system with single boundary conditions. Under one recharge boundary condition, the drawdown in piezometer can be given as

$$s = \frac{2.3Q}{4\pi T}\left[\lg\left(\frac{2.25Tt}{r^2 S}\right) - \lg\left(\frac{2.25Tt}{{r_{r1}}^2 r^2 S}\right)\right] \tag{5.14}$$

In this region, the drawdown derivatives are characterized as

$$\frac{\mathrm{d}s}{\mathrm{dlg}t} = 0 \tag{5.15}$$

$$\frac{\mathrm{dlg}s}{\mathrm{dlg}t} = 0 \tag{5.16}$$

For a single barrier boundary system, the drawdown in the piezometer is

$$s = \frac{2.3Q}{4\pi T}\left[\lg\left(\frac{2.25Tt}{r^2 S}\right) + \lg\left(\frac{2.25Tt}{{r_{r1}}^2 r^2 S}\right)\right] \tag{5.17}$$

The derivatives of drawdown and logarithm drawdown are

$$\frac{\mathrm{d}s}{\mathrm{dlg}t} = 2 \times \frac{2.3Q}{4\pi T} \tag{5.18}$$

$$\frac{\mathrm{dlg}s}{\mathrm{dlg}t} = \frac{2}{\ln\left(\frac{1}{r_{r1}{}^2}\right)+2\times\ln\left(\frac{2.25Tt}{r^2S}\right)} \tag{5.19}$$

In the case of the aquifers with two boundaries, the image system for the aquifers with two boundaries at right angle to each other is assumed to have a pumping well and three image wells; the image system for the aquifers with two parallel boundaries is constructed by a pumping well and seven image wells (Ferris et al., 1962). Using the similar derivation method in the case of one boundary systems, the drawdown derivative patterns for pumping tests in the aquifers with two boundaries are described in Table 5-1.

Table 5-1 Drawdown derivative patterns for two boundaries condition systems

Boundary conditions system		**d*s*/dlg*t***	**dlg*s*/dlg*t***
two boundaries at right angle to each other	one barrier and one recharge boundary	0	0
	two barrier boundaries	$4 \times \frac{2.3Q}{4\pi T}$	$f(4)$*
	two recharge boundaries	0	0
two parallel boundaries	one barrier and one recharge boundary	0	0
	two barrier boundaries	$8 \times \frac{2.3Q}{4\pi T}$	$f(8)$*
	two recharge boundaries	0	0

*$f(n) = \frac{n}{\ln[\prod_{i=2}^{n} r_{r(i-1)}^2]^{-1}+n\times\ln\left(\frac{2.25Tt}{r^S S}\right)}$, where n is the number of pumping and image wells in an image system.

As mentioned above, different boundary conditions can be represented by different drawdown derivative plots. Uses of plots of d*s*/dlg*t* and dlg*s*/dlg*t* can be adopted for identifications of single barrier boundary and two barrier boundaries conditions. For plots of d*s*/dlg*t*, derivative patterns for different barrier boundary conditions can be simply explained as integer factors of that of radial flows immediately before boundary effect dominations as,

$$\frac{\mathrm{d}s}{\mathrm{dlg}t} = n \times \frac{2.3Q}{4\pi T} \tag{5.20}$$

For plots of dlg*s*/dlg*t*, derivative patterns for different barrier boundary systems can be gained as follows,

$$\frac{\mathrm{dlg}s}{\mathrm{dlg}t} = \frac{n}{\ln[\prod_{i=2}^{n} r_{r(i-1)}^{2}]^{-1} + n \times \ln\left(\frac{2.25Tt}{r^{S}S}\right)} \tag{5.21}$$

where n is the number of pumping and image wells in the image system of interest. The values of d*s*/dlg*t* and dlg*s*/dlg*t* are both equal to 0 whenever recharge boundaries are involved during pumping tests (Table 5-1).

5.1.3 Derivative Plot for Dual-Porosity Aquifer

One frequent flow response of pumping tests in fractured rock is a dual-porosity behavior. In this case, a fractured reservoir is assumed to consist of two media: matrix and fractures, which can be represented by an equivalent homogeneous dual-porosity system (Warren and Root, 1963). Kazemi et al. (1969) extended use of the drawdown analysis method, developed by Warren and Root (1963), for pumped wells to express drawdown data recorded in observation wells. A semi-lg drawdown plot for a constant rate test in a double-porosity aquifer, as shown in Figure 5-3, is revealed as two parallel straight lines connected by a transitional pattern.

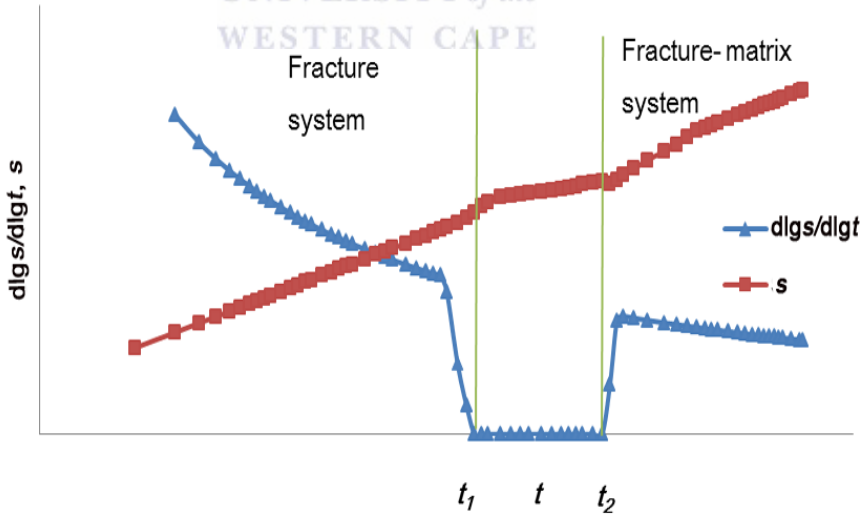

Figure 5-3 Conceptual plots of drawdown and dlg*s*/dlg*t* for double-porosity behavior without wellbore storage in a semi-lg scale.

Figure 5-3 also presents a conceptual derivative plot of dlg*s*/dlg*t* for the double-porosity behaviour. Two radial flow patterns, one for fracture system at the early time ($t<t_1$) and other for fracture-matrix system at the late time ($t>t_2$), can be identified in the plot of dlg*s*/dlg*t*.

Recall the expression of drawdown response (s) presented by Kazemi et al. (1969) for the fracture system is

$$s = \frac{2.3Q}{4\pi T_f} \lg \frac{2.25T_f t}{r^2 S_f} \tag{5.22}$$

$$\lg s = \lg \frac{2.3Q}{4\pi T_f} + \lg \left[\lg \left(\frac{2.25T_f t}{r^2 S_f} \right) \right] \tag{5.23}$$

where T_f and S_f are the effective transmissivity and the storativity of the fracture, respectively. Based on Eqs. (5.22) and (5.23), the drawdown derivatives are produced as

$$\frac{\mathrm{d}s}{\mathrm{dlg}t} = \frac{2.3Q}{4\pi T_f} \tag{5.24}$$

$$\frac{\mathrm{dlg}s}{\mathrm{dlg}t} = \frac{1}{\ln\left(\frac{2.25T_f t}{r^2 S_f} \right)} \tag{5.25}$$

According to Eqs. (5.24) and (5.25), the values of T_f and S_f are assessed as

$$T_f = \frac{2.3Q}{4\pi \frac{\mathrm{d}s}{\mathrm{dlg}t}} \tag{5.26}$$

$$S_f = \frac{5.2Qt}{4\pi r^2 \frac{\mathrm{d}s}{\mathrm{dlg}t} \times \exp\left(\frac{\mathrm{dlg}t}{\mathrm{dlg}s} \right)} \tag{5.27}$$

At the late time, the drawdown expression for the fracture-matrix system is given as

$$s = \frac{2.3Q}{4\pi T_f} \lg \frac{2.25T_f t}{r^2 (S_f + \beta S_m)} \tag{5.28}$$

$$\lg s = \lg \frac{2.3Q}{4\pi T_f} + \lg \left[\lg \frac{2.25T_f t}{r^2 (S_f + \beta S_m)} \right] \tag{5.29}$$

where β is a factor defined as 1/3 for orthogonal system or 1 for strata type by Warren and Root (1963) and S_m is the storativity of the matrix. The drawdown derivative plots of the fracture-matrix system are obtained as

$$\frac{\mathrm{d}s}{\mathrm{dlg}t} = \frac{2.3Q}{4\pi T_f} \tag{5.30}$$

$$\frac{\mathrm{dlg}s}{\mathrm{dlg}t} = \frac{1}{\ln\left[\frac{2.25T_f t}{r^2 (S_f + \beta S_m)} \right]} \tag{5.31}$$

From Eqs. (5.30) and (5.31), a term of $S_f + \beta S_m$ can be shown that

$$S_f + \beta S_m = \frac{5.2Qt}{4\pi r^2 \frac{\mathrm{d}s}{\mathrm{dlg}t} \times \exp\left(\frac{\mathrm{dlg}t}{\mathrm{dlg}s} \right)} \tag{5.32}$$

Using Eqs. (5.27) and (5.32), the storativity of the matrix (S_m) and the storativity ratio(ω) are calculated as

$$S_m = \frac{\left[\frac{5.2Qt}{4\pi r^2 \frac{\mathrm{d}s}{\mathrm{dlg}t}\times\exp\left(\frac{\mathrm{dlg}t}{\mathrm{dlg}s}\right)} - S_f\right]}{\beta} \tag{5.33}$$

$$\omega = \frac{S_f}{S_f+\beta S_m} \tag{5.34}$$

Bourdet and Gringarten (1980) also introduced that the drawdown during the transition period could be expressed as $[2.3Q\lg(1.26/\gamma)]/(4\pi T_f)]$, where γ is the interporosity flow coefficient. Hence, the drawdown derivative values of dlg*s*/dlg*t* and d*s*/dlg*t* are both equal to 0 when transition occurs.

It is highlighted that the proposed derivative analysis in this subsection can also be applied to analyze the drawdown data recorded in pumped wells in dual-porosity aquifers if the distance from the observation well to the pumped well (r) is replaced with an effective radius of the pumped well (r_w) in Eqs. (5.22)-(5.34).

5.2 Differentiation and Algorithm

Noisy components during numerical differentiation of drawdown data could be generated due to incorrect field data or numerical differentiation itself. To remove such noisy effect, the Lagrange Interpolation Regression (LIR) based on the Lagrange polynomial (Meijering, 2002) is introduced for numerical differentiation of drawdown data in the thesis. The Lagrange polynomial was developed and published by Lagrange (Meijering, 2002). For the LIR, the corresponding slope of a point of interest is calculated based on data of adjacent three points in row. The weighted function of the LIR is expressed as Eq. (5.35).

$$\frac{\mathrm{d}y_i}{\mathrm{d}x_i} = y_{i-1}\frac{x_i-x_{i+1}}{(x_{i-1}-x_i)(x_{i-1}-x_{i+1})} + y_i\frac{2x_i-x_{i-1}-x_{i+1}}{(x_i-x_{i-1})(x_i-x_{i+1})} + y_{i+1}\frac{x_i-x_{i-1}}{(x_{i+1}-x_{i-1})(x_{i+1}-x_i)} \tag{5.35}$$

where *i* = the point of interest, *i*-1 = the point immediately before *i*, *i*+1 = the point immediately after *i*, *y* = the drawdown or the logarithm of drawdown, *x* = the logarithm of time function.

Advantages and disadvantages of use of different differentiation algorithms, including the LIR, the Least Square Regression (LSR) and other standard methods, for numeric derivative

calculations are discussed and demonstrated via two following case studies. Involved mathematics of the LIR and the LSR are programed in an Excel workbook (Appendix D) for simultaneous matching of any type-curve solution to both drawdown and its derivative data, whilst the other standard methods (the nearest neighbours, the Bourdet, the Spane and the Smoothing methods) are implemented in the software entitled *AQTESOLV* (Duffield, 2007).

5.3 Case Studies

Two case studies are described in detail to demonstrate practical applications of purposed derivative analysis in the following. In the two case studies, the LIR is employed to calculate the values of dlg*s*/dlg*t*, while the values of d*s*/dlg*t* are evaluated by the uses of the standard methods from the *AQTESOLV*, the LIR and the LSR.

5.3.1 Variable Discharge test - Hypothetical Case

Drawdown data in the case study are taken from a hypothetical variable discharge test conducted in a fully penetrating confined aquifer (Kruseman and Ridder, 1991). Pertinent test information includes discharge rates of three pumping periods (500 m^3/d, 700 m^3/d and 600 m^3/d), distance from pumping well (5 m), reported analysis results of hydraulic properties (T= 102 m^2/d, S= 9.6X10^{-4}).

The values of $ds_i/dlgt_e$ calculated by different differentiation algorithms are plotted against normal time (Figure 5-4a). It is assumed that the "noise" values during the process of the numeric derivative calculations are transiently produced in the first and the last points of each pumping period due to the changes of pumping rates. These "noise" values are results of the limitations of these differentiation algorithms themselves. According to Eq. (5.6), a basic assumption is that the analytical value of $ds_i/dlgt_e$ is calculated based on an unchanged pumping rate (Q). In reality, this rule cannot be achieved during the numerical differentiation of drawdown data in the first and the end points of each pumping period. As the weighted function (Eq. (5.35)) of the LIR, the numeric value of $ds_i/dlgt_e$ of the first point of each pumping period at the discharge rate Q_n is determined based on the data of the last point of the preceding pumping period at the discharge rate Q_{n-1} and the data of second point of the pumping period at the discharge rate Q_n; the value of $ds_i/dlgt_e$ of the last point of the pumping

period with discharge rate Q_n is evaluated based on the second last point of the same pumping period and the first point of the next pumping period with the discharge rate Q_{n+1}. Due to the fact that the numeric derivative calculation of the first and end points requires the data from adjacent pumping periods, the LIR is bound to introduce errors or "noises" the numerical differentiation of drawdown data. The same situations can be observed using the other differentiation algorithms. In those cases, the "noise" derivative values in the first and the end points of each pumping period are set up as null.

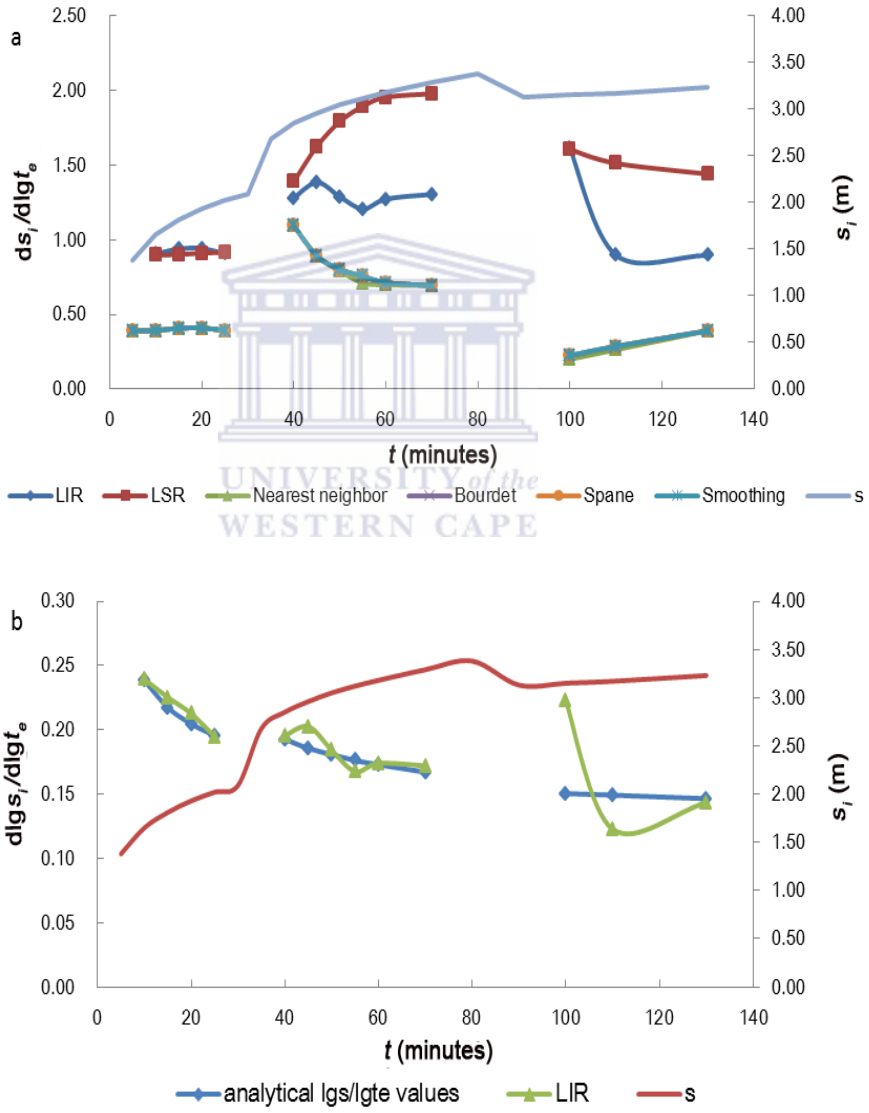

Figure 5-4 Derivative plots for the hypothetical pumping test: (a) plots of $ds_i/dlgt_e$; (b) plots of $dlgs_i/dlgt_e$.

Table 5-2 $ds_i/d\lg t_e$ and T values during the radial flows by different differentiation algorithms and the analytical method

Method	Differentiation Algorithm	period	Mean values of $ds_i/d\lg t_e$	$T(m^2/d)$
Analytical method	Eq. (5.6)*	period 1	0.90	102.00
		period 2	1.25	102.00
		Mean	***1.24***	***102.00***
This study	LIR	period 1	0.92	99.29
		period 2	1.29	99.63
		Mean	***1.12***	***99.46***
Standard Derivative	LSR	period 1	0.90	100.84
		period 2	1.77	77.69
		Mean	***1.33***	***86.60***
Standard Derivative Methods from *AQTESOLV*	Nearest neighbor	period 1	0.40	228.54
		period 2	0.81	157.68
		Mean	***0.60***	***193.11***
	Bourdet	period 1	0.40	228.54
		period 2	0.77	166.24
		Mean	***0.59***	***197.39***
	Spane	period 1	0.40	228.54
		period 2	0.82	155.39
		Mean	***0.61***	***191.96***
	Smoothing	period 1	0.40	228.13
		period 2	0.82	155.29
		Mean	***0.61***	***191.39***

* The data using for the calculations of the analytical values of $ds_i/d\lg t_e$ by Eq. (5.6) are Q_1 (500 m^3/d) and T (102 m^2/d) for period 1; Q_2 (700 m^3/d) and T (102 m^2/d) for period 2.

In Figure 5-4a, the plots of $ds_i/d\lg t_e$ are depicted as fairly straight lines over different pumping periods, indicating that the radial flows prevail. However, the plot of $ds_i/d\lg t_e$ from the LIR shows an obvious curve over the third pumping period, suggesting that the "noise" is generated during derivative process in the third pumping period by use of the LIR. Analytical values of $ds_i/d\lg t_e$ by Eq. (5.6) are also calculated for the first and the second pumping periods as given in Table 5-2. The results show that the values of $ds_i/d\lg t_e$ using the LIR (0.92) and the LSR (0.90) are identical to the analytical one (0.90) in the first pumping period; however, the value of $ds_i/d\lg t_e$ (1.77) using the LSR is greater than the analytical one (1.25) in the second pumping period. This certifies that both the LIR and the LSR are recommended to calculate the numeric values of $ds_i/d\lg t_e$ for the points of interest in first pumping period without

wellbore storage effect or "noise" data in the beginning of pumping tests. In the later pumping periods, the LIR is better fitted for the calculations of the numeric values of $ds_i/d\lg t_e$, whilst the use of the LSR are negatively influenced by the changes of pumping rates (Q). For the other options provided by *AQTESOLV*, their values of $ds_i/d\lg t_e$ during the radial flows are significantly smaller than the analytical results.

In this case study, T values in Eq. (5.8) are evaluated for both the first and the second pumping periods. As shown in Table 5-2, the evaluated T value by the LIR (99.46 m^2/d) is almost identical to that (102 m^2/d) by the Birsoy-Summers method. However, the evaluated T values by the other differentiation algorithms, including the LSR, the nearest neighbor, the Bourbet, the Spane and the smoothing methods, are obtained as 86.60 m^2/d, 193.11 m^2/d, 197.39 m^2/d, 191.96 m^2/d and 191.39 m^2/d, respectively, which are significantly different from the analytical one. The discrepancies are attributed to the noisy values of $ds_i/d\lg t_e$ by using the LSR and the differentiation algorithms from *AQTESOLV* (Table 5-2). Therefore, the use of the LIR is preferred for the $ds_i/d\lg t_e$ calculations in a variable discharge test.

Table 5-3 $d\lg s_i/d\lg t_e$ and S values during the radial flows from the LIR and the analytical method

period	t (minutes)	$d\lg s_i/\lg t_e$ values		S values	
		Analytical method*	LIR	Analytical method	LIR
period 1	10.00	0.238	0.239	9.3×10^{-4}	9.47×10^{-4}
	15.00	0.217	0.225	9.3×10^{-4}	10.9×10^{-4}
	20.00	0.205	0.213	9.3×10^{-4}	11.2×10^{-4}
	25.00	0.196	0.195	9.3×10^{-4}	9.11×10^{-4}
period 2	27.00	0.193	0.195	9.3×10^{-4}	9.99×10^{-4}
	33.00	0.186	0.206	9.3×10^{-4}	14.7×10^{-4}
	38.00	0.181	0.184	9.3×10^{-4}	10.3×10^{-4}
	44.00	0.177	0.168	9.3×10^{-4}	7.00×10^{-4}
	49.00	0.173	0.174	9.3×10^{-4}	9.66×10^{-4}
	60.00	0.167	0.172	9.3×10^{-4}	11.1×10^{-4}
		Mean		***9.3×10^{-4}***	***10.4×10^{-4}***

* The data using for the calculations analytical values of $d\lg s_i/d\lg t_e$ by Eq. (5.7) are T (102 m^2/d), S (9.6×10^{-4}) and r (5 m)

Numeric and analytical values of $d\lg s_i/d\lg t_e$ by use of the LIR and Eq. (5.7), respectively, are presented in Figure 5-4b and Table 5-3. The derivative plots of $d\lg s_i/d\lg t_e$ without straight lines as given in Eq. (5.3) imply that there is no effect of wellbore storage at the onset of the

pumping test. The shape of the plot of $dlgs_i/dlgt_e$ using the LIR has a good match with that of the analytical one during the first and the second pumping periods, indicating manifestation of the radial flows. The "noise" values cropped out in the third pumping period may be induced by the errors in the field work, which cannot be used for the determination of the *S* value. Two series of the evaluated *S* results by Eq. (5.9) based on the numerical and the analytical derivative patterns ($dlgs_i/dlgt_e$ and $ds_i/dlgt_e$), respectively, are listed in Table 5-3 for the points during the radial flows in the first and the second pumping periods. A mean value of the *S* series by using the LIR is estimated as $10.4X10^{-4}$, which is almost identical to the analytical one ($9.3X10^{-4}$).

Consequently, the LIR is the more appropriate method for use in model identifications and parameter determinations for a variable discharge test. It is also interesting to notice that the use of the LSR is limited to numeric derivative calculations of the first pumping period without wellbore storage effect or "noise" data before the radial flow.

5.3.2 Constant Rate Test in the Cape Flats Aquifer System in South Africa

The Cape Flats, covering a surface area of about 630 km^2, is located in the City of Cape Town Water Management Area (WMA) in South Africa. Relevant geological (Figure 5.5a-b) and hydrogeological background of the Cape Flats has been comprehensively documented by Adelana and Xu (2008). The aims of this case study are to evaluate hydraulic properties of the Cape Flats aquifer system in the test site at the University of the Western Cape and demonstrate a practical application of the proposed derivative analysis method (Xiao and Xu, 2014) for a constant rate test.

5.3.2.1 Regional Geological and Hydrogeological Setting

The Cape Flats aquifer system comprises two main terrains of low-lying sandy plains and rocky mountains. Figure 5.5a shows the stratigraphy of the Cape Flats. It indicates that the Sandveld Group of sand and Malmesbury Group of rock dominate the Cape Flats aquifer system (Johnson et al., 2006). The test site at the University of the Western Cape is located in G22C Quaternary catchment (Figure 5.5b), where the Witzand Formation of the Sandveld Group and the Tygerberg Formation of the Malmesbury Group prevail (Figures 5.5c-d). The

Witzand Formation is composed of the Quaternary deposit originated from the adjacent beaches for thousands years. The thickness of the Witzand Formation changes horizontally from 20 to 40 m. The Tygerberg Formation underlying the Witzand formation is characterized by rhythmic alternations of greywacke, phyllitic and siltstone, immature quartzite and a few thin impure limestone and conglomerate beds. Additionally, heterogeneous layers consisting of clay and peat develop in some places at the test site. These clayey layers usually occur within about 15 to 60 m underground.

a

Group	Formation	Lithology	Description
Sandveld	Witzand		Aeolian, calcareous, quartzose sand
	Springfontyn		Aeolian, quartzose sand with intermittent peaty clays
	Langebaan		Aeolian, calcrete-capped, calcareous sandstone
	Velddrif		Littoral, calcrete-capped coquina
	Varswater		Quartzose and muddy sand, and shelly gravel, phosphate -rich
	Elandsfontyn		Angular quartzose gravely sand
Malmesbury	Populierbos		Phyllitic shale
	Magrug		Conglomerate and quartzite
	Brandwacht		Conglomerate, Volcanic rocks and Greywacke
	Porterville		Phyllitic shale
	Norree		Greywacke, quartzite, dolomite
	Piketberg		Conglomerate and quartzite
	Franschhoek		Conglomerate and quatzite
	Bridgetown		Greenstone, dolomite, chert and graphitic schists
	Moorreesburg		Greywacke and phyllitic
	Killpplaat		Quartz, sericite and chlorite
	Berg river		Chlorite schist, greywacke with impure limestone lenses and quartz schist
	Tygerberg		Greywacke, phyllitic and siltstone, immature quartzite

Quartz sand
Pebbles and cobbles
Greywacke
Cross-bedding
Phyllitic shale
Sandstone/quartzite
Calcrete
Conglomerate
Limestone/dolomite
Calcareous sand
Volcanic rocks
Clayey sand/silt

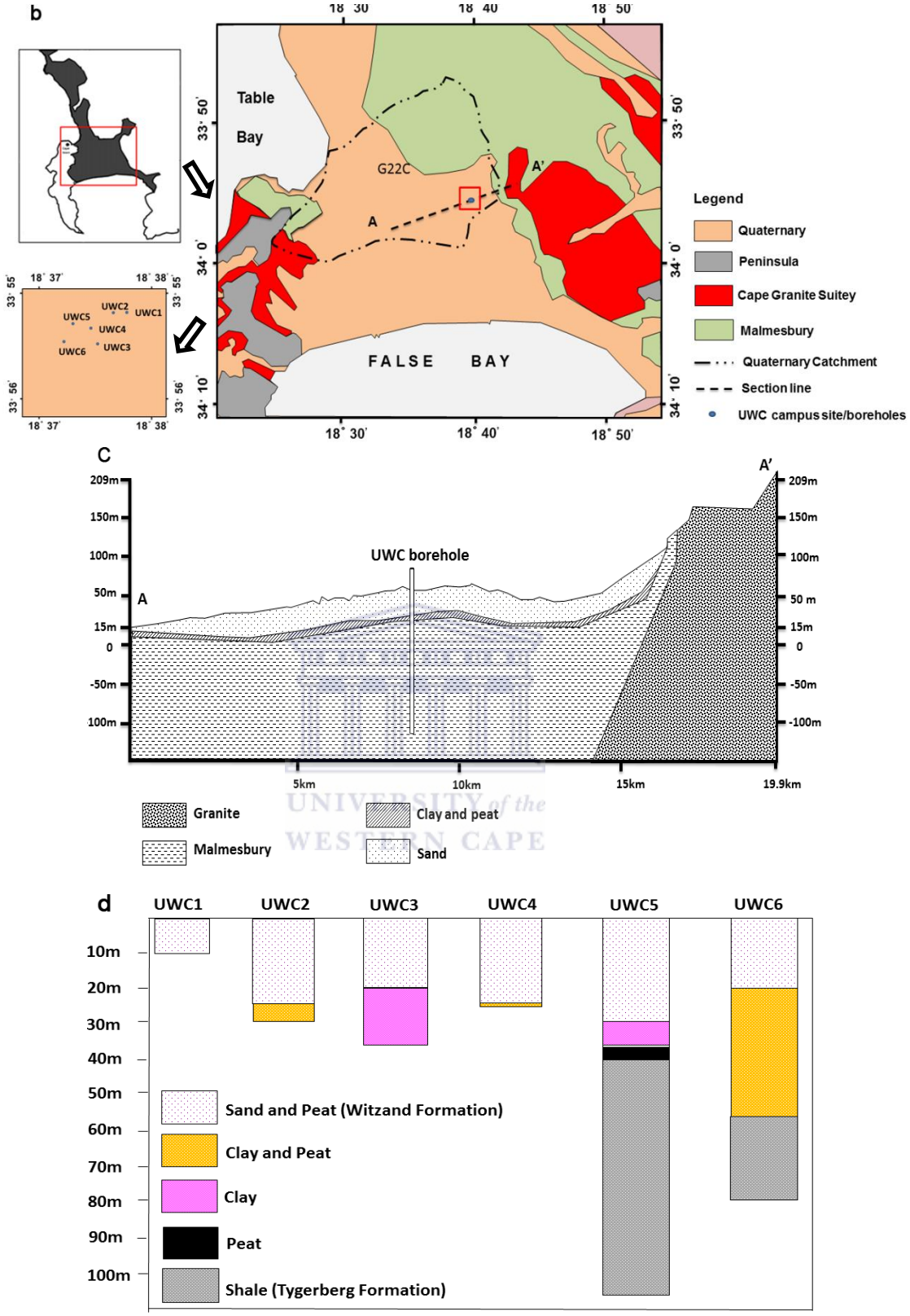

Figure 5-5 (a) stratigraphy of the Cape Flats (after Johnson et al., 2006); (b) map of the test site in University of the Western Cape, showing the location and geological information of the test site; (c) schematic cross-section of the line A-A' in Figure 5-5(b); (d) geological logs of the six boreholes drilled at the campus test site (vertical distance is in meters horizontal distance is not to scale) (Adelana et al., 2010).

The aquifer in the test site is vertically divided into two parts: (1) sandy aquifer on top and (2) hard rock aquifer on bottom. The sandy aquifer consisting of the Quaternary deposit is unconfined, in which the groundwater levels are generally less than 2m underground. The hydraulic properties of the unconfined aquifer given by Adelana et al. (2010) were T= 618.8 m^2/d, S= 1.0X10^{-2}. It is worth noting that the presence of the clayey layers should result in large variations of hydraulic properties of the unconfined aquifer. The bottom hard rock aquifer is confined or semi-confined, in which the borehole yield is low.

5.3.2.2 Hydraulic Properties of the Confined Aquifer

The confined aquifer at the test site is assumed to extend infinitely and anisotropically. As shown in Figure 5.5d, there were a total of six boreholes drilled to different depth. The four boreholes, namely UWC 1-4, were drilled into the unconfined aquifer, whilst the other two boreholes (UWC 5 and 6) were drilled into the confined aquifer. To obtain the hydraulic properties of the confined aquifer of interest, a test was done with a constant rate pumped from a borehole (UWC 5) and the drawdown measured in an observation borehole (UWC 6). For comparison purpose, the Theis' method and proposed derivative method are applied to calculate the hydraulic properties of the confined aquifer. The detail information of the constant rate test is listed in Table 5-4. Pertinent test information includes discharge rate is 718.85 m^3/d, distance between the UWC 5 and the UWC 6 is 18.75 m. The hydraulic properties of the confined aquifer by use of the Theis' method are T= 87.76 m^2/d and S= 2.01X10^{-3}, which are different from those in Adelana et al. (2010).

Figure 5-6a is the derivative plots of ds/dlg$t$ values versus normal time. The fairly straight lines are observed from 15 minutes to the pumping end, indicating occurrence of a radial flow. Fifteen points in beginning of the pumping test are identified as "noise" data. The mean values of ds/dlg$t$ in the radial flow by using different differentiation algorithms and an analytical value of ds/dlg$t$ by using Eq. (5.6) are listed in Table 5-5. It is suggesting that the mean value of ds/dlg$t$ (1.56) by using the LIR is almost identical to the analytical one (1.49) whilst the other values of ds/dlg$t$ from the standard derivative methods are much smaller than the analytical one.

Table 5-4 Information and drawdown data of the constant test

Pumping test information		**Aquifer parameters by the Theis' method**	
Pumping well type	**Fully penetrating**	**Transmissivity (m^2/d)**	**87.76 m^2/d**
Distance between the observation and the pumping wells	**17.88 m**	**Storativity**	**2.01 X 10^{-3}**
t (minutes)	***Q (m^3/d)***		***s(m)***
1	718.85		0.18
2	718.85		0.28
3	718.85		0.37
4	718.85		0.43
5	718.85		0.51
6	718.85		0.57
7	718.85		0.62
8	718.85		0.67
9	718.85		0.72
10	718.85		0.75
11	718.85		0.80
12	718.85		0.84
13	718.85		0.87
14	718.85		0.9
15	718.85		0.93
16	718.85		0.97
17	718.85		1.00
18	718.85		1.02
19	718.85		1.05
20	718.85		1.08
25	718.85		1.23
30	718.85		1.3
40	718.85		1.51
50	718.85		1.67
60	718.85		1.89
75	718.85		1.97
90	718.85		2.19
120	718.85		2.38
150	718.85		2.60

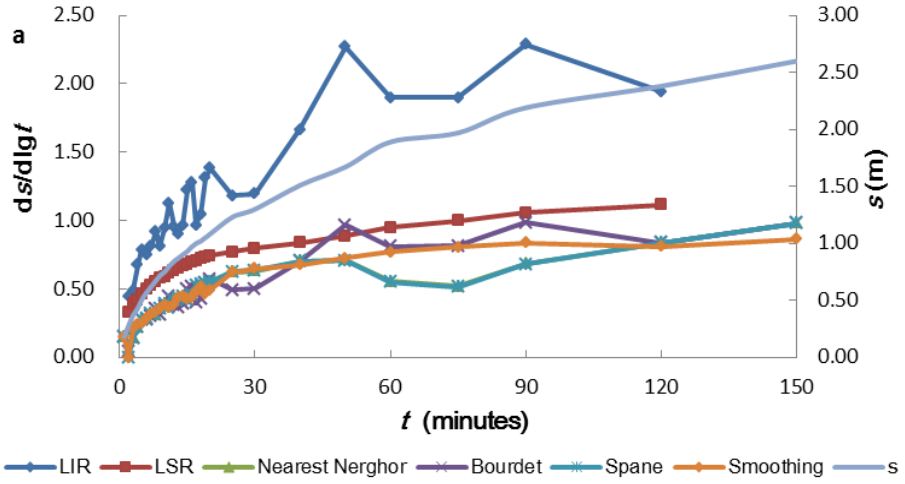

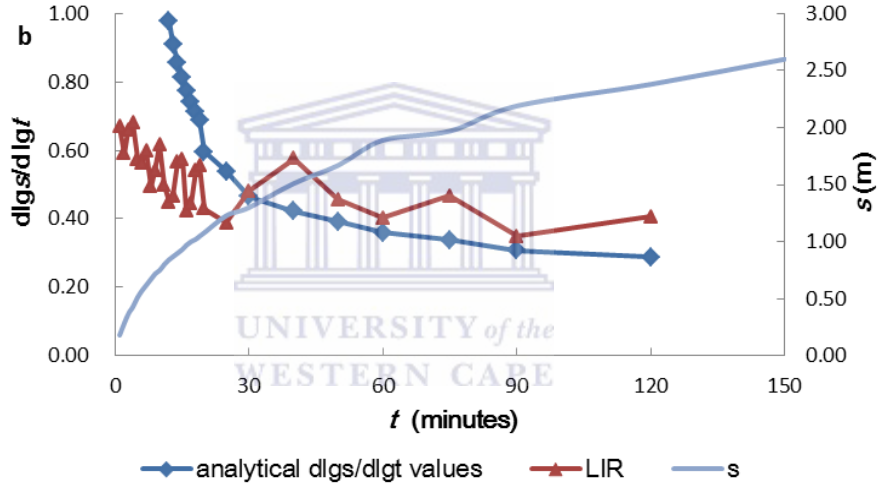

Figure 5-6 Derivative plots for the constant rate test: (a) plots of d*s*/dlg*t*; (b) plots of dlg*s*/dlg*t*.

Using Eq. (5.8), *T* values of the pumped aquifer can be calculated. As shown in Table 5-5, the evaluated *T* value (84.15 m^2/d) from the LIR is basically identical to that (87.76 m^2/d) from the Theis' method. However, the small values of d*s*/dlg*t* from the other differentiation algorithms lead to the overestimations of the *T* values. This indicates that the LIR can be used to effectively prevent noise data from being cumulated in the numeric derivative calculations of the value of d*s*/dlg*t* and the use of the other differentiation algorithms would produce noisy data during the numeric derivatives calculation in this case study.

Table 5-5 d*s*/dlg*t* and *T* values for the radial flow by different differentiation algorithms and the analytical method

Method	Differentiation Algorithm	Mean values of ds/dlg*t*	*T*(m^2/d)
Analytical method	Eq. (5.6)*	1.49	87.76
This study	LIR	1.56	84.15
Standard Derivative	LSR	0.86	153.67
Standard Derivative Methods from *AQTESOLV*	Nearest neighbor	0.63	202.52
	Bourdet	0.68	193.58
	Spane	0.62	212.31
	Smoothing	0.65	202.51

* The data using for the calculation of the analytical value of ds/dlg*t* by Eq. (5.6) are *Q* (718.85 m^3/d) and *T* (87.76 m^2/d).

Numeric and analytical values of dlg*s*/dlg*t* by the LIR and Eq. (5.7), respectively, are given in Figure 5-6b and Table 5-6. It is shown that the numeric values of dlg*s*/dlg*t* using the LIR from 15 minutes to the pumping end are almost the same as the analytical ones, indicating dominance of a radial flow. Two series of *S* results by use of Eq. (5.9) based on the analytical and numeric derivative patterns, respectively, are given for the points of interest during the radial flow (Table 5-6). A mean value of the *S* series by using the LIR is $1.94X10^{-3}$, which is similar to that ($2.01X10^{-3}$) by means of the Theis' method.

Table 5-6 dlg*s*/dlg*t* and *S* values during the radial flow from the LIR and the analytical method

t (minutes)	dlg*s*/dlg*t* values		*S* values	
	LIR	Analytical method*	LIR	Analytical method
15	0.567	0.858	$1.06 X 10^{-3}$	$2.01 X 10^{-3}$
16	0.575	0.813	$1.16 X 10^{-3}$	$2.01 X 10^{-3}$
17	0.422	0.775	$0.66 X 10^{-3}$	$2.01 X 10^{-3}$
18	0.444	0.742	$0.78 X 10^{-3}$	$2.01 X 10^{-3}$
19	0.543	0.713	$1.24 X 10^{-3}$	$2.01 X 10^{-3}$
20	0.555	0.688	$1.36 X 10^{-3}$	$2.01 X 10^{-3}$
25	0.429	0.596	$1.00 X 10^{-3}$	$2.01 X 10^{-3}$
30	0.388	0.538	$0.94 X 10^{-3}$	$2.01 X 10^{-3}$
40	0.482	0.466	$2.07 X 10^{-3}$	$2.01 X 10^{-3}$
50	0.577	0.422	$3.63 X 10^{-3}$	$2.01 X 10^{-3}$
60	0.457	0.392	$2.77 X 10^{-3}$	$2.01 X 10^{-3}$
75	0.403	0.360	$2.59 X 10^{-3}$	$2.01 X 10^{-3}$
90	0.468	0.338	$4.34 X 10^{-3}$	$2.01 X 10^{-3}$
120	0.349	0.308	$2.83 X 10^{-3}$	$2.01 X 10^{-3}$
	mean		***$1.94 X 10^{-3}$***	***$2.01 X 10^{-3}$***

* The data using for the calculation of analytical values of dlg*s*/dlg*t* by Eq. (5.7) are *T* (87.75 m^2/d), *S* ($2.01X10^{-3}$) and *r* (17.85m).

In the case study, the hydraulic properties of the confined aquifer in the test site at the University of the Western Cape are evaluated by using the proposed derivative method. The results suggest that the hydraulic properties by the proposed derivative method (T= 84.16 m^2/d and S= 1.89X10^{-3}) are fairly identical to the analytical ones (T= 87.76 m^2/d and S= 2.01X10^{-3}) by the Theis' method. Additionally, the case study also demonstrates the advantages and disadvantages of various differentiation algorithms for use in numeric derivative calculation. It is indicated that the use of the LIR is better fitted to the numeric derivative calculation of the values of ds/dlgt and dlgs/dlgt in the constant rate tests. However, the LSR can be used for the derivative analyses of the constant test without effect of wellbore storage or "noise" data before radial flow. The use of other differentiation algorithms from *AQTESOLV* cannot effectively prevent noisy data from producing during the numeric derivative calculation in this case study.

5.4 Discussion

Compared to traditional derivative analysis by using plot of ds/dlg*t* alone and existing differentiation algorithms, advantages of the proposed derivative analysis method based on combined plot of dlg*s*/dlg*t* and d*s*/dlg*t* and the LIR are now discussed.

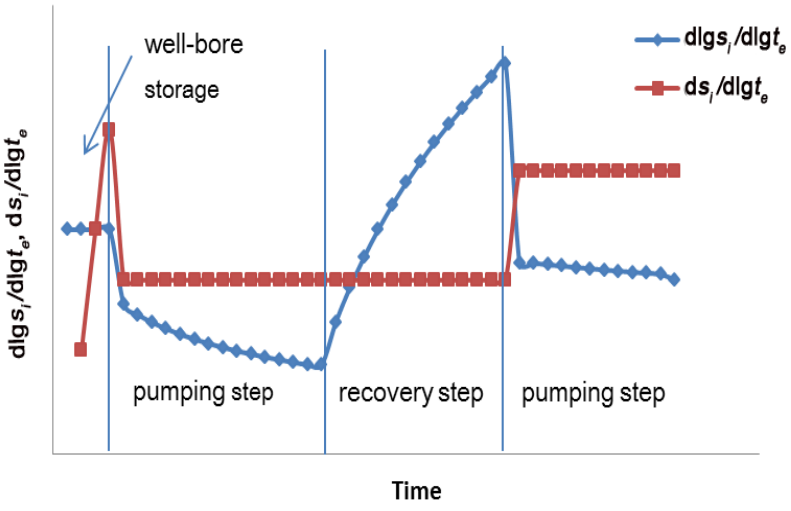

Figure 5-7 Conceptual derivative curves of dlgs_i/dlgt_e and ds_i/dlgt_e in normal time scale for intermittent variable discharge tests.

One of two important applications of the drawdown derivative analysis is model

identifications. For comparison purpose, a conceptual derivative plot of dlgs_i/dlgt_e for intermittent variable discharge tests is presented against that of traditional derivative method (ds_i/dlgt_e) in Figure 5-7. During the wellbore storage period in the early time as the pumping starts, the plot of dlgs_i/dlgt_e is done as a horizontal straight line with the value equal to 1, while the plot of ds_i/dlgt_e is made as a straight line with a fixed slope $2.3Q_1/(\pi r_c^2)$ (Renard et al., 2009). When the radial flow prevails, the plot of dlgs_i/dlgt_e can be used to reveal the differences between pumping and its following recovery periods, which are otherwise not achieved by using the plot of ds_i/dlgt_e alone. In the plot of ds_i/dlgt_e, all the values of ds_i/dlgt_e from pumping and its following recovery periods lie along a straight line with the value equal to $2.3Q_i/(4\pi T)$, as seen in Eqs. (5.6) and (5.10). In the plot of dlgs_i/dlgt_e, the derivative pattern of dlgs_i/dlgt_e for pumping and its following recovery periods are expressed as $1/\ln[2.25Tt_e/(r^2S)]$ and $1/\ln t_e$, respectively. This makes it easy for hydrologists to identify pumping and its following recovery periods in the plot of dlgs_i/dlgt_e.

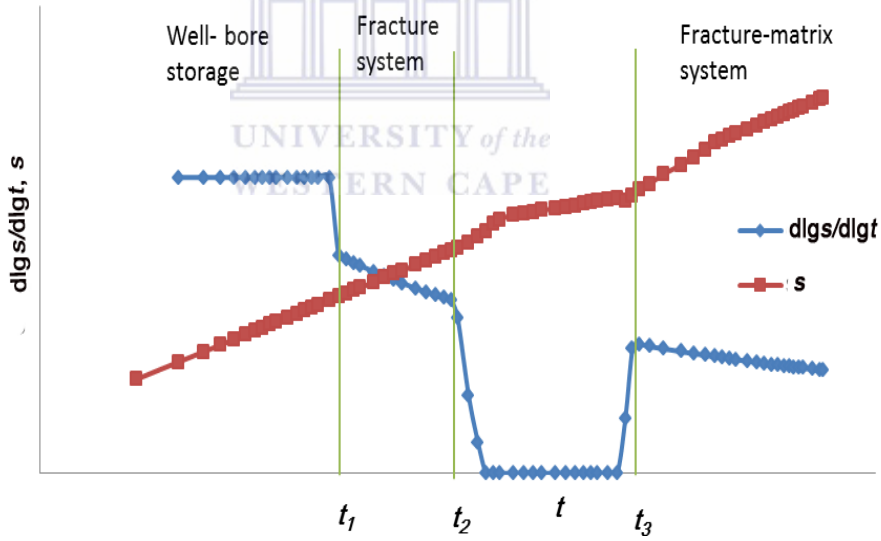

Figure 5-8 Conceptual plots of drawdown and dlgs/dlg*t* for double-porosity behaviors with wellbore storage effects using a semi-lg scale.

In double-porosity aquifers, fracture flow systems are often masked by effects of wellbore storage in semi-lg drawdown plots. Figure 5-8 shows conceptual plots of drawdown and dlg*s*/dlg*t* for double-porosity behaviors with wellbore storage effects. In this case, the wellbore storage region ($t<t_1$) is often misidentified as the radial flow in the time-drawdown plot, which could result in wrong parameter estimates of pumped aquifers by Kazi at al.'s

straight-line method. The sensitivity of the plot of dlg*s*/dlg*t* makes it feasible to remove the negative effect of wellbore storage on the fracture system identification. In the plot of dlg*s*/dlg*t*, the wellbore storage effect is depicted as a straight line as Eq. (5.3). The characteristic pattern ($t_1<t<t_2$) for fracture flow system is described as Eq. (5.25) at the early pumping time and another characteristic pattern ($t_3<t$) is gained as Eq. (5.31) for fracture-matrix system at the late pumping time.

Other important application of the drawdown derivative analysis is parameter determinations. The traditional derivative analysis by using plot of d*s*/dlg*t* alone can only be applied to estimate the transmissivity (*T*) but not the storativity (*S*) of pumped aquifers. In this chapter, a comprehensive quantitative analysis is proposed for the parameter determinations of pumped aquifers concerned. Based on accurate identifications of radial flows during pumping phases in variable discharge tests, the transmissivity (*T*) and the storativity (*S*) of pumped aquifers can be assessed by Eqs. (5.8) and (5.9), respectively. In double-porosity aquifers, derivative values of dlg*s*/dlg*t* and d*s*/dlg*t* of fracture flow and matrix-fracture flow systems can be used to calculate effective transmissivity of the fracture (T_f) (Eq. (5.26)), storativity of the fracture (S_f) (Eq. (5.27)), storativity of the matrix (S_m) (Eq. (5.33)) and storativity ratio (ω) (Eq. (5.34)) for a double-porosity behaviour.

An appropriate differentiation approach should be adopted to prevent "noise" effects from being cumulative during numerical differentiation of drawdown data. Two differentiation algorithms, the LIR and the LSR, are discussed in two case studies. The results give rise to a recommendation that the LIR is preferred for derivative analysis of aquifer tests (constant rate tests, variable discharge tests and double-porosity tests) without "noise" field data during radial flows.

With regard to the LSR, it can be used for numerical differentiation of drawdown data under strict conditions. According to weighted function of the LSR ($\mathrm{dy}_i/\mathrm{dx}_i = [n\sum_{j=1}^{i}(y_j x_j) - (\sum_{j=1}^{i} y_j \sum_{j=1}^{i} x_j)]/[n\sum_{j=1}^{i} x_j^2 - (\sum_{j=1}^{i} x_j)^2$), the corresponding slope of a point of interest is affected by data of all points before the point of interest. It is assumed that changes of flow segments (e.g. changes of flow segments from wellbore storages to radial flows, changes of pumping rates in variable discharge tests and changes of

flow segments from radial flow in fracture system to transition period) or "noise" field data before each flow segment should have negative effects on accuracy of derivative calculations using the LSR. However, the negative effects would benefit from self-cancellation by the LSR at the late time of long radial flow segments. Hence, use of the LSR is only accepted for derivative analysis of constant rate tests with "noise" data in long radial flow segments.

Other differentiation algorithms, including the nearest neighbours, the Bourdet, the Spane and the Smoothing methods, implemented in the software *AQTESOLV* cannot be applied to effectively remove "noise" effects during numerical differentiation of drawdown data as these methods tended to give smaller derivative values in these case studies.

5.5 Summary

This chapter discusses the possibility of use of dlg*s*/dlg*t* for the derivative analysis of aquifer tests and clarifies differences between the LIR and the traditional differentiation algorithms of use in numerical derivative calculations. Uses of the plots of dlg*s*/dlg*t* and the LIR are proved to improve the applications (model identifications and parameter determinations) of the derivative analysis of aquifer tests. Comprehensive assessments of different characteristic flow segments, including the wellbore storage effect, the radial flow, the boundary condition and the double-porosity behavior, can be achieved by using the combined plot of dlg*s*/dlg*t* and d*s*/dlg*t* and the LIR. Compared with standard derivative analysis, advantages of the proposed derivative method are identified. The main points are highlighted as follows,

1. Plot of dlg*s*/dlg*t* is preferred for use in distinguishing pumping and its following recovery periods in intermittent variable discharge tests;
2. Storativity (*S*) of pumped aquifers can be evaluated by using combined plot of dlgs/dlgt and ds/dlgt;
3. Combined plot of d*s*/dlg*t* and dlg*s*/dlg*t* has shown to be particularly powerful for diagnostic analysis of pumping tests involving double-porosity behaviours. Negative effects of wellbore storages on fracture system identifications are avoided by means of the plot of dlg*s*/dlg*t*. Parameters of a dual-porosity aquifer are easy to be assessed in aid of the combined derivative plot of d*s*/dlg*t* and dlg*s*/dlg*t*;
4. Use of the LIR is recommended for derivative analysis of pumping tests, including

constant rate tests, variable discharge tests, tests in bounded aquifer and tests involving double-porosity behaviors, without "noise" data during radial flows, whilst use of the LSR is preferred for derivative analysis of constant rate tests with "noise" data during long radial flow segments.

Consequently, the chapter provides hydrologists with an additional method for use in the aquifer characterization by the combined derivative plot of ds/dlg*t* and dlgs/dlg*t*. It is also pointed out that a caution must be exercised with use of numeric algorithms in *AQTESOLVE* for derivative analysis of aquifer tests.

Nomenclature

lg logarithm to the base 10;
ln logarithm to the base *e*;
Q pumping rate, [L^3/t];
Q_i pumping rate in *i* th pumping period, [L^3/t];
s drawdown, [L];
s_d drawdown from real discharging well, [L];
s_i drawdown in *i* th pumping period, [L];
s_r drawdown from image well, [L];
S storativity;
S_f storativity of the fracture;
S_m storativity of the matrix;
t time, [d];
t_e adjusted time. [d];
T transmissivity, [L^2/t];
T_f effective transmissivity of the fracture, [L^2/t];
r distance between piezometer and real discharging well, [L];
r_c stress well casing radius, [L];
r_i distance between piezometer and *i* th image well, [L];
$r_{r1\rightarrow n}$ ratio equal to r_i/r;
r_w effective radius of the pumping well, [L];
u argument of W function;
W Theis well function;
β factor of pump test analysis in double-porosity aquifer;
ω storativity ratio;

Chapter 6

Hydrochemical and Environmental Isotopic Approach to Groundwater Flow Dynamics of Dolomite Spring System in South Africa

This chapter discusses flow dynamics of the dolomitic spring system in South Africa by using a hydrogeochemistry and environmental isotopes method. The aim is to assess groundwater mean residence time (MRT) and reveal its temporal trend by a lumped-parameter model with time series of ^{14}C measurements of spring samples during 1970s and 2010s. New data on geochemistry and environmental isotopes of spring samples are added to achieve understanding of the flow dynamics in the dolomite aquifer. The recharge sources and areas of the dolomite aquifer are identified. The effect of climate change, especially rainfall variability, on the groundwater cycle is also investigated. The results would be valuable for sustainable management of the strategic dolomite aquifer in South Africa.

6.1 Hydrogeological Setting

Geology and hydrogeology settings of the dolomite aquifer have been well documented by Rosewarne (2006). The dolomite aquifer comprises three morphological groups named as Far East to Far West Rand (FE-FW), North-West (NW) and Ghaap Plateau (GP). All the three areas are characterized by development of karst features due to leaching of dolomite dissolution, compartmentalization by dykes and sills and occurrence of cold springs.

In the FE-FW region, total areas of dolomite outcrops are about 2850 km^2 (Figure 6-1a). The dolomites belong to the Malmani Subgroup of the Transvaal Sequence, which are further divided into four formations (Table 6-1) as the Eccles, the Lyttelton, the Monte Christo and the Oaktree based on chert content, presence and type of algal structure (Rosewarne, 2006). Generally, chert-rich formations (Eccles and Monte Christo) display a higher degree of karstification and thus contain more groundwater than chert-poor or chert-free dolomite (Lyttelton and Oaktree). The average depth of weathering deposits zones because of carbonate solution or karstification is up to about 150 m. The dolomitic aquifer was compartmentalized

by the dolerite dykes. Brink (1979) revealed that major tensional fractures due to the development of the dolerite dykes provided ready conduits and controlled direction of groundwater flow in the weathering deposits zones. The key aquifer parameters including transmissivity (*T*) and storage show a wide range of variation because of different natural karst conditions involved. The *T* value has an apparent increase along N-S dykes (DE Freitas and Wolmarans, 1978). The storage changes from <1% to 15% with depths.

Table 6-1 Lithostratigraphy of different dolomitic formations in the study area (after Rosewarne, 2006)

Morphological groups	Sequence	Group	Subgroup	Formation	Lithology	
FE-FW and NE	Transvaal	Pretoria		Rooihoogte	Shales	
		Chuniespoort	Malmani	Frisco	Dark and chert-poor dolomite	
				Eccles	Chert-rich dolomite	
				Lyttleton	Dark, chert-free dolomite	
				Monte Christo	Light coloured, recrystallised dolomite with abundant chert	
				Oaktree	Dolomite, becoming darker upwards;chocolate coloured weathering	
	Ventersdorp SG			Ventersdorp lava	Lava	
GP	Griqualand West	Griquatown		Asbestos Hills	Kuruman	Banded ironstone with bands of amphibolite
		Campbell		Ghaap Plateau	Lime Acres	Dolomite with lenses of limestone and chert
					Grootfonteint	Mainly chert with interbedded layers of dolomite
					Fairfield	Coarsely crystalline recrystallized dolomite
						Banded ironstone marker - Kanguru layer
					Ulco	Mainly fine grained dolomite and limestone

The sampling springs, namely Gerrit Minnebron and Turfontein eyes, occur on the downstream side of the compartmentalizing dykes at the lowest topographic points and maintain high magnitude discharges (Figure 6-1a). Figure 6-1b shows the E-W schematic cross section of the upstream of Gerrit Minnebron and Turfontein eyes in the cross line

A-A'-A'' in Figure 6-1a, indicating the relative aquifer compartments and the vertical location of each dolomitic formation. In general, Gerrit Minnebron and Turfontein eyes were fed by four aquifer compartments, namely the Zuurbekon Compartment, the Bank Compartment, the Ohlz Compartment and the Tuffontein Compartment (Winde and Erasmus, 2011). The highly chert-rich dolomite of the Eccles and the Monte Christo formation cover the most of the dolomite outcrop area. In contrast, chert-poor and therefore water free formations such as the Oak Tree and the Lyttelton cover only a comparably small proportion of the outcrop area. The groundwater storage volumes in associated compartments are different between the individual compartments. The Tuffontein Compartment has the largest groundwater storage volumes with about 7.700 X 10^9 m^3 (Winde and Erasmus, 2011).

A dewatering area overlying goldfields exists in the Zuurbekon Compartment, the Bank Compartment and the Ohlz Compartment. Before dewatering, most of the groundwater was stored in the upper 40 to 100 m of the dolomite aquifer. However, the large-scale dewatering lowered the water table by up to 1000 m in some places. Located on downstream of goldfields, Gerrit Minnebron and Turfontein eyes are assumed to be impacted by the mining-related water, especially, with acid pollution. The former investigations (Winde and Erasmus, 2011) revealed that the polluted effluents discharged in the dewatering area could permeate into the underlying dolomite aquifer.

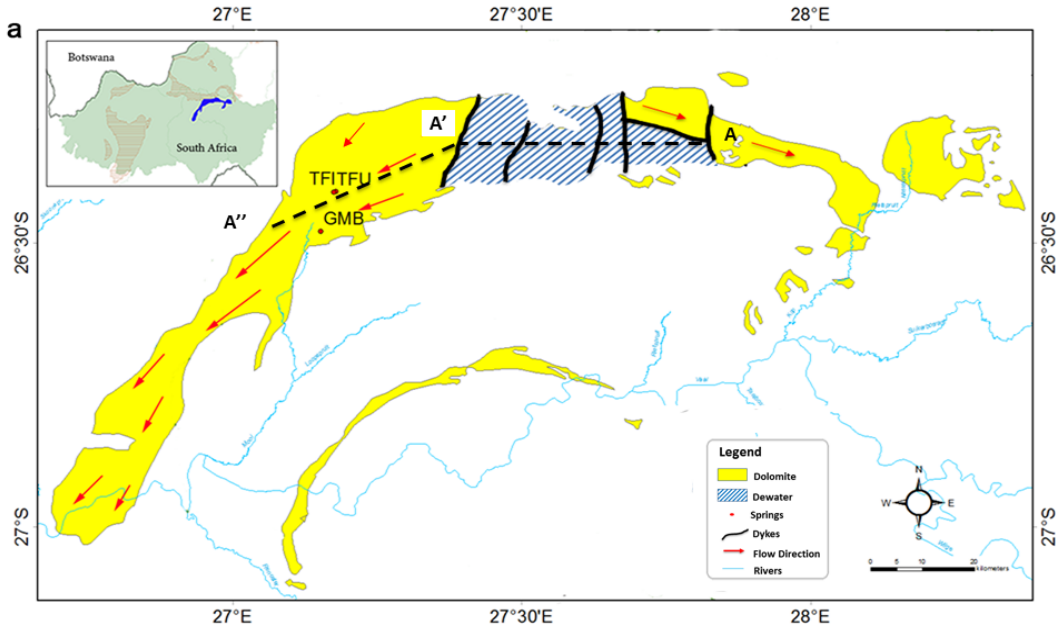

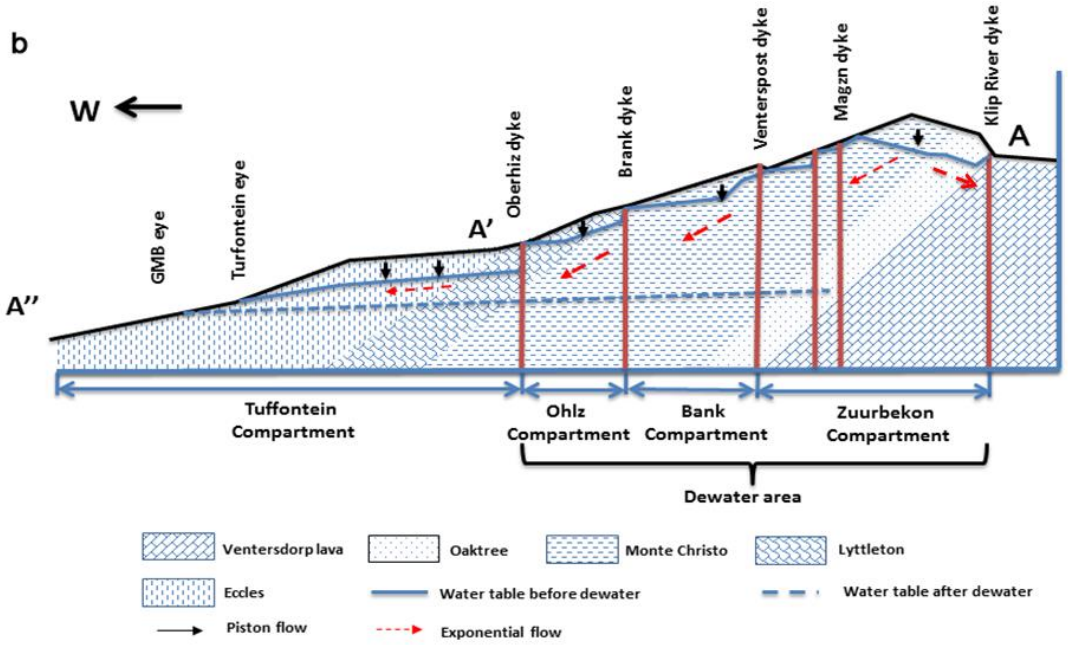

Figure 6-1 (a) map of the Far East to Far West Rand (FE-FW), showing dyke developments, spring locations and flow directions (after Rosewarne, 2006); (b) schematic E-W cross section of the dolomitic compartments upstream of the Gerrit Minnebron and Turfontein eyes in the line A-A'-A'' (after Winde and Erasmus, 2011).

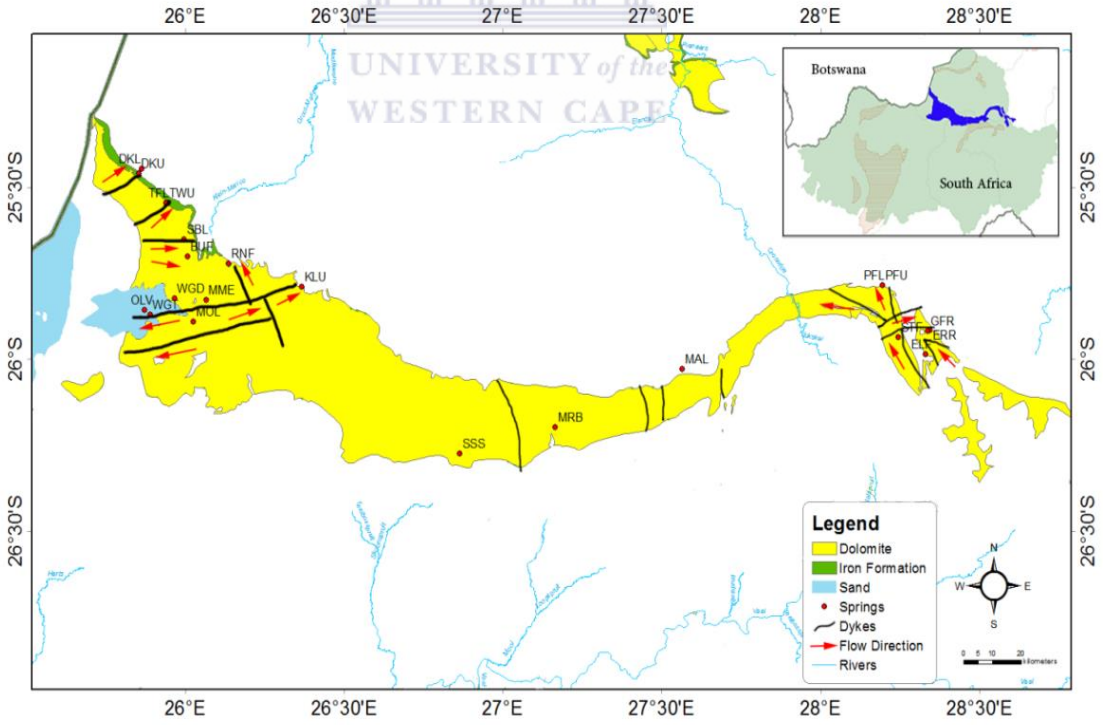

Figure 6-2 Map of the North-West (NW), showing dyke developments, spring locations and flow directions (after Rosewarne, 2006).

The dolomites in the NE cover an area of about 5500 Km^2 (Figure 6-2). The geological sequence is similar to that in the FE-FW. Additionally, the Frisco Formation (Table 6-1)

characterized by a dark and chert-poor dolomite lies at the top of the sequence (Rosewarne, 2006). Numerous intrusive dolerite dykes appear in NE. Springs occur at the topographic lows along the dykes and towards the edge of the dolomite outcrop area.

The dolomite outcrops in the GP are shown in Figure 6-3, of which covering area is about 19035 km^2. The dolomites form a part of the Campbell Group in the Griqualand West Sequence. Areas along the foothills of the Kuruman Hills are covered by recent deposits of windblown sand and scree whilst surface limestone covers large areas of the flat plains to the east, which are postulated as the main recharge site in the Kuruman area (Rosewarne, 2006). The values of transmissivity (T) is variable from almost impervious to >10,000 m^2/day (Van Rensburg, 1995). The highest transmissivity happens along the western side of the Kuruman Hills. Similar to transmissivity, storage is highly variable due to the heterogeneous nature of the dolomites. An average value of storage ranges from 1% to 5%. Controlled yield tests conducted in many boreholes indicated the storage values ranging from 0.01% to 2%.

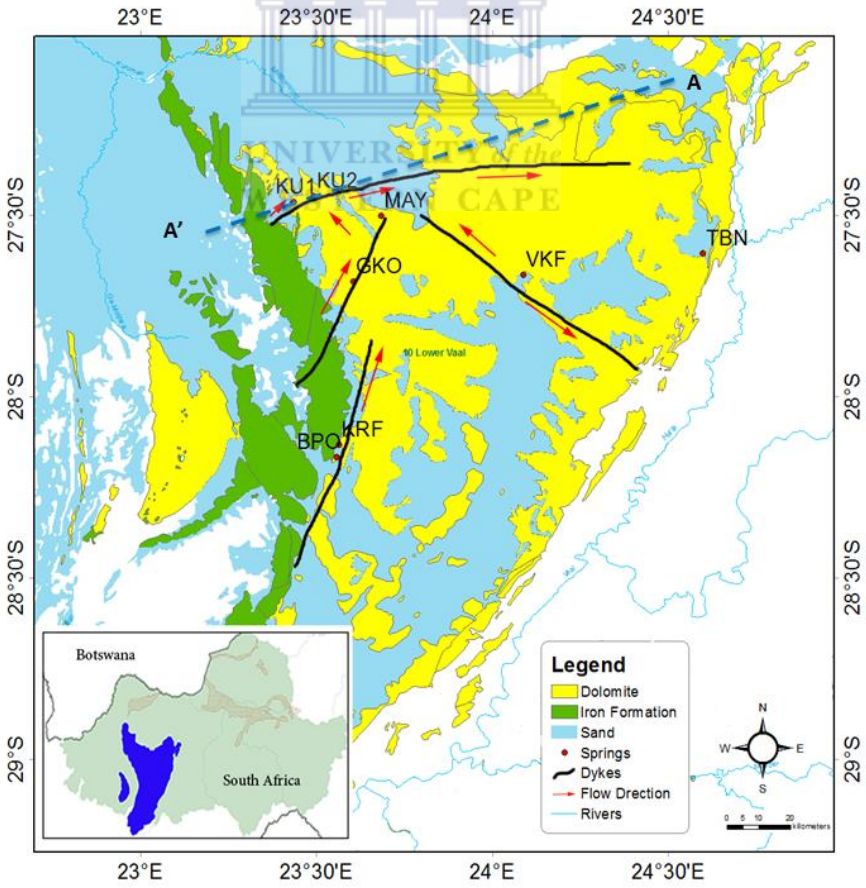

Figure 6-3 Map of the Ghaap Plateau (GP), indicating main dyke developments, spring locations and flow directions (after Rosewarne, 2006). The cross section A-A' is displayed in Figure 6-18.

6.2 Methods

Based on existing data and information, a supplement survey had been conducted. The spring samples were collected for measurements of $^{87}Sr/^{86}Sr$ ratio and CO_2 in the field works in 1992 and 1993 (Talma et al., 2001). Representative samples were collected for measurements of ^{14}C values of dissolved inorganic carbon (^{14}C-DIC), ^{13}C values of dissolved inorganic carbon ($\delta^{13}C$-DIC), oxygen-18 ($\delta^{18}O$), hydrogen (δD), tritium (^{3}H) and major chemistry components between 17 October and 29 November 2007. Methods of samplings and analyses are detailed below.

6.2.1 Samplings and Analyses

Groundwater samples were collected from outflow of 33 springs in the Far East to Far West Rand, the North-West and the Ghaap Plateau. The detail information on the springs can be found in Table 6-2 (Talma et al., 2001). Spring locations are shown in Figures 6-1, 6-2 and 6-3.

Whenever feasible, water samples were collected at the point of emergence, however, at some sites, the inflow of spring water into a large pool (and outflow from the rock) is ill-defined and samples were necessarily collected at a weir. In these cases, the springs are termed as open springs in the chapter. In the other cases (e.g. Kaaloog, Malmani Spring and Molopo Spring), it was possible to collect samples in both inflow and outflow pools for the possibility of obtaining various results.

Radiocarbon samples were collected in 25 to 60 litre plastic drums and concentrated into 300ml NaOH and analyzed in the CSIR-NRE-Quadru laboratory. The error of the radiocarbon measurements was ± 0.1-3.6 Pmc. ^{3}H samples were collected in 1 litre plastic drums and analyzed in the iThemba laboratory in Gauteng. The error of the ^{3}H measurements was ± 0.2 TU. Water samples for ^{2}H and ^{18}O data were collected in 200 ml Plastic medical flats and analyzed by mass spectrometry at the CSIR-NRE-Quadru laboratory and the iThemba laboratory in Gauteng. Field measurements of temperature, pH and dissolved oxygen were taken either in-stream or in a bucket with quick-flowing water delivered by the Whale pump. $^{87}Sr/^{86}Sr$ ratio was analyzed on a number of samples collected from all three study areas. Samples for strontium (Sr) isotope analyses were collected, filtered through 0.45μm Millipore

filters into acid rinsed plastic bottles, acidified, extracted and analyzed by solid source mass spectrometry at Ematek, CSIR in Pretoria. The error of $^{87}Sr/^{86}Sr$ ratio measurements was $\pm 1X10^{-5}$ - $5X10^{-5}$. CO_2 was extracted by NaOH and analyzed.

Table 6-2 Information on the sampled springs

Area	Spring name	Lat south	Long east	Source type	Map label
Far East to Far West Rand	Gerrit Minnebron	26.47988	27.15153	Spring	GMB
	Turffontein Spring at inflow point	26.40962	27.17749	Spring	TFI
	Turffontein Spring upper	26.41019	27.17444	Open spring	TFU
North-West	Buffelshoekoog	25.70125	26.00808	Spring	BUF
	Dinokane lower eye	25.44436	25.86208	Spring	DKL
	Dinokane upper eye	25.45742	25.85300	Spring	DKU
	Kaaloog at Palm	25.78944	26.36710	Open spring	KLU
	Malmani upper eye	25.82642	26.06550	Spring	MME
	Molopo Spring	25.88947	26.02592	Spring	MOL
	Olievendraai spring	25.85725	25.87142	Spring	OLV
	Rhenosterfontein	25.72111	26.13539	Spring	RNF
	Stinkhoutboom Spring lower	25.65064	25.99594	Spring	SBL
	Tweefontein lower	25.54414	25.94556	Open spring	TFL
	Tweefontein upper	25.54536	25.94081	Spring	TWU
	Welgedachtoog	25.82317	25.96653	Spring	WGD
	Wondergat	25.86954	25.88938	Sinkhole	WGT
Ghaap Plateau	Elandsfontein	25.98592	28.33139	Spring	ELF
	Erasmus Rietvlei	25.91569	28.34381	Spring	ERR
	Grootfontein Rietvlei	25.91708	28.33833	Spring	GFR
	Pretoria Fountains lower eye	25.78481	28.19458	Spring	PFL
	Pretoria Fountains upper eye	25.78475	28.19492	Open spring	PFU
	Sterkfontein Spring	25.93619	28.24492	Open spring	STF
	Maloneys eye	26.02683	27.56406	Spring	MAL
	Mooirivier Boonste Spring	26.1981	27.16490	Spring	MRB
	Schoonspruit southern eye	26.27522	26.86444	Spring	SSS
	Boplaas Spring	28.16630	23.55677	Spring	BPO
	Groot Kono Spring	27.68258	23.60428	Open spring	GKO
	Kramasfontein	28.13323	23.56361	Spring	KRF
	Kuruman Spring A	27.46406	23.43624	Spring	KU1
	Kuruman Spring B	27.44827	23.49162	Spring	KU2
	Manyeding Spring	27.50204	23.68413	Open spring	MAY
	Tamasikwe north	27.60482	24.60085	Spring	TBN
	Vlakfontein	27.66359	24.08791	Open spring	VKF

6.2.2 Determination of Groundwater MRTs

Generally, the spring water is assumed to store and flow in a mobile groundwater system. According to the local hydrogeological conditions of the dolomite aquifer in South Africa (Figure 6-1b), the dolomite aquifer includes two flow patterns in line. In the area between the ground surface and water table, the flow lines are approximated to have the same transit time, and the hydrodynamic dispersion and diffusion are negligible. The kind of flow part is recognized as a piston flow. It is followed by the second one with the distribution approximated by an exponential flow during the flow period from water table to the recharge site. Hence, the Exponential-piston model (EPM) is selected and adopted in the thesis. Recall the convolution integral for the EPM is

$$C_{out}(t) = \int_0^{\infty} C_{in}(t-\tau)h(\tau)\exp(-\lambda\tau)\mathrm{d}\tau \tag{6.1a}$$

The response functions are

For the piston flow pattern

$$h(\tau) = 0 \text{ for } \tau < t_t(1-f) \tag{6.1b}$$

For the exponential flow pattern

$$h(\tau) = (f t_t)^{-1} \exp\left[-\left(\frac{\tau}{f t_t}\right) + \left(\frac{1}{f}\right) - 1\right] \text{ for } \tau > t_t(1-f) \tag{6.1c}$$

where C_{in} and C_{out} are the input and the output concentrations of a radioisotope. τ is the entry time of groundwater and $t-\tau$ is the groundwater residence time. $h(\tau)$ is the response function of a hydrological system. λ is the radioactive decay constant, expressing as $\lambda = \ln 2/T_{1/2}$. $T_{1/2}$ is the half-life of a radioisotope. f is the ratio of the exponential volume to the total volume. $t_t(1-f)$ is the time required for groundwater in the piston flow.

6.3 Results

Results of field measurements and laboratory analyses are listed in Appendix E. Discussion of these results is given in following subsections.

6.3.1 Chemical Measurements

Temperatures of the spring samples are within the range of 18 to 21℃. For the open springs, their temperatures generally follow the adjacent air temperatures. A piper diagram of chemical compositions (Figure 6-4) indicates that the major ion compositions are calcium (Ca^{2+}), bicarbonate (HCO_3^{1-}) and magnesium (Mg^{2+}) ions. The concentrations of sodium (Na^{1+}) and chloride (Cl^{1-}) are used as an indicator of recharge source. Most springs reflect low Na^{1+} and Cl^{1-} measured values, suggesting a major rainfall influence on groundwater recharge. The extra concentrations of sulphate (SO_4^{2-}) and Cl^{1-} in the study areas may indicate springs contamination. Seven springs, including Pretoria Lower Fountain and Sterkfontein in the North-West, Turffontein lower, Turffontein Upper and Gerrit Minnebron in the Far East to Far West Rand and Tamasikwe north in the Ghaap Plateau, have clear signs of elevated concentrations of SO_4^{2-} and Cl^{1-}, indicating possibility of spring water being contaminated in these sites.

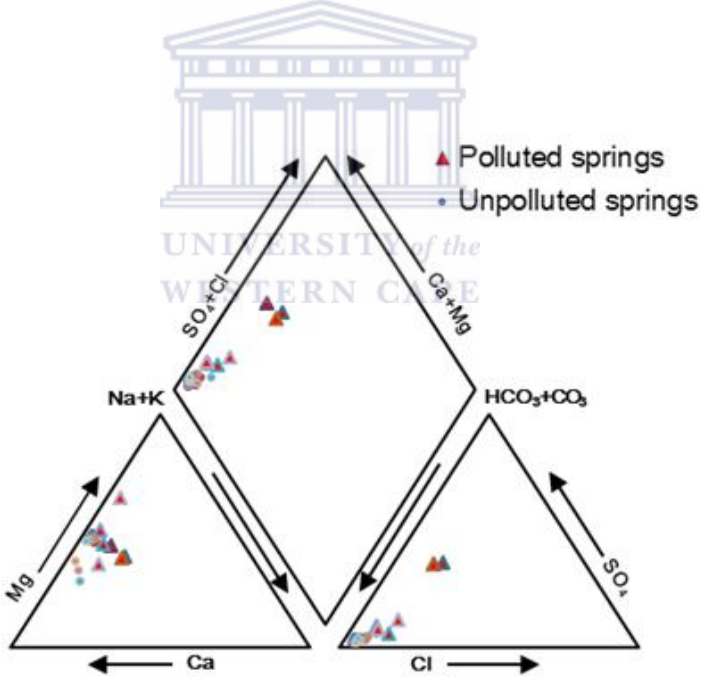

Figure 6-4 Piper diagram shows water types of spring samples. The samples at six springs have high SO_4^{2-} and Cl^{1-} data indicating contaminated component of spring water.

The ratio of Ca^{2+} to Mg^{2+} mole concentrations can be used to unveil the solubility system in a carbonate aquifer. Figure 6-5 shows a plot of Ca^{2+} versus Mg^{2+} concentrations and two expected solubility equilibrium lines of $[Ca^{2+}]/[Mg^{2+}]$ ratio at 20℃ and 15℃, respectively. Most plots of samples in the Far East to Far West Rand and the North-West are located between the two expected solubility equilibrium lines, indicating an expected Ca-Mg-HCO_3

rich water system from a dolomite aquifer. In the Ghaap Plateau, plots of Boplaas spring, Kuruman springs and Groot Kono spring show a lower slope than the expected solubility equilibrium lines, suggesting a substantial increase in Ca^{2+} values with a slight increase in Mg^{2+} values. This chemical evolution is accompanied by a mixing system of Ca-Mg-HCO_3 rich water and Ca-HCO_3 rich water from a dolomite-calcite aquifer. It is consistent with the field observation that groundwater in these areas is mainly recharged in the hilly area along western edge represented by limestone. In contrast, the plots of Vlakfontein, Kramasfontein and Manyeding Spring are scattered between the expected solubility equilibrium lines, indicating a Ca-Mg-HCO_3 rich water system. For a special case of Tamasikwe north, the extra concentration of Mg^{2+} is assumed to be in response to SO_4^{2-} and Cl^{1-} addition from contamination.

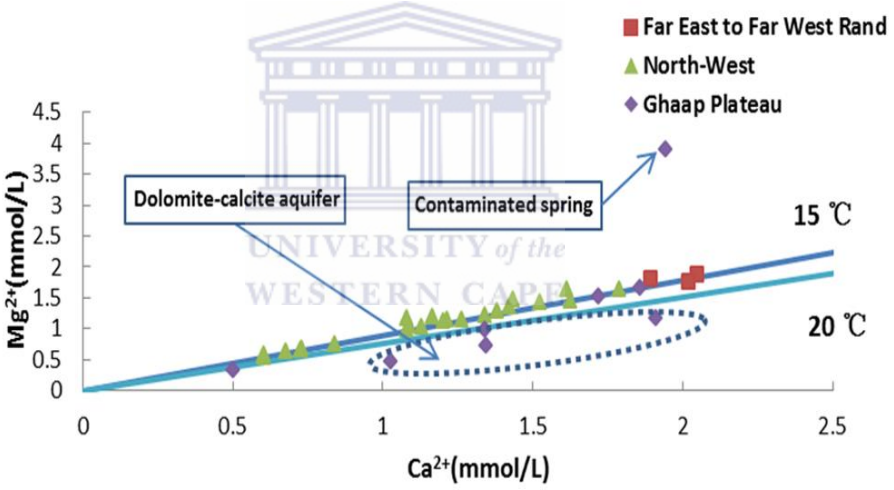

Figure 6-5 Plot of Ca^{2+} versus Mg^{2+} mole concentrations; the two straight lines are expected solubility equilibrium lines of $[Ca^{2+}]/[Mg^{2+}]$ ratio at 20℃ and 15℃, respectively.

Generally, a mole concentration of $[Ca^{2+}+Mg^{2+}]$ is equal to a HCO_3^{1-} mole concentration according to charge balance of groundwater in an expected saturated dolomite aquifer. However, extra $Ca^{2+}+Mg^{2+}$ values could be introduced into groundwater by the acid contamination. A plot of $Ca^{2+}+ Mg^{2+}$ versus HCO_3^{1-} concentrations of 2007 samplings and an expected line of $[Ca^{2+}+Mg^{2+}]/[HCO_3^{1-}]$ ratio in charge balance condition of dolomite-water system are given in Figure 6-6. It shows that the plots of most springs are near ionization equilibrium with respect to calcite and dolomite. However, the plots of six polluted springs,

such as Pretoria Lower Fountain and Sterkfontein in the North-West, Turffontein lower, Turffontein upper and Gerrit Minnebron in the Far East to Far West Rand and Tamasikwe north in the Ghaap Plateaun, are distinctly scattered below the expected line indicating an additional Ca^{2+} and Mg^{2+} source. The extra Ca^{2+} and Mg^{2+} concentrations were assumed to be coincidence with the elevated concentrations of SO_4^{2-} and Cl^{1-} at these springs.

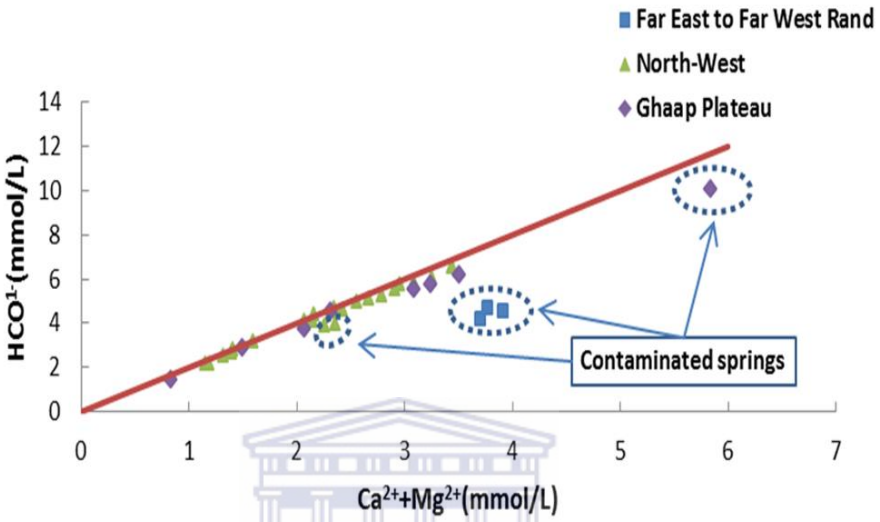

Figure 6-6 Plot of $[Ca^{2+} + Mg^{2+}]$ versus HCO_3^{1-} mole concentrations; the straight line is an expected line of $[Ca^{2+} + Mg^{2+}]/[HCO_3^{1-}]$ ratio with respect to electrically neutral condition in saturated dolomite-water system. Extra Ca^{2+} and Mg^{2+} are accompanied by elevated concentrations of SO_4^{2-} and Cl^{1-} at six contaminated springs.

6.3.2 ^{18}O and D Measurements

$\delta^{18}O$ and δD values of spring samples are given in Appendix E. However, an inter-calibration exercise of $\delta^{18}O$ and δD values was arranged in four South African stable isotope laboratories and the IAEA isotope hydrology laboratory in Vienna in 2010. The corrected values of $\delta^{18}O$ cover a range between -2.75‰ with -6.13‰, whilst the calibrated results of δD vary from -16.5 to -38.9‰. Figure 6-7 is a plot of $\delta^{18}O$ versus δD values in 2007 samplings. A local meteoric water line (LMWL) based on these $\delta^{18}O$ and δD data is $\delta D = 6.13 \times \delta^{18}O - 0.97$.

$\delta^{18}O$ and δD values of groundwater samples are variably affected by recharge conditions and evaporation. Generally, groundwater recharged during a period with low rainfall in dry air conditions contains a δD-excess value (Mook, 2000). High evaporation can lead to a slight increase of δD values with a considerable increase of $\delta^{18}O$ values. As shown in Figure 6-7, all samples plot above global meteoric water line (GMWL), suggesting the springs have been

recharged by the low rainfall in dry air conditions. The high evaporation in the dolomite area results in a shallower slope of LMWL than that of GMWL. Additionally, $\delta^{18}O$ and δD distributions are also controlled by a continental effect. Table 6-3 shows $\delta^{18}O$ and δD distributions towards western edge. It indicates that there is a tendency for $\delta^{18}O$ and δD values to decrease from eastern edge to western edge.

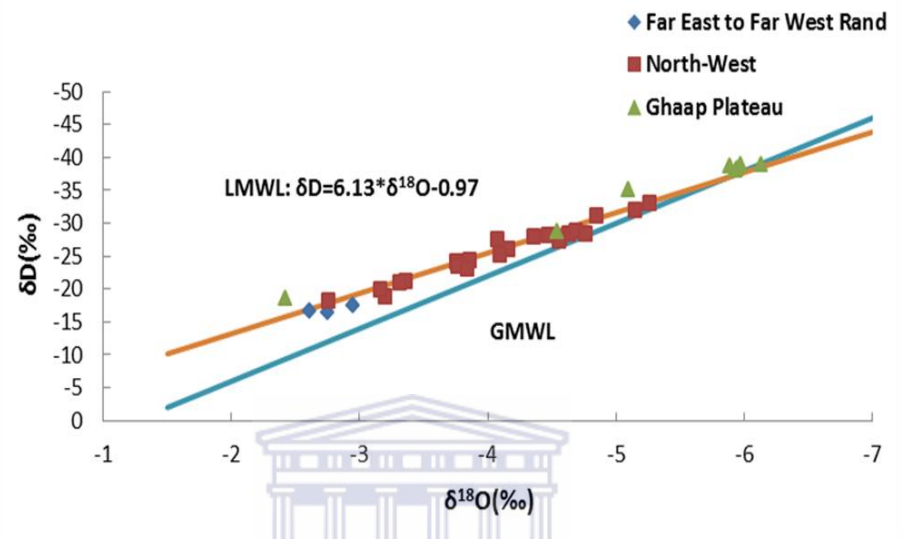

Figure 6-7 Plot of δD versus $\delta^{18}O$ values of spring samples in the dolomite aquifer.

Table 6-3 Summary of continental effect on $\delta^{18}O$ and δD distributions in spring samples

Longitude	$\delta^{18}O$ (‰)	δD (‰)
29 ℮-26 ℮	-3.56	-21.74
26 ℮ -24 ℮	-4.33	-27.16
24 ℮ -22 ℮	-4.64	-30.81

6.3.3 ^{3}H Measurements

^{3}H values sampled during 1992 to 2007 range from 0-3.2 TU. The samples at twenty seven springs contain lower ^{3}H values than the background one (2 TU) in atmosphere, whilst the other six spring samples have the higher ^{3}H values. The highest ^{3}H value is 3.2 TU in Pretoria Fountains lower eye.

6.3.4 ^{13}C Measurements

δ^{13}C-DIC in groundwater can be affected by mineral dissolution, bacterial methanogenesis and acetate fermentation by vegetation when groundwater flows through a dolomite aquifer (Cartwright, 2010). Bacterial methanogenesis can be ignored in this study due to absence of methane and presence of dissolved oxygen in water samples. Low SO_4^{2-} values at uncontaminated springs imply that there is no effect of the acetate fermentation by vegetation on the geochemistry of spring samples. Hence, δ^{13}C-DIC of spring samples in the research site is mainly controlled by the mineral dissolution as follows,

$$CaMg(CO_3)_2+2CO_2+2H_2O \text{ ---- } Ca^{2+}+Mg^{2+}+4HCO_3^{1-} \quad (6\text{-}1)$$

$$CaCO_3+CO_2+H_2O \text{ ---- } Ca^{2+}+2HCO_3^{1-} \quad (6\text{-}2)$$

As a starting condition, δ^{13}C-DIC at the soil root zone is assumed as -13 ‰ which is consistent with dominance of C3 plants in semi-arid region (Chen et al., 2005; Vogel, 1993) and the marine source of the dolomite. The δ^{13}C-DIC of groundwater samples is examined to evaluate the mineral dissolution in the dolomite aquifer. In the Far East to Far West Rand and North-West, the δ^{13}C-DIC ranges from -12.7 ‰ to -7 ‰. The lowest δ^{13}C-DIC is -12.7 ‰ at Buffelshoekoog. It is almost the same as the starting condition of δ^{13}C-DIC, indicating slight mineral dissolution. The highest δ^{13}C-DIC is -7 ‰ at Schoonspruit southern eye, suggesting a strong mineral dissolution. The reaction (6-1) is considered as the main chemical process of the Mg-Ca-HCO_3 rich water system in these areas. In the Ghaap Plateau, the δ^{13}C-DIC varies from -12.1 ‰ to -10 ‰. They are close to the starting condition of δ^{13}C-DIC, indicating slight dolomite dissolution. Both reactions (6-1) and (6-2) are realized to prevail at Boplaas spring, Kuruman springs and Groot Kono spring, corresponding to the domination of the dolomite-calcite aquifer in these sites. The reaction (6-1) is assumed to control the distribution of δ^{13}C-DIC at the other springs from a pure dolomite aquifer in the Ghaap Plateau.

6.3.5 $^{87}Sr/^{86}Sr$ Measurements

Sr isotopes are produced by decay of the radioactive alkali metal rubidium (^{87}Rb). The $^{87}Sr/^{86}Sr$ ratio provides a valuable independent evaluation of the ion exchange reaction between groundwater and mineral in the dolomite aquifer (Gosselin et al., 2004; Cartwright et al., 2007; Klaus et al., 2007; Cartwright, 2010), which is built based on the facts that (1)

mineral dissolution or isotopic exchange reaction change the $^{87}Sr/^{86}Sr$ ratios in the mineral-water system; (2) mineral precipitation does not separate $^{87}Sr/^{86}Sr$ ratios from the mineral-water system; and (3) the long half-life of ^{87}Rb leads that the change of $^{87}Sr/^{86}Sr$ ratios is not due to the decay of ^{87}Rb in groundwater.

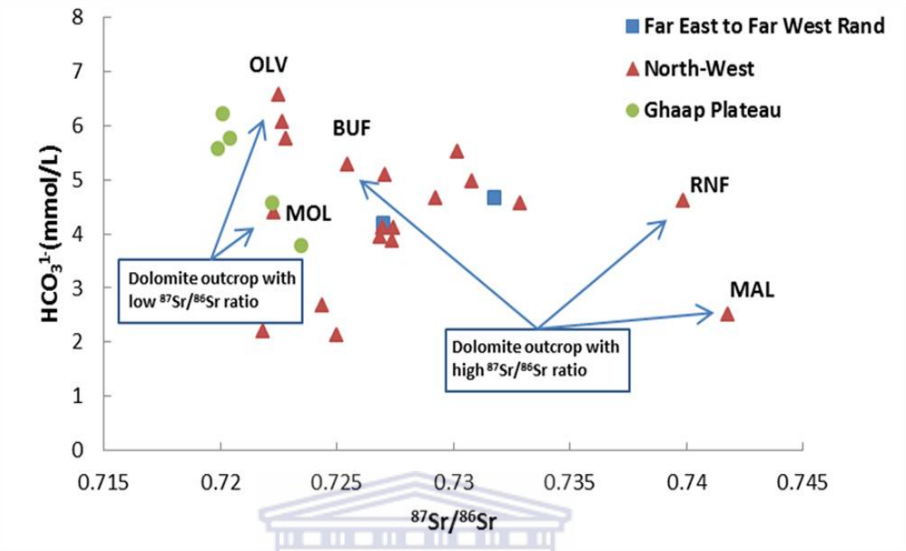

Figure 6-8 Plot of $^{87}Sr/^{86}Sr$ ratios versus HCO_3^{1-} values of spring samples.

In the 1992-1993 samplings, $^{87}Sr/^{86}Sr$ data was analyzed on a number of samples collected from all three study areas as shown in Appendix E. The groundwater samples have $^{87}Sr/^{86}Sr$ ratios of 0.716957-0.741761 which are higher than that of modern seawater (0.70918) (Jones and Jenkyns, 2001), indicating additional resource of Sr isotopes. Figure 6-8 is a plot of $^{87}Sr/^{86}Sr$ ratios versus HCO_3^{1-} values of spring samples, presenting a direct correlation between $^{87}Sr/^{86}Sr$ ratios and HCO_3^{1-} values in most sampling sites. However, the correlation is invalid in the Ghaap Plateau, which is presumed to be associated with the domination of mixing dolomite-calcite groundwater system. This would be explained by mineral dissolution, rather than ion exchange reaction between carbonate and groundwater, being critical for distribution of Sr isotopes in the groundwater samples.

Additionally, $^{87}Sr/^{86}Sr$ ratios of dolomite rock also affect the regional distribution of $^{87}Sr/^{86}Sr$ ratios of groundwater samples. A low $^{87}Sr/^{86}Sr$ ratio of dolomite rock nearby the spring can result in a low $^{87}Sr/^{86}Sr$ ratio of groundwater, however, in the case of strong dolomite dissolution took place. Table 6-4 shows analysis results of $^{87}Sr/^{86}Sr$ ratios of spring samples and dolomite rock samples collected nearby the sampled springs in the North-West.

In general, $^{87}Sr/^{86}Sr$ ratios of carbonate from dolomite outcrop are smaller than those of the accompanying groundwater. $^{87}Sr/^{86}Sr$ ratios of dolomite rock at Molopo Spring (MOL) and Olievendraaispring (OLV) are smaller than those at Buffelshoekoog (BUF) and Rhenosterfontein (RNF), which results in that the spring samples at MOL and OLV with stronger dolomite dissolutions contain relatively smaller $^{87}Sr/^{86}Sr$ ratios than those at BUF and RNF(as shown in Figure 6-8).

Table 6-4 Comparison of $^{87}Sr/^{86}Sr$ ratios between spring water and dolomite rock

Spring	$^{87}Sr/^{86}Sr$ ratios of dolomite rock	$^{87}Sr/^{86}Sr$ ratios of groundwater	Difference
Buffelshoekoog	0.713139	0.725464	0.012325
Molopo Spring	0.711497	0.722284	0.010787
Olievendraai spring	0.709538	0.722511	0.012973
Rhenosterfontein	0.723364	0.739861	0.016497

6.3.6 ^{14}C Measurements

^{14}C-DIC of 2007 samples covers a range from pre-bomb (70 pmc) to recent (110 pmc) values. ^{14}C-DIC in a groundwater sample can be affected by mineral dissolution in a carbonate aquifer. The highest ^{14}C-DIC is captured at Groot Kono Spring in the Ghaap Plateau (Figure 6-9).

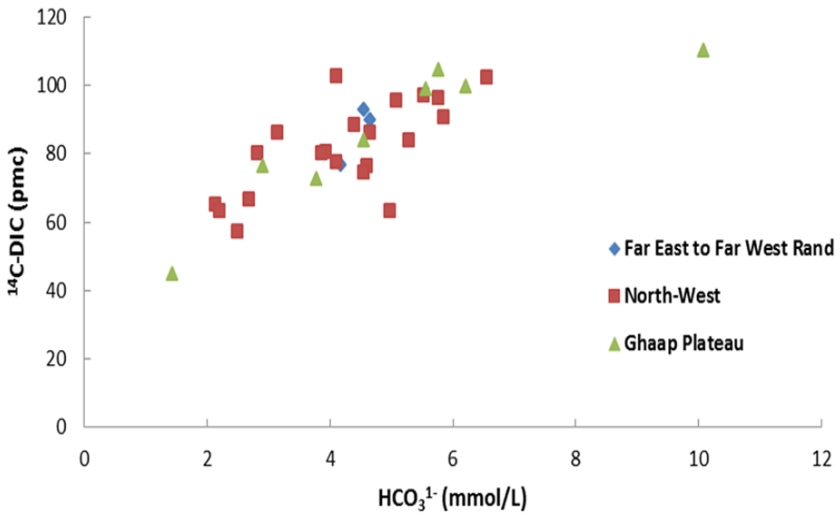

Figure 6-9 Plot of HCO_3^{1-} versus ^{14}C-DIC in 2007 samplings.

Compared to former measurement results (Appendix E), ^{14}C-DIC in 2007 samplings shows a slow increase, decrease or constancy within a few pmc in most springs. However, ^{14}C-DIC of Tweefontein upper and Erasmus have significant increases (10 pmc or more) above the historic measurements, whilst ^{14}C-DIC of Tweefontein lower and Groot Kono Spring show substantial decreases (10 pmc or more).

6.4 Discussion

Determination of corrected ^{14}C MRTs in the dolomite spring system is presented in this section. Applying geochemical data and groundwater MRTs, the flow dynamics, including the effect of rainfall on temporal trend of groundwater MRTs and the groundwater flow circulation, of the spring system are also discussed.

6.4.1 Corrected Groundwater ^{14}C MRTs

To assess accurate ^{14}C MRTs of the dolomite spring system by the EPM, a dilution factor (q) is introduced to calculate the initial ^{14}C activities (C_{in}) in Eq. (2.1). Corresponding to the fact that the dilution effect on initial ^{14}C activities is the produce of the mineral dissolution in the dolomite aquifer of South Africa, two empirical approaches are selected and applied to calibrate the initial ^{14}C activities. The first one is the Pearson model which is proposed to present an approximation of the dilution effect of dolomite dissolution by Pearson and Hanshaw (1970). The model is an isotopic mixing model and based on the assumption that ^{14}C has same chemical behaviour as ^{13}C. δ^{13}C-DIC measurements are used to estimate the dilution factor by means of the following equation.

$$q = \frac{\delta_s - \delta_m}{\delta_g - \delta_m} \tag{6.2}$$

where δ_s is the δ^{13}C-DIC of water sample. δ_m is the δ^{13}C-DIC of mineral. δ_g is the δ^{13}C -DIC of soil gas.

The second correction model is a chemical mixing model namely the Tamers model (Tamers, 1975). The calculation of the dilution factor by the Tamers Model is made with the following assumptions: (1) half of bicarbonate comes from CO_2 gas and the other half is from the carbonate minerals and (2) all the CO_2 comes from the soil zone and all the bicarbonate is

from the dissolution of carbonate minerals. The CO_2 and HCO_3^{1-} mole concentrations are used to calculate dilution factor as follows,

$$q = \frac{m_{CO_2} + 0.5 m_{HCO_3^{1-}}}{m_{CO_2} + m_{HCO_3^{1-}}} \tag{6.3}$$

where m_{CO_2} is the mole concentration of CO_2 in water sample. $m_{HCO_3^{1-}}$ is the mole concentration of HCO_3^{1-} in water sample. Based on dilution factor, q, the convolution integral of the EPM is rewritten as

$$C_{out}(t) = \int_0^{\infty} q C_{in}(t-\tau) h(\tau) \exp(-\delta\tau) \mathrm{d}\tau \tag{6.4}$$

In the dolomite aquifer of South Africa, δ^{13}C-DIC of soil gas (δ_g) in Eq. (6.2) is assumed to be -13 ‰ which is a mean δ_g of soil gas in root zone under semi-arid condition (Vogel, 1993; Chen et al., 2005). The δ^{13}C-DIC of mineral (δ_m) in Eq. (6.2) is assumed to be 0 ‰ for marine carbonate minerals (Vogel, 1993; Chen et al., 2005). A mean value of δ^{13}C-DIC in water samples during 1970s and 2000s is given for δ_s (Appendix F) in Eq. (6.2). An average value of HCO_3^{1-} measurements in 1992-1993 is given for $m_{HCO_3^{1-}}$ (Appendix F) in Eq. (6.3). A concentration of CO_2 was collected in 1992-1993 (Appendix F). The time series of ^{14}C activities in atmosphere from 1922 to 2002 is used as an input function (C_{in}) in Eq. (6.4). The parameter, f, in Eq. (6.1c) is assumed to be equal to 0.75.

According to the convolution integral and the relative response functions of each lumped-parameter model as mentioned in Chapter 1, an Excel program as shown in Appendix G is designed to automate the lumped-parameter models. However, limitations of the use of the EPM based on the existing ^{14}C measurements are necessarily noted. The useful ^{14}C-DIC of spring water has been sampled from 1970s to 2000s and the initial ^{14}C activities of atmosphere have been measured since 1922 in the research site. The ^{14}C-DIC sample collected in 2007 is not involved in the calculation of groundwater MRTs due to the lack of the measurement of initial ^{14}C activities from 2002 to 2010. Figure 6-10 shows the model simulations of the ^{14}C time series with different MRTs by the input of uncalibrated initial ^{14}C activities during 1922 and 2002 into the EPM with parameter *f=0.75*. It hints that the simulation curves of ^{14}C time series with 1 year and 10 years MRTs are difficult to be

distinguished during 1975 and 2002. Consequently, the EPM is only useful when groundwater MRTs of spring samples distribute in the range from 10 to 80 years in this case.

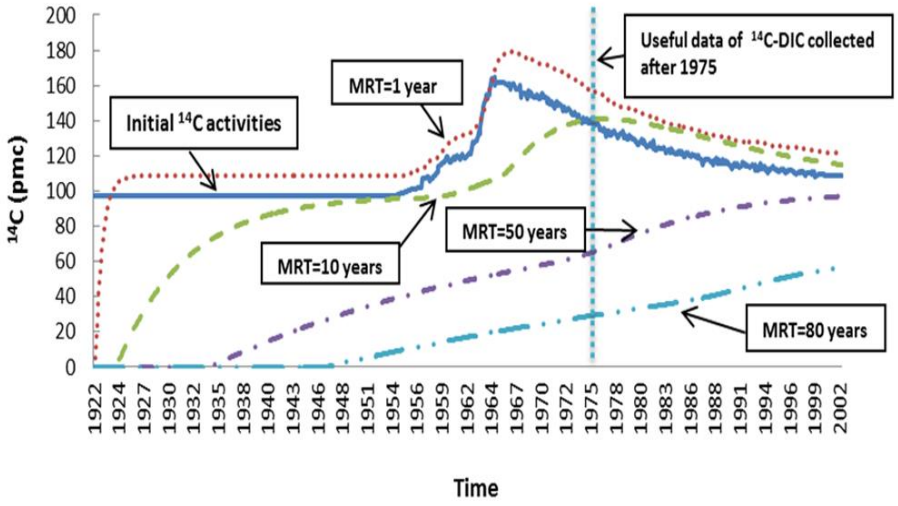

Figure 6-10 Model simulation of the ^{14}C time series with different MRTs by the input of atmospheric ^{14}C into the EPM with parameter *f=0.75.*

6.4.2 Calculation Results and Verification of Groundwater MRTs

Two series of dilution factors are given by using the Pearson and the Tamers models, respectively. As shown in Appendix F, in the Far East to Far West Rand and Ghaap Plateau, the dilution factors by means of the Pearson model are fairly similar to those from the Tamers model. An exception is Kuruman B in which the dilution factor by using the Pearson model is 0.18 larger than that from the Tamers model. It leads the groundwater MRT by the Pearson model is about 20 years older than that by the Tamers model at Kuruman B. In the North-West, the dilution factors of five selected springs from the two models are almost identical. However, the dilution factors of the other eight selected springs by the Pearson model are about 0.1-0.2 larger than those generated by the Tamers model. At these springs, it results in about 10-20 years difference of MRT calculation results by different models. The greatest difference of groundwater MRT evaluation is about 20 years captured in Pretoria Fountains upper eye.

With regard to the Tamers model (Eq. (6.3)), the calculation of dilution factor is sensitive to the CO_2 measurements (Tamers, 1975). There is a critical importance to carrying out the chemical analyses rapidly. However, in the 1992-1993 samplings, the spring samples were

transferred from field to laboratory, and then CO_2 was extracted in NaOH before being analyzed. The data collection method of CO_2 may lead to loss of dissolved CO_2. This coincides with the fact that pH values in fieldwork are generally lower than those measured in laboratory. Spurious dilution factors should be given in Eq. (6.3) based on the faking CO_2 measurements. In this case, the validity of the use of the Tamers Model is doubtful, and the Pearson model is preferred for the dilution factor calculation in this chapter.

The evaluation results of dilution factor by the Pearson model (Eq. (6.2)) show the spring samples have about 50% to 80% initial ^{14}C activities in the dolomite aquifer (Appendix F). The groundwater MRTs of spring samples by using the EPM with corrected ^{14}C activities range from ≤10 to 51 years (Appendix F). In the North-West, there are nine springs which contain old groundwater with >10 years MRTs, whilst the spring samples at other six selected springs have 10 years or less MRTs. In the Far West to Far East Rand and the Ghaap Plateau, all the five selected springs have >10 years MRTs. Erasmus Rietvlei spring contain the oldest groundwater with 51 years MRT.

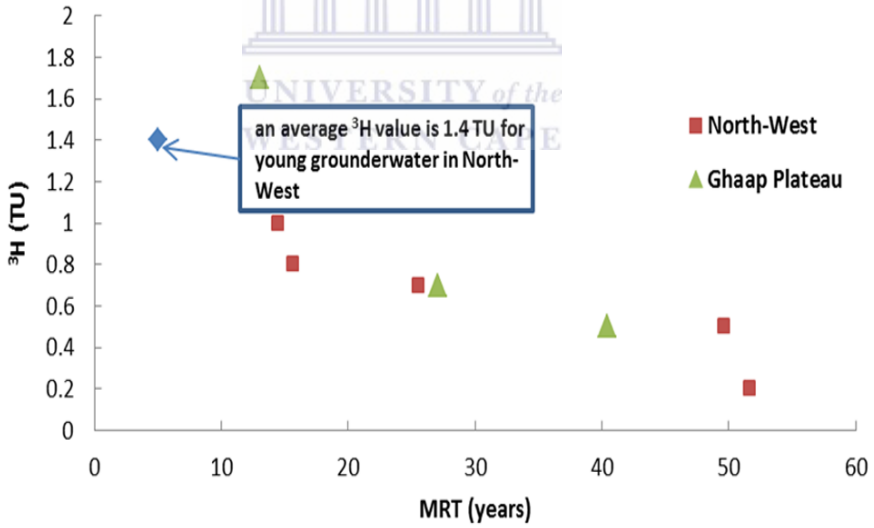

Figure 6-11 Plot of ^{3}H values versus groundwater MRTs by the Pearson model at uncontaminated spring samples. It indicates there is a negative correlation between groundwater MRTs and ^{3}H values.

Compared to former results of groundwater MRTs from Bredenkamp (2007) and Bredenkamp et al. (2007), the groundwater MRTs by the Pearson model in fourteen springs are older than those from the previous researches, whilst the groundwater MRTs in four springs using the Pearson model are younger than the former ones (Appendix F). ^{3}H value, an

indicator of groundwater recharge occurring in the last 60 years, is applied to verify the groundwater MRTs of spring samples in this study. The appearance of ^{3}H indicates that the groundwater contains an element of modern recharge. However, extra ^{3}H are supposed to be introduced through contamination component at the contaminated selected springs, such as Turffontein upper, Gerrit Minnebron, Sterkfontein Spring, Pretoria Fountains lower eye and Pretoria Fountains upper eye. Figure 6-11 is a plot of ^{3}H values versus groundwater MRTs at the uncontaminated sampling sites, displaying a negative correlation between groundwater MRTs and ^{3}H values. The groundwater MRT distributions are sensitive to the variability of ^{3}H values in the spring sampling sites. An average ^{3}H value of young groundwater samples with 10 years or less MRTs in the North-West is about 1.4 TU, while the old spring samples with >10 years MRTs often have low ^{3}H values (1 TU or less). In the case, the calculation results of groundwater MRTs of spring samples from this study are accepted.

6.4.3 Effect of Rainfall on Temporal Trend of Groundwater MRTs

Spring water represents dynamical mixing of different recharge events with different ages from an entire catchment. According to the geochemical measurements above, the spring water in the dolomite aquifer is mainly recharged by local rainfall. Hence, the effect of rainfall on the temporal trend of groundwater MRTs is investigated in the following.

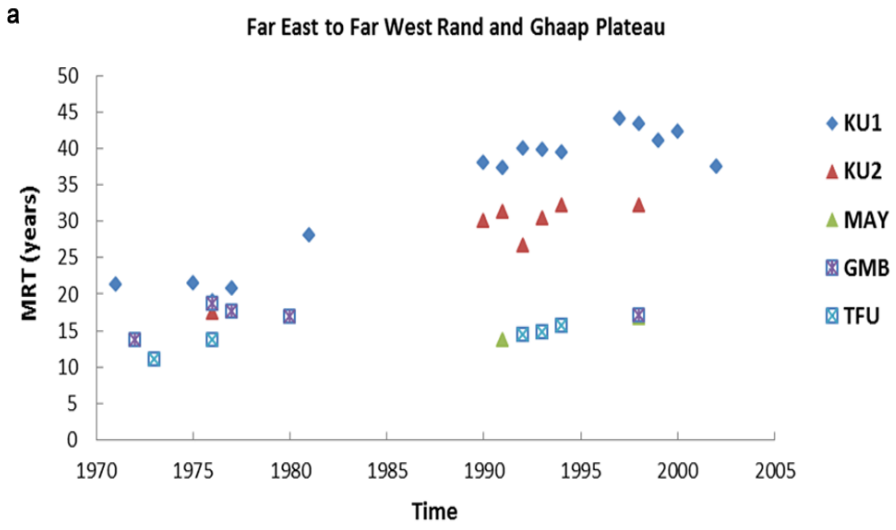

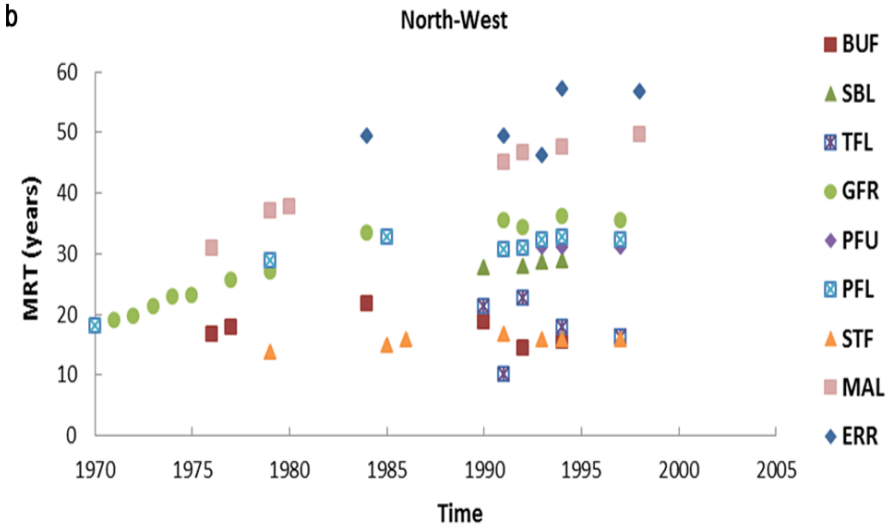

Figure 6-12 Temporal trends of groundwater MRTs of spring samples (a-b) from 1970s to 2000s.

Two temporal trends of groundwater MRTs calculated by the Pearson model are identified in fifteen springs with >10 years MRTs. As shown in Figure 6-12, groundwater MRTs at five springs, including Grootfontein Rietvlei, Pretoria Fountains lower eye, Manloys, Kuruman A and Kuruman B, have significant increases (10 years or more) during 1970s and 2000s. At the other nine springs, their plots of groundwater MRTs display stable trends or small changes with few years (<10 years).

Figure 6-13 is the model simulation of ^{14}C time series by the EPM at the five springs where the groundwater MRTs display significant increases (10 years or more) during the sampling period. It indicates that the time series of ^{14}C-DIC cannot be fitted approximately with a single MRT. The most variation of groundwater MRT takes place in Kuruman A where the groundwater MRT has increased by about 20 years since 1970s.

The Kuruman springs have been closely monitored (Bredenkamp, 2000, 2007; Bredenkamp et al., 2007), in which the time series of ^{14}C-DIC are analyzed with being given special attention for the effect of rainfall on the temporal trend of groundwater MRTs. Figure 6-14 is a plot of MRT variations and rainfall data at the Kuruman springs during 1970s and 2000s. The positive temporal trends of groundwater MRTs are developed with the decreases of rainfall, indicating distinct rainfall effect on temporal trends of groundwater MRTs in spring samples. In 1970s, the Kuruman springs had about 20 years MRTs. Consistent with the decreases of rainfall in 1990s-2000s, the MRTs of Kuruman A (Fig.6.14 d) and Kuruman B

(Fig.6.14 e) increase to 41 and 27 years, respectively, suggesting that the groundwater MRTs distribution in Kuruman A is more sensitive to the change of rainfall than that in Kuruman B.

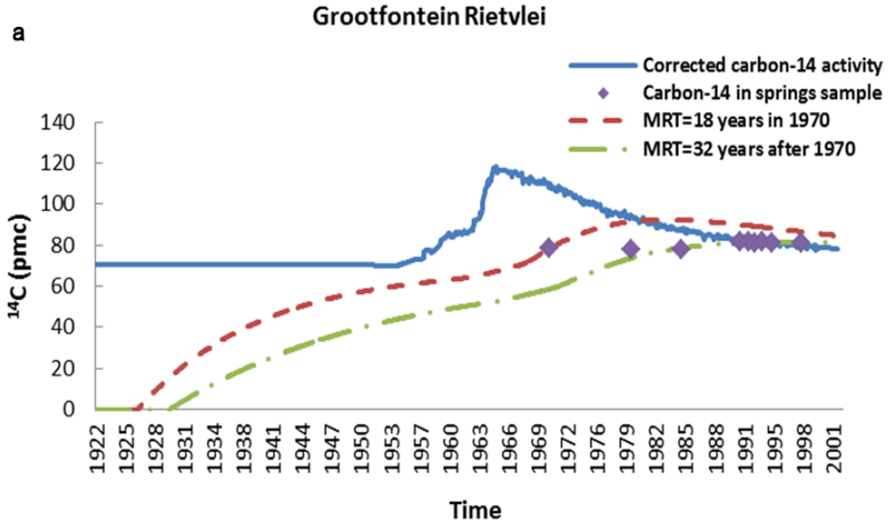

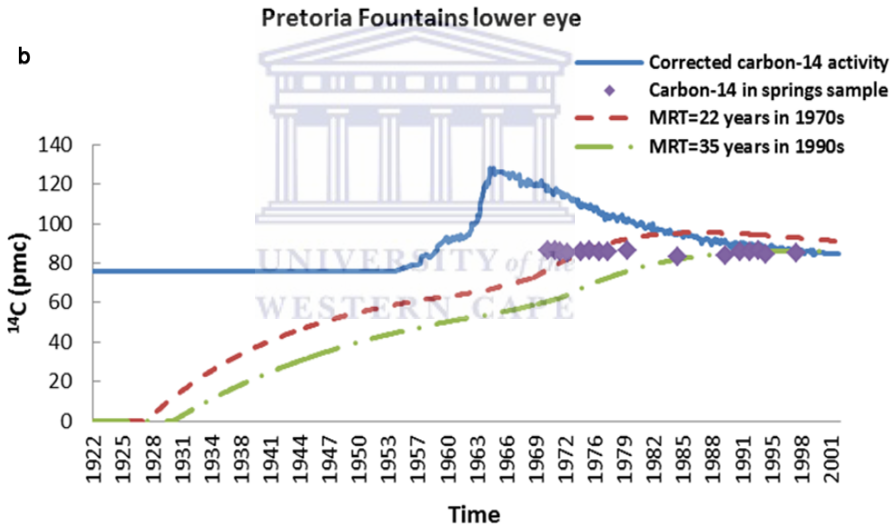

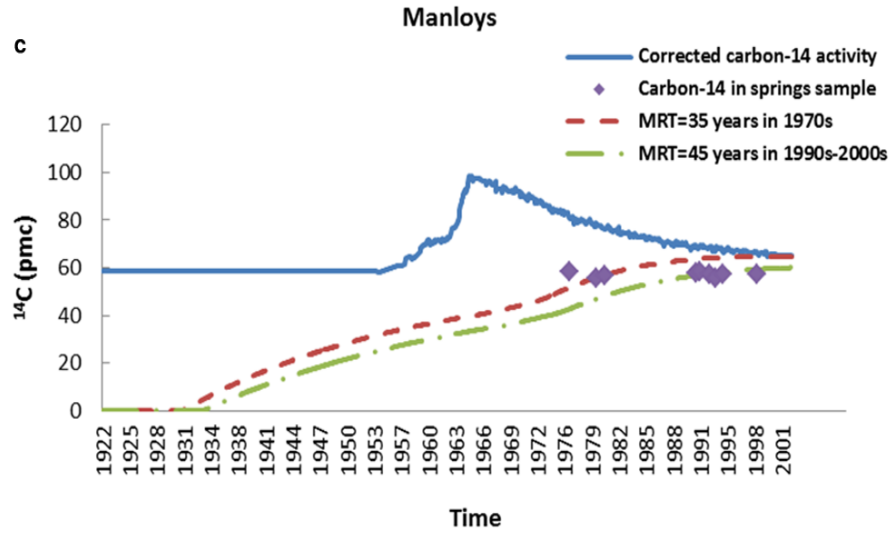

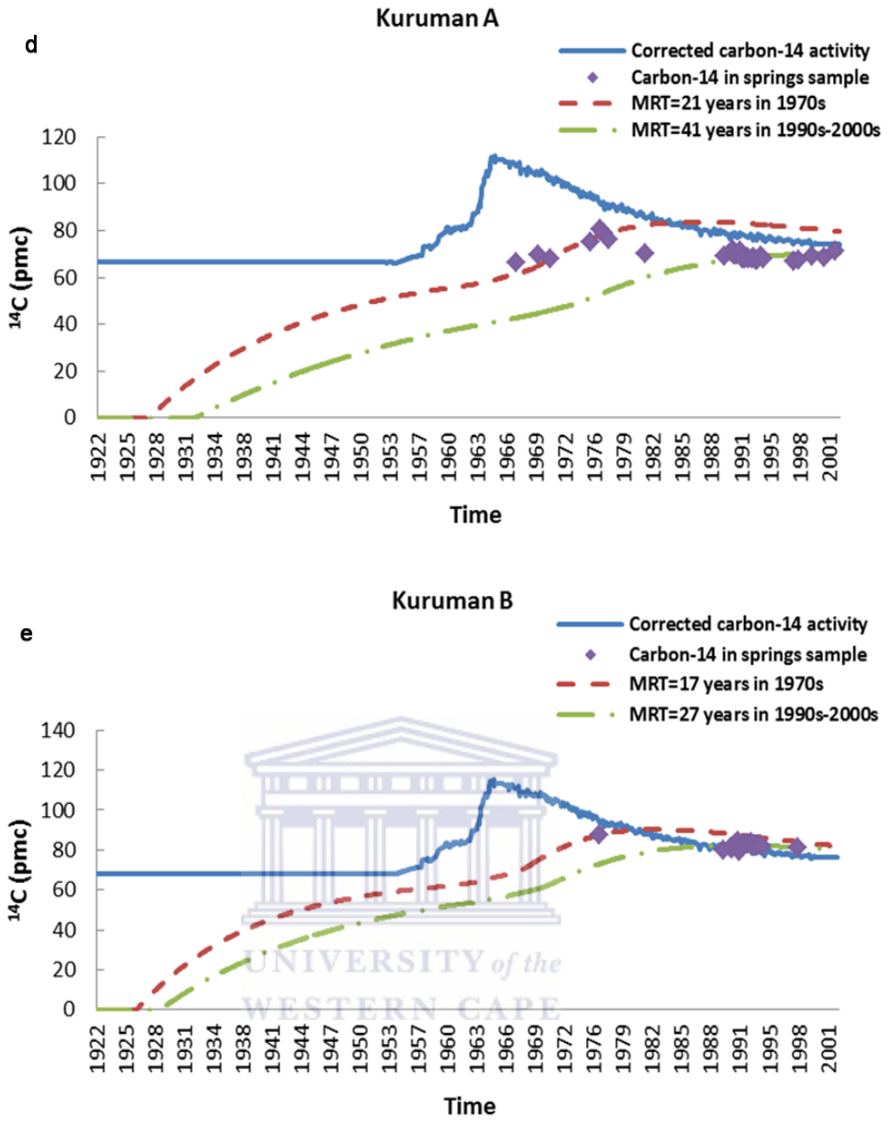

Figure 6-13 Model calculation of ^{14}C progress for five selected springs (a-e) by using the EPM.

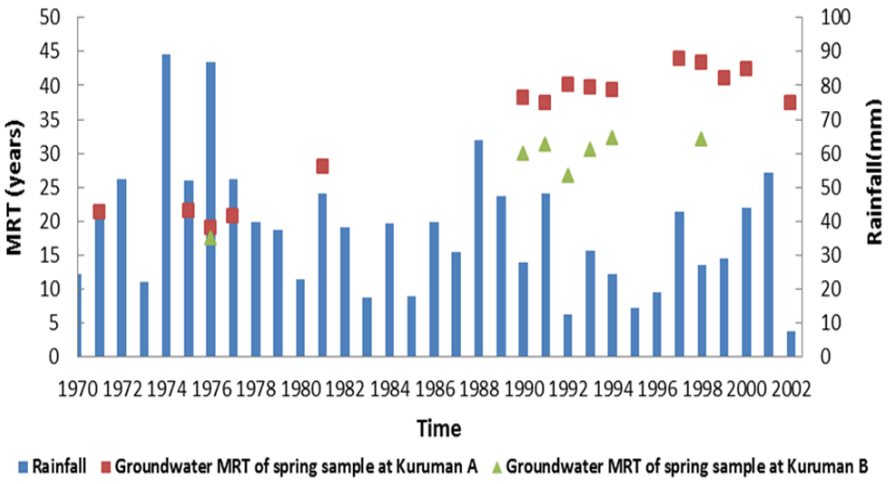

Figure 6-14 MRTs variations and rainfall data over the sampling period in the Kuruman springs.

At the other nine selected springs, the temporal trends of groundwater MRTs are steady or changed with few years during 1970s and 2000s. Figure 6-15 shows the model simulation of the ^{14}C time series at five examples of such springs. It proved that their ^{14}C-DIC of spring samples is approximately fitted with a single MRT. In this case, the rainfall change is recognized to have a slight effect on the MRT distribution of spring samples. Figure 6-16a shows the plot of rainfall data versus groundwater MRTs of spring samples over 1970s and 2000s at Buffelshoekoog. The considerable change of rainfall at Buffelshoekoog from 30 to 90 mm is accompanied by a slight change of groundwater from 16 to 21 years. It indicates the groundwater MRT of spring samples is not sensitive to rainfall variability. A similar phenomenon is observed at Gerrit Minnebron (Figure 6-16b).

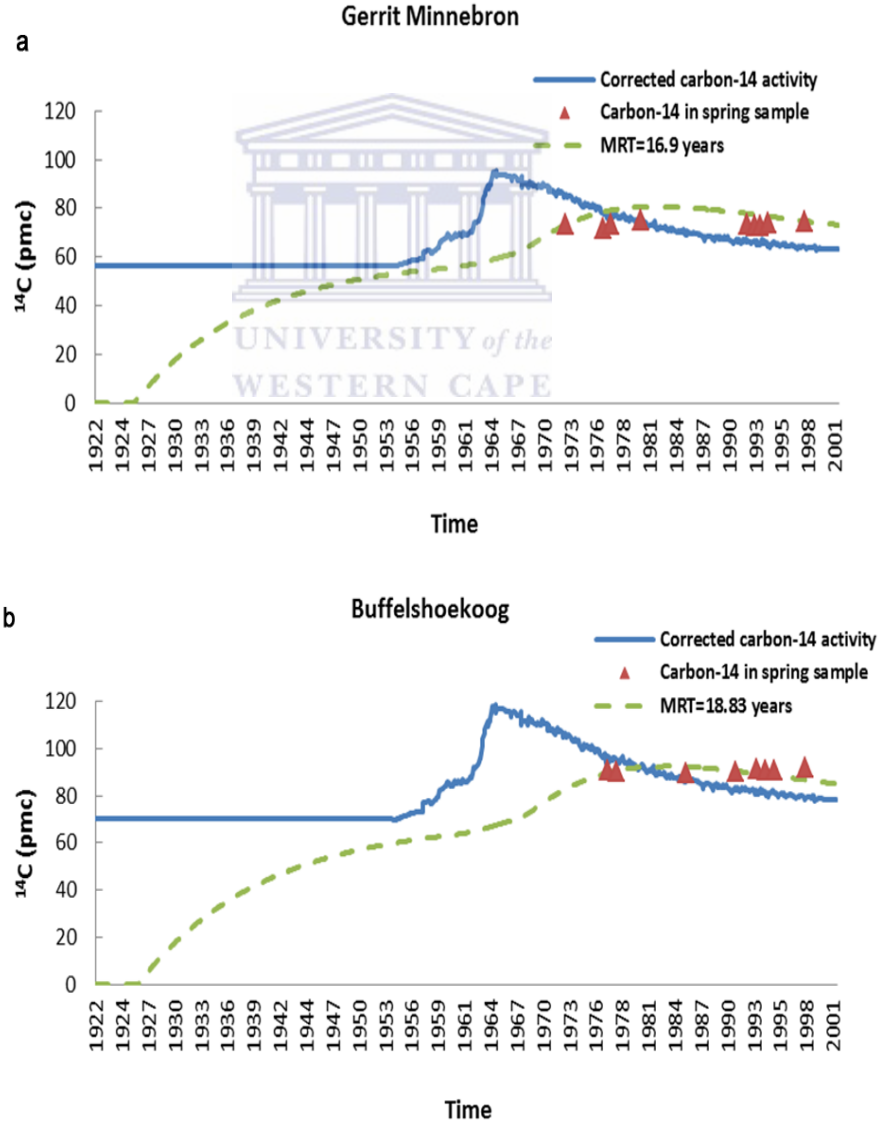

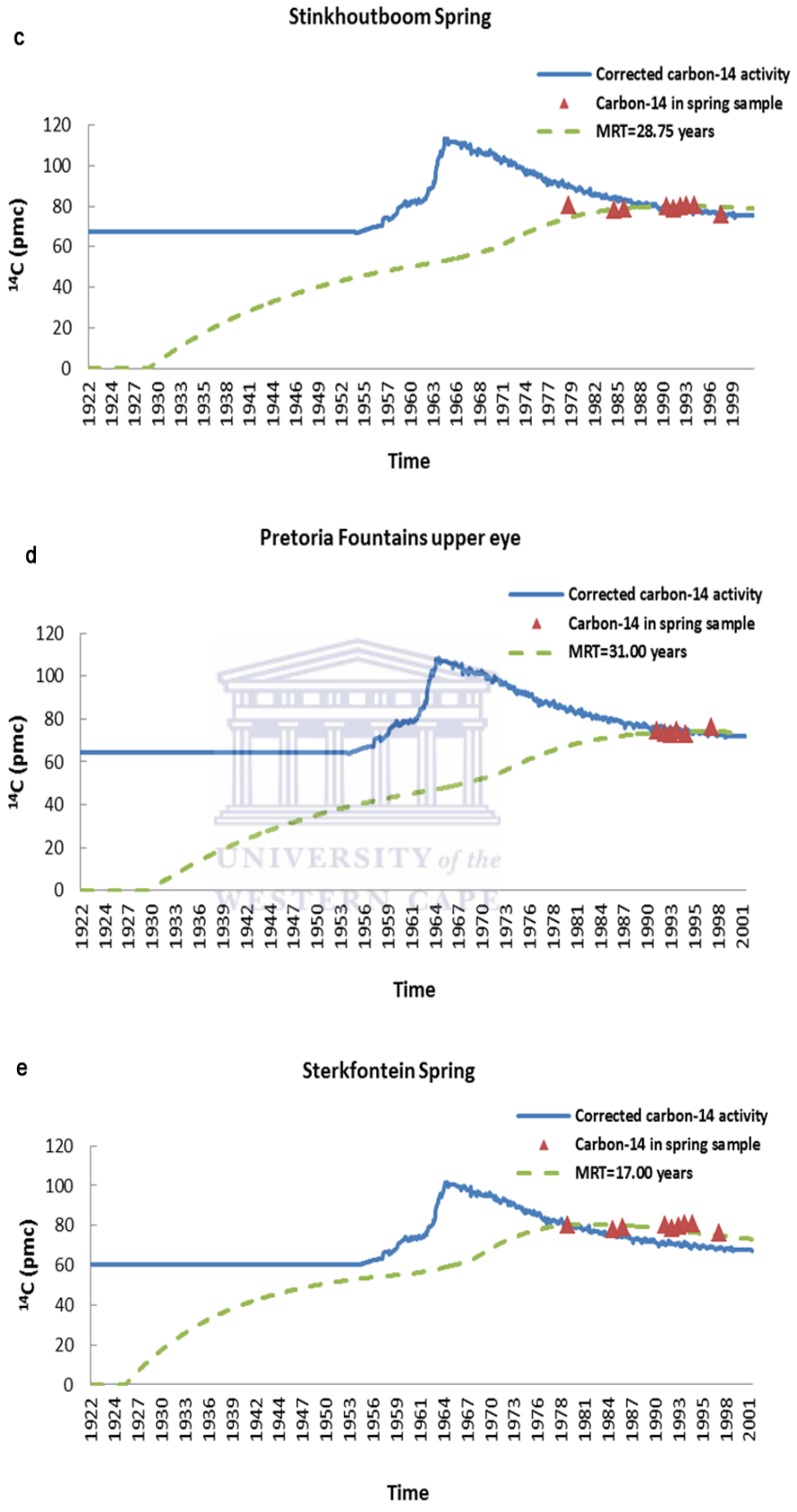

Figure 6-15 Model simulation of ^{14}C time series for five selected springs (a-e) by using EPM.

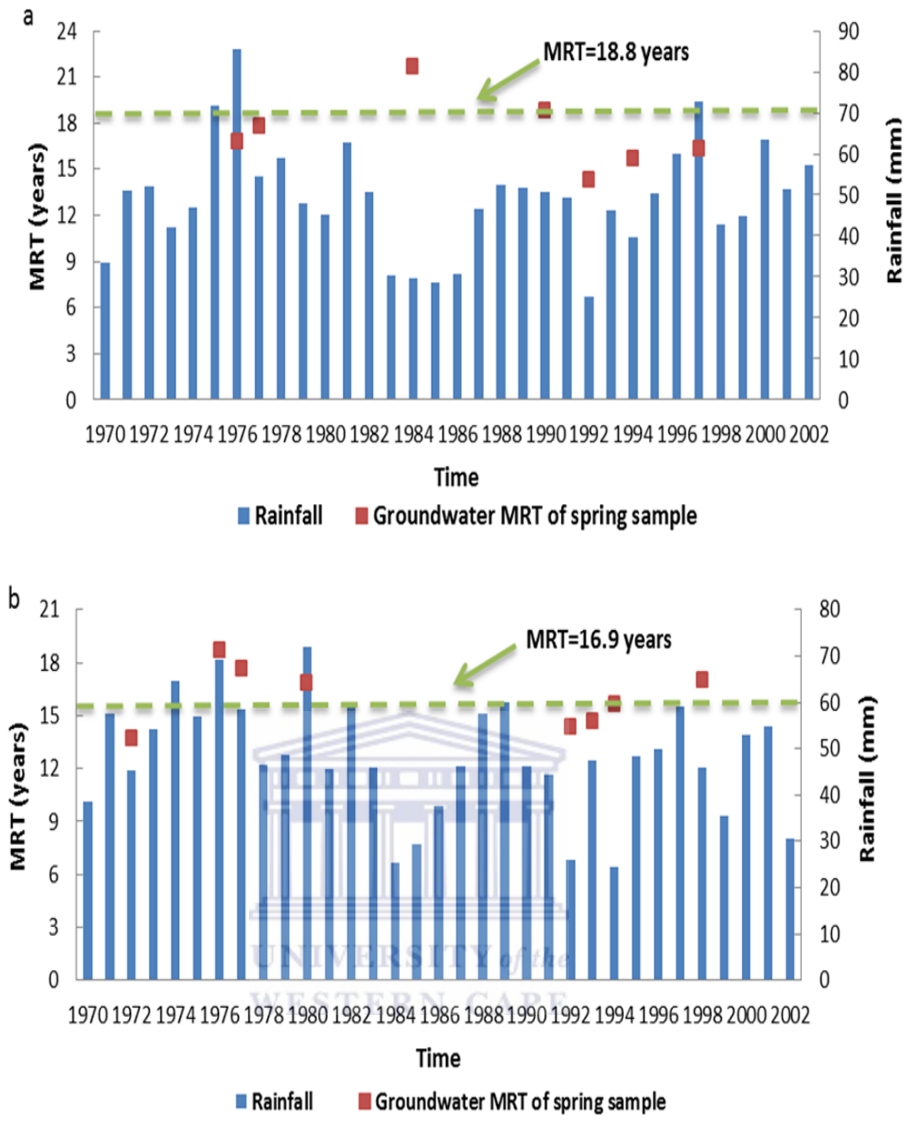

Figure 6-16 Temple trend of MRTs and rainfall during 1970s and 2000s at (a) Buffelshoekoog and (b) Gerrit Minnebron.

6.4.4 Groundwater Flow Circulation

Hydrochemical evolution (e.g. $[Ca^{2+}]/[Mg^{2+}]$ ratio) and groundwater MRTs of spring samples provide qualitative indicators of groundwater circulation in a dolomite aquifer. Generally, $[Ca^{2+}]/[Mg^{2+}]$ ratios and groundwater MRTs are assumed to present an increasing trend along flow direction. However, a role of deep groundwater inflow to springs in the study area remains uncertain, and the contaminated spring water should make the trend invalid.

In the Far East to Far West Rand, groundwater flow is in a westerly direction as shown in Figure 6-1. The groundwater movement can be confirmed to exclusively occur along the transverse fault zone by the hydrochemical evolution and groundwater MRTs of spring

samples. An increasing trend of groundwater MRTs can be observed from 13.7 years at Turffontein Springs to 16.9 years at Gerrit Minnebron. The spring samples with anomalously SO_4^{2-} and Cl^{1-} concentrations also indicate the movement of acid contaminant from dewatering area in the eastern area. The concentrations of SO_4^{2-} (152 mg/L) and Cl^{1-} (40.3 mg/L) at Turffontein Upper Spring are obviously higher than those at Gerrit Minnebron (137 mg/L for SO_4^{2-}; 31 mg/L for Cl^{1-}). It results in a lack of positive trend of $[Ca^{2+}]/[Mg^{2+}]$ ratio of spring sample along the flow direction from the Turffontein Springs to Gerrit Minnebron. Over such a distance, a small age increase and an unnoticeable hydrochemical evolution should be observed due to the fast movement of groundwater through the aquifer and unimportant effect of deep groundwater on the spring outflow.

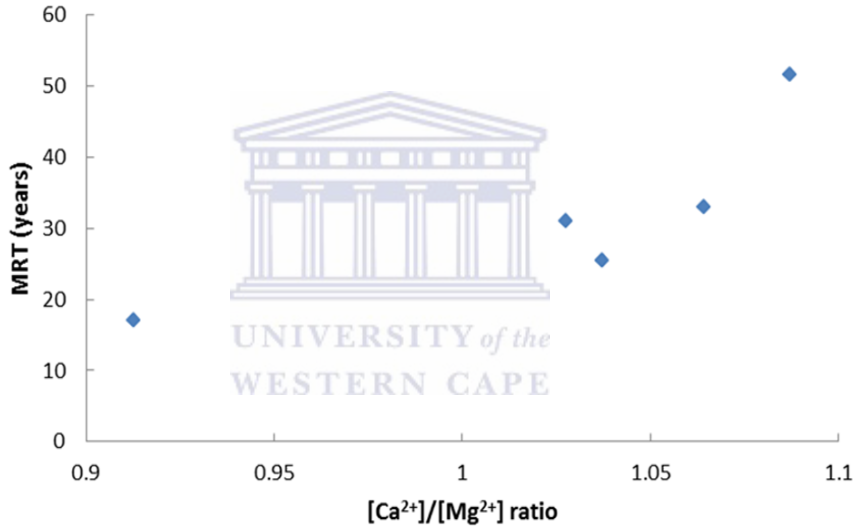

Figure 6-17 Plot of $[Ca^{2+}]/[Mg^{2+}]$ ratio versus groundwater MRT at the spring samples in the eastern area of North-West.

In the North-West, the flow directions generally mimic the topography and the dyke distribution. The springs are mainly distributed in two areas along the eastern edge and western edge of the dolomite outcrops, respectively. The flow directions are shown in Figure 6-2. In the area along eastern edge, the distribution of groundwater MRTs strictly agrees with the distribution of $[Ca^{2+}]/[Mg^{2+}]$ ratio (Figure 6-17). Old groundwater from deep aquifer should be assumed to play an important role in the outflow of springs because the spring water generally has 20-50 years MRTs. Compared to the springs in the eastern edge, the unpolluted spring samples contain younger groundwater with 10 years or less MRTs in the

area along western edge. However, there are three special cases at Buffelshoekoog, Stinkhoutboom Spring and Tweefontein lower where the MRTs of spring samples are 18.8, 28.8 and 17.5 years, respectively. It indicates an unimportant role of deep groundwater inflow in spring water and fast movement of groundwater through the aquifer in this area.

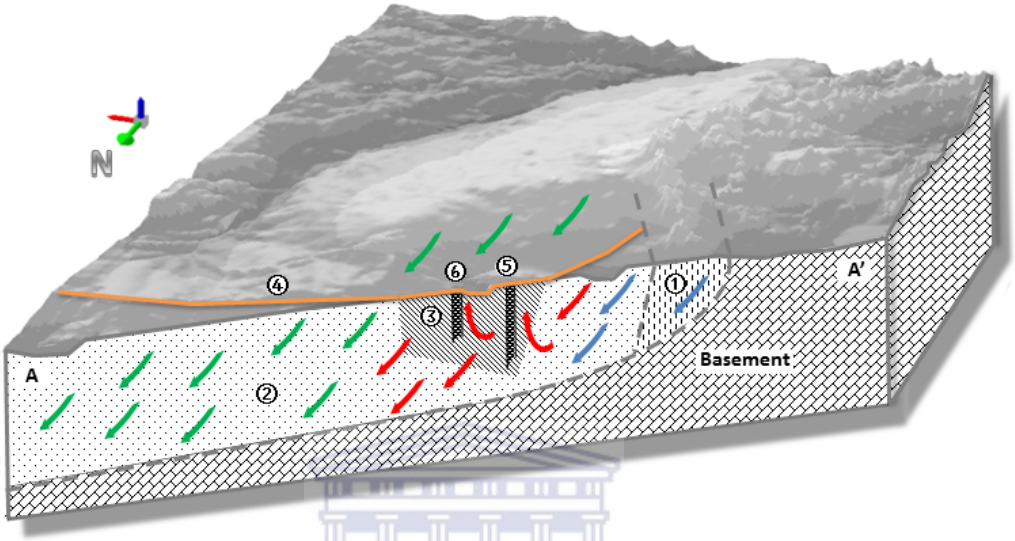

(1) Main recharge (➡) occurs in hilly area along western edge (①) of the Ghaap Plateau represented by limestone;

(2) Recharge occurs (➡) in the dolomite outcrop area (②) in the Ghaap Plateau. Ca-HCO_3 rich water is introduced to dolomite aquifer along dykes (④). A mix system (➡) of Ca-Mg-HCO_3 rich water and Ca-HCO_3 rich water are observed at the outflows of springs (⑤ and ⑥) along fault zone (③) due to development of dykes in the Kuruman area;

(3) the spring samples in Kuruman A (⑤) would come from deeper aquifers than those in Kuruman B (⑥).

Figure 6-18 Conceptual model of groundwater origin and flow circulation in the Ghaap Plateau shown on a cross-section. The location of the cross-section A-A' and its view direction were shown in Figure 6-3.

In the Ghaap Plateau, the hilly area developing along the western edge is generally considered as the major recharge area (Figure 6-3). The flow directions also agree with topography and the development of dyke patterns. The hydrochemical evolution from a mixing dolomite-calcite system to a dolomite system leaves little doubt that there is an easterly groundwater movement in the Kuruman area. However, there is a lack of positive trend of groundwater MRTs along the flow movement. Kuruman B has younger groundwater with 27.1 years MRT than that (40.4 years) at Kuruman A, although Kuruman B is farther than Kuruman A from the major recharge area. In this case, the burial depth of groundwater

resource of spring samples is considered. It would be explained that the burial depth of groundwater resource of Kuruman A is deeper than that of Kuruman B (Figure 6-18). Additionally, the $[Ca^{2+}]/[Mg^{2+}]$ ratio (1.37) in Kuruman B is obviously smaller than that (1.87) in Kuruman A, suggesting there is a stronger component of groundwater from the young Ca-Mg-HCO_3 rich system in the outflow of Kuruman B than that in Kuruman A. It would also be concluded that the groundwater MRTs in Kurman B is smaller than that in Kurnman A.

6.5 Summary

The analysis of the geochemical and isotopic data of spring samples has contributed to gaining a better understanding of the flow dynamics, including recharge areas and sources, groundwater MRTs and flow circulation, of the dolomite spring system in South Africa. The results will be useful for the sustainable management of these strategic groundwater resources.

The recharge of the spring system is suggested to be mainly influenced by local rainfall. Most of the spring samples contain Ca-Mg-HCO_3 rich water from an expected dolomite aquifer. However, the chemical evolution of four springs (Boplaas spring, Kuruman springs and Groot Kono spring) in the Ghaap Plateau is corresponding to a mixing system with Ca-Mg-HCO_3 and Ca-HCO_3 rich water from the dolomite-calcite aquifer. It verifies that groundwater in these areas is mainly recharged from hilly areas along western edge of the Ghaap Plateau represented by limestone. Contamination components with high values of SO_4^{2-} and Cl^{1-} were captured at eight springs. A local meteoric water line (LMWL) based on $\delta^{18}O$ and δD values of spring samples is $\delta D=6.13X\delta^{18}O-0.97$. Distribution of the stable isotopes of spring samples is controlled by a continental effect. Mineral dissolution is considered as the main process of controlling $\delta^{13}C$-DIC and $^{87}Sr/^{86}Sr$ ratio in the spring water.

^{14}C dating is used to evaluate young groundwater (MRT<100 years) containing bomb carbon in this chapter. However, it may not generally be the method of choice when other better methods are available (e.g. ^{3}H). The lumped-model is adapted and applied to date the spring samples with a range of ages. Calibration of initial ^{14}C activities is made based on $\delta^{13}C$-DIC. The time series of calculated ^{14}C activities and ^{14}C-DIC from spring samples are

interpreted by the EPM with exponential fraction of 0.75. The results show that the corrected groundwater MRTs of spring samples range from ≤10 year to 51 years. Their acceptance is verified by comparison with the ^{3}H distribution of spring samples. During the sampling period between 1970s and 2000s, the temporal trends of groundwater MRTs in nine selected springs were fairly stable, whilst there were gradual increases of the groundwater MRTs in other five selected springs where the temporal trends of groundwater MRTs is assumed to be influenced by the climate changes, especially the rainfall variability.

It is worth noting that effect of deep circulating groundwater on outflow of spring must be considered. The springs in the area along eastern edge of North-West and the Kuruman area in the Ghaap Plateau often contain the old groundwater with >10 years MRTs. An important role of deep groundwater in spring water should be clarified. In order to improve the understanding of effect of deep groundwater, further geochemical and isotopic data collection of borehole water sample would be necessary. The further investigation would include vertical distribution of groundwater MRTs in the area concerned.

Chapter 7

Summary and Recommendation

7.1 Summary

The flow theories on the Theis problem and transient confined-unconfined flow are investigated in this thesis. A new derivation of the Theis equation is given. A new analytical solution for the transient confined-unconfined flow induced by a fully penetrating well is developed. To improve the diagnostic analysis of pumping tests, a new drawdown derivative method based on a lg-lg derivative pattern, dlg*s*/dlg*t*, and the differentiation algorithm namely the Lagrange Interpolation Regression is presented. Practical application of hydrochemistry and environmental tracer tests to assess flow dynamics of hydrogeological systems is demonstrated via a case study in the dolomite aquifer of South Africa. Consequently, the main conclusions of the thesis are presented as follows.

Derivation of the Theis equation

This thesis proposed a new approach to derivation of the Theis equation by making use of Boltzmann transform. It does not only provide a theoretical mathematical treatment of this fundamental theory of hydraulic testing for aquifers, but also provide the hydrogeologists with a new perspective to understand the Theis solution and associated assumptions.

Analytical solution for transient confined-unconfined flow

The proposed new analytical solution provides a comprehensive understanding of the transient flow towards a fully penetrating well in a confined aquifer. The proposed analytical solution can be used to investigate the effect of the change of the hydraulic properties during the confined-unconfined conversion. Estimates of the distance of the conversion interface from the pumping well and the variable diffusivity in the unconfined region can be made by using the proposed analytical solution and a constant rate test.

The applicability of the proposed analytical solution is demonstrated by a comparison with the previous solutions, namely the MP and the Chen models. The comparison results also demonstrate the disadvantages of the use of the two previous models. The MP model is only

developed for the transient confined-unconfined flow with a constant transmissivity. The Chen model, given as a special case of the proposed model, is limited to the analysis of the transient confined-unconfined flow with a fixed diffusivity.

Derivative analysis of pumping tests

The new drawdown derivative analysis method based on the lg-lg derivative pattern, dlg*s*/dlg*t*, and the differentiation algorithm namely Lagrange Interpolation Regression (LIR) is certified to improve the applications (model identifications and parameter determinations) of the diagnostic analysis of constant rate tests with infinite conditions, variable discharge tests with infinite conditions, constant rate tests in bounded aquifers and tests involving double-porosity behaviours. An emphasis is placed on the conceptualization of the combined derivative plots of dlg*s*/dlg*t* and d*s*/dlg*t*. The proposed drawdown derivative method possesses certain advantages, over the traditional one using plot of d*s*/dlg*t* alone, as follows: (1) pumping and its following recovery periods in intermittent variable discharge tests can be identified in the plot of dlg*s*/dlg*t*; (2) storativity (*S*) of pumped aquifers can be evaluated using the combined derivative plot; and (3) quantitative analyses of dual-porosity behaviors can also be achieved. The advantages and disadvantages of the use of the LIR and the other methods in numerical differentiation of drawdown data are demonstrated via two practical case studies. The result indicates that the use of the LIR is preferred for derivative analysis of pumping tests as it can be used to effectively minimise noisy effects during numerical differentiation processes.

Flow dynamics of the dolomite spring system in South Africa

The flow dynamics of the dolomite spring system in South Africa is assessed by using a hydrogeochemistry and environmental isotope method. The recharge area is confirmed by use of the interpretation of hydrogeochemical types of the spring samples. In an example, the hilly area along the western edge of the Ghaap Plateau represented by limestone is identified as a main recharge area of the dolomite aquifer in the Ghaap Plateau. An important role of local rainfall in groundwater recharge is suggested by the low Na^+ and Cl^- measurements or $\delta^{18}O$ and δD measurements of the spring samples. A local meteoric water line (LMWL) based on$\delta^{18}O$ and δD values of spring samples is $\delta D=6.13X\delta^{18}O-0.97$.

To obtain the calibrated ^{14}C MRTs in the dolomite aquifer, the measurements of $\delta^{13}C$-DIC are used to evaluate the dissolution of carbonate mineral and assess the initial ^{14}C activities of the spring samples. The results imply that the spring samples have about 50% to 80% initial ^{14}C activities. Using a lumped-parameter model with the input of calibrated initial ^{14}C activities and time series of ^{14}C-DIC of the spring samples, the calibrated ^{14}C MRTs are given within a range from ≤ 10 to 50 years in the dolomite aquifer. The effect of rainfall on the temporal trend of groundwater MRTs and the groundwater flow circulation are also discussed for the possible management interventions in the dolomite aquifer.

7.2 Recommendation

Based on this study, a number of fields for future researches of interest are recommended,

1. The Boltzmann transform is used to solve partial differential equations with simply initial and boundary conditions, such as the Theis problem and the initial boundary-value problem on the transient confined-unconfined flow induced by an infinitesimal fully penetrating well in a confined aquifer, in the thesis. In future, the possibility of the use of the Boltzmann transform to solve complicated cases should be investigated.
2. For the analytical solution of transient confined-unconfined flow in a confined aquifer, the practical application of the proposed general analytical solution is not presented in this study. In future, some case studies should be conducted to investigate the accuracy and applicability of the proposed model in practice. Additionally, two interesting topics that deserve further research have also been highlighted in chapter 4. They are (1) the effect of the wellbore storage on the transient confined-unconfined flow and (2) the effect of the unsaturated flow on the transient confined-unconfined flow.
3. For the diagnostic analysis of pumping tests, the use of the combined derivative plot of dlg*s*/dlg*t* and d*s*/dlg*t* and Lagrange Interpolation Regression is made for the diagnostic analysis of pumping tests. However, there were only two case studies to demonstrate the practical applications of the purposed derivative analysis. In future, more case studies should be analyzed to investigate the disadvantage and advantage of the use of different derivative analysis methods in practice.

4. For the determination of groundwater age of a hydrogeological system, a novel application of ^{14}C techniques to date young groundwater (MRT<100 years) containing bomb carbon is attempted in the thesis. However, it may not generally be the method of choice when other better methods are available (e.g. tritium). Hence, the use of tritium to date the spring sample should be conducted to verify and calibrate the results from this study in the future study. Additionally, the effect of deep groundwater inflow on the spring water remains uncertain. An investigation on hydrogeochemical and isotopic data of the groundwater sample collected in a certain burial depth will be necessary. It will be helpful to understand the vertical distribution of groundwater MRT and assess the role of deep water inflow to the springs.

References

Adelana, S., Xu, Y.X., 2008. Impacts of land-use changes on a shallow coastal aquifer, South-Western Cape, South Africa. Proc. XXXVI Congress of the International Association of Hydrogeologists (IAH), 28 October - 2 November 2008, Toyama, Japan.

Adelana, S., Xu, Y.X., Vrbka, P., 2010. A conceptual model for the development and management of the Cape Flats aquifer, South Africa. Water SA 36(4): 461-474.Anderson, M.P., Woessner, W.W., 1992. Applied Groundwater Modeling. Academic Press, New York.

Bear, J., 1972. Dynamics of fluids in porous media. Elsevier, New York.

Beauheim, R.L., Pickens, J.F., 1986. Applicability of pressure derivative to hydraulic test analysis. Paper presented at poster session at the Annual Meeting of America Geophysical Union, Baltimore, Maryland.

Bethke, C.M., Johnson T.M., 2008. Groundwater age and groundwater age dating. Annual Review of Earth and Planetary Sciences 36:121–152.

Birkhoff, G., 1950. Hydrodynamics. Princeton University Press, Princeton.

Birsoy, Y.K., Summers, W., 1980. Determination of aquifer parameters from step tests and intermittent pumping data. Groundwater 18(2): 137–146.

Bourdet, D., 2002. Well Test Analysis: The Use of Advanced Interpretation Models. Elsevier, New York.

Bourdet, D., Ayoub, J., Pirard. Y., 1989. Use of pressure derivative in well test interpretation. SPE Formation Evaluation 4(2): 293–302.

Bourdet, D., Gringarten, A.C., 1980. Determination of fissure volume and block size in fractured reservoirs by type-curve analysis. Paper SPE 9293 Presented at the SPE Annual Technical Conference and Exhibition, Dallas, September 21–24.

Bourdet, D., Whittle, T., Douglas, A.A., Pirard Y.M., 1983. A new set of type curves simplifies well test analysis. World Oil 196(6): 95–106.

Bredenkamp, D.B., 2000. Groundwater monitoring: a critical review of groundwater monitoring in water resources evaluation and management. Pretoria. Water Research Commission, Report 838/1/00.

Bredenkamp, D.B., 2007. Use of natural isotopes and groundwater quality for improved

estimation of recharge and flow in dolomitic aquifers. Water SA 33(1): 87-94.

Bredenkamp, D.B., Botha, L.J., Esterhuyse, C., 1992. The geohydrology of the Kuruman eye and quantitative estimation of recharge and storativity of the aquifer. Pretoria. Department of Water Affairs and Forestry, Report GH3790.

Bredenkamp, D.B., Botha, L.J., van Tonder, G.J., 1995. Manual on Quantitative Estimation of Groundwater Recharge and Aquifer Storativity. Pretoria. Water Research Commission, Report TT 73/95.

Bredenkamp, D.B., Schutte, J.M., Du Toit, G.J., 1974. Recharge of a dolomitic aquifer as determined from tritium profiles. In: Isotope Techniques in groundwater Hydrology. IAEA, Vienna: 73-95.

Bredenkamp, D.B., Vogel, J.C., 1970. A study of a dolomitic aquifer with ^{14}C and tritium. In: Isotope Hydrology. IAEA, Vienna: 349-372.

Bredenkamp, D.B, Vogel, J.C., Wiegmans, F.E., Xu, Y.X., Janse van Rensburg H., 2007. Use of Natural Isotopes and Groundwater Quality for improving estimation of Recharge and Flow in Dolomitic Aquifers. Pretoria. Water Research Commission, Report KV177/07.

Brink, A.B.A ,1979. Engineering geology of southern Africa. Building Publications, Pretoria.

Cartwright, I., 2010. Using groundwater geochemistry and environmental isotopes to assess the correction of ^{14}C ages in a silicate-dominated aquifer system. Journal of Hydrology 382 (1–4): 174–187.

Cartwright, I., Weaverb, T., Petridesa, B., 2007. Controls on $^{87}Sr/^{86}Sr$ ratios of groundwater in silicate-dominated aquifers: SE Murray Basin, Australia. Chemical Geology 246 (1): 107–123.

Cassiani, G., Kabala, Z.J., Medina, M.A. Jr., 1999. Flowing partially penetrating well: solution to a mixed-type boundary value problem. Advances in Water Resources 23:59–68.

Chang, C.C., Chen, C.S., 2003. A flowing partially penetrating well in a finite-thickness aquifer: a mixed-type initial boundary value problem. Journal of Hydrology 271: 101 - 118.

Chen, Z.Y., Nie, Z.L., Zhang, Z.J., Qi, J.X., Nan, Y.J., 2005. Isotopes and sustainability of ground water resources, North China Plain. Groundwater 43 (4): 485–493.

Chow, V.T., 1952. On the determination of transmissibility and storage coefficients from pumping test data. Transactions, American Geophysical Union 33(3): 397–404.

Coetsiers, M., Walraevens, K., 2009. A new correction model for ^{14}C ages in aquifers with complex geochemistry – application to the Neogene Aquifer, Belgium. Applied Geochemistry 24(5): 768–776.

Cooper, H.H., Jacob., C.E., 1946. A generalized graphical method for evaluating formation constants and summarizing well field history. Transactions, American Geophysical Union 27(4): 526–534.

Darcy, H., 1856. Les Fontaines Publiques de la Ville de Dijon. Dalmont, Paris.

Debnath, L., 2004. Nonlinear Partial Differential Equations for Scientists and Engineers, 2nd ed. Birkhäuser, Boston, Massachusetts.

De Freitas, M.H., Wolmarans, J.F., 1978. Dewatering and settlement in the Bank Compartment of the far West Rand, South Africa. SAIMOS-78 Conference proceedings, Granada (Spain).

Djebbar, T., Kumar., A., 1980. Application of the p'D function to interference analysis. Society of Petroleum Engineers 32(4): 1465–1470.

Douglas, A.A., Osiensky J.L., Keller C.K., 2007. Carbon-14 dating of ground water in the Palouse Basin of the Columbia River basalts. Journal of Hydrology 334 (3): 502–512.

Duffield, G.M., 2007. AQTESOLV for Windows Version 4.0 Professional . Reston, Virginia: HydroSOLVE, Inc. Ehlig-Economides, C. 1988. Use of the pressure derivative for diagnosing pressure-transient behavior. Journal of Petroleum Technology 40(10): 1280–1282.

Ehlig-Economides, C., 1988. Use of the pressure derivative for diagnosing pressure-transient behavior. Journal of Petroleum Technology 40(10): 1280–1282.

Elango, K., Swaminathan, K., 1980. Finite-element model for concurrent confined–unconfined zones in an aquifer. Journal of Hydrology 46(3): 289–299.

Ferris, J.G., Knowles, D.B., Brown, R.H., Stallman, R.W., 1962. Theory of Aquifer Tests. US Geological Survey, Denver, Colorado.

Goode, D.J., 1997. Composite recovery type curves in normalized time from Theis' exact solution. Groundwater 35(4): 672–677.

Gosselin, D.C., Harvey, F.E., Frost, C., Stotler, R. Macfarlane, P.A., 2004. Strontium isotope geochemistry of groundwater in the central part of the Dakota (Great Plains) aquifer, USA.

Applied Geochemistry 19: 359–377.

Hantush, M.S., 1960. Modification of the theory of leaky aquifers. Journal of Geophysical Research. 65(11): 3713–3725.

Hermance, J.F., 1999. A Mathematical Primer on Ground Water Flow. Prentice Hall, Englewood Cliffs, New Jersey.

Hoque, M.A., Burgess, W.G., 2012. ^{14}C dating of deep groundwater in the Bengal Aquifer System, Bangladesh: Implications for aquifer anisotropy, recharge sources and sustainability. Journal of Hydrology 444: 209–220.

Horn, R.N., 1995. Modern Well Test Analysis: A Computer Aided Approach, 2nd ed. Petroway Inc, Palo Alto, California.

Hu, L., Chen, C., 2008. Analytical Methods for Transient Flow to a Well in a Confined-Unconfined Aquifer. Groundwater, 2008 46(4): 642–646.

Jacob, C.E., 1940. On the flow of water in an elastic artesian aquifer. Transactions of the American Geophysical Union 21: 574–586.

Johnson, M.R., Anhaeusser, C.R., Thomas, R.J., 2006. The geology of South Africa. Council for Geoscience, Johannesburg.

Jones, C.E., Jenkyns, H.C., 2001. Seawater strontium isotopes, Oceanic Anoxic Events, and seafloor hydrothermal activity in the Jurassic and Cretaceous. American Journal of Science 301: 112-149.

Karasaki, K.J., Long, C.S., Witherspoon, P.A., 1988. Analytical models of slug tests. Water Resources Research 24(1): 115–126.

Kazemi, A.G., Lehr, J.H., Perrochet, P., 2008. Groundwater Age. Wiley-Interscience, New York.

Kazemi, H., Seth, M.S., Thomas, G.W., 1969. The interpretation of interference tests in naturally fractured reservoirs with uniform fracture distribution. Society of Petroleum Engineers 9(4): 463–472.

Klaus, J.S., Hansen, B.T., Baupeng, S., 2007. $^{87}Sr/^{86}Sr$ ratio: a natural tracer to monitor groundwater flow paths during artificial recharge in the Bangkok area, Thailand. Hydrogeology Journal 15: 745–758.

Konikow, L.F, 2001. Use of numerical models to simulate groundwater flow and transport, in

Environmental Isotopes in the Hydrological Cycle: Principles and Applications, Modeling, vol. 6, edited by W. G. Mook, 75–116, Int. At. Energy Agency, Vienna.

Kronfeld, J., Vogel, J.C., Talma, A.S., 1994. A new explanation for extreme $^{234}U/^{238}U$ disequilibria in a dolomitic aquifer. Earth and Planetary Science Letters 123(1): 81-93.

Kruseman, G.P., Ridderna, D.E., 1991. Analysis and Evaluation of Pumping Test Data, 2nd ed. International Institute for Land Reclamation and Improvement, Wageningen, the Netherland.Le Gal La Salle, C., Marlin, C., Leduc, C., Taupin, J.D., Massault M., Favreau G., 2001. Renewal rate estimation of groundwater based on radioactive tracers (^{3}H, ^{14}C) in an unconfined aquifer in a semi-arid area, Iullemeden Basin, Niger. Journal of Hydrology 254 (1): 145–156.

Li, W.H., 1972. Differential Equations of Hydraulic Transients, Dispersion, an Ground Water Flow. Prentice Hall, Englewood Cliffs, New Jersey.

Lo áciga, H.A., 2009. Derivation approaches for the Theis (1935) equation. Groundwater 48(1): 2–5.

Maloszewski, P., Zuber, A., 1993. Principles and practice of calibration and validation of mathematical models for the interpretation of environmental tracer data. Advances in Water Resources 16: 173–190.

Maloszewski, P., Zuber, A., 1996. Lumped parameter models for the interpretation of environmental tracer data. In: Manual on Mathematical Models in Isotope Hydrogeology. TECDOC-910. IAEA, Vienna, Austria: 9–58.

Maloszewski, P., Stichler W., Zuber, A., 2004. Interpretation of environmental tracers in groundwater systems with stagnant water zones. Isotopes in Environmental and Health Studies 40(1): 21-23.

Maloszewski, P., Zuber, A., 1998. A general lumped parameter model for the interpretation of tracer data and transit time calculation in hydrologic systems (Journal of Hydrology 179 (1996) 1–21), comments. Journal of Hydrology 204 (1–4), 297–300.Masoodi, R., Ghanbari, R.N., 2012. Comment of “Derivation of the Theis (1935) equation by substitution”. Groundwater 50(1): 7–8.

Mathias, S.A., Butler, A.P., 2006. Linearized Richards’ equation approach to pumping test analysis in compressible aquifers. Water Resources Research 42: W06408.

Mattar, L., Zaoral, K., 1992. The primary pressure derivative (PPD) – A new diagnostic tool in well test interpretation. Journal of Canadian Petroleum Technology 4: 63–70.

McConnell, C.L., 1993. Double porosity well testing in the fractured carbonate rocks of the Ozarks. Groundwater 31(1): 75–83.

Meijering, E., 2002. A chronology of interpolation: From ancient astronomy to modern signal and image processing. Proceedings of the IEEE 90(3): 319–342.

Mishra, P., Vesselinov, V., Kuhlman, K., 2012. Saturated-unsaturated flow in a compressible leaky-unconfined aquifer. Advances in Water Resources 42; 62-70.

Moench, A.F., 2008. Analytical and numerical analyses of an unconfined aquifer test considering unsaturated zone characteristics. Water Resources Research 44: W06409.

Moench, A.F., Prickett, T.A., 1972. Radial flow in an infinite aquifer undergoing conversion from artesian to water table conditions. Water Resources Research 8(2): 494–499.

Mokrik, R., Mažeika, J., Baublytė, A., Martma, T., 2008. The groundwater age in the Middle–Upper Devonian aquifer system, Lithuania. Hydrogeology Journal 17 (4): 871–889.

Mook, W.G., 2000. Environmental isotopes in the hydrological cycle: principles and applications. IAEA, Vienna.

Muennich, K.O., 1957. Messung des ^{14}C-Gehaltes von hartem Grundwasser. Naturwissenschaften 34:32–3.

Muennich, K.O., 1968. Isotopen-Datierung von Grundwasser. Naturwissenschaften 55:158–63.

Neuman, S.P., 1972. Theory of flow in unconfined aquifers considering delayed response of the water table. Water Resources Research 8(4): 1031–1045.

Nwankwor, G.I., Gillham R.W., van der Kamp G., Akindunni F.F., 1992. Unsaturated and saturated flow in response to pumping of an unconfined aquifer: field evidence of delayed drainage. Groundwater 30(5): 690–700.

Ostrowski, L.P., Kloska, M.B., 1989. Use of pressure derivatives in analysis of slug test or DST flow period data. Society of Petroleum Engineers 18595: 13–23.

Partridge, T.C., 1985. Spring flow and tufa accretion. In: Tobias, P.V. (editors). Hominid Evolution: Past, Present and Future. Alan R. Liss Inc, New York: 171-188.

Pearson, F.J., Hanshaw, B.B., 1970. Sources of dissolved carbonate species in groundwater and their effects on carbon-14 dating. In: Isotope Hydrology, Proceedings, IAEA, 1978. IAEA, Wien.

Perina, P., 2010. Derivation of the Theis (1935) equation by substitution. Groundwater 48(1): 6–7.

Renard, P., 2005. The future of hydraulic tests. Hydrogeology Journal 13(1): 259–262.

Renard, P., Glenz, D., Mejias, M., 2009. Understanding diagnostic plots for well-test interpretation. Hydrogeology Journal 17(3): 1–12.

Rosewwarne, P.N, 2006. Groundwater Resource Assessment: Dolomite Aquifer. Pretoria. Department of Water Affairs and Forestry, Report P RSA C000/00/4406/06.

Rushton, K.R., Wedderburn, L.A., 1971. Aquifers changing between the confined and unconfined state. Groundwater 9(5): 30–38.

Samani, N., Pasandi, M., Barry, D.A., 2006. Characterizing a heterogeneous aquifer by derivative analysis of pumping and recovery test data. Journal of Geological Society of Iran 1: 29–41.

Spane, J.F., Wurstner, S., 1993. DERIV: A computer program for calculating pressure derivatives for use in hydraulic test analysis. Groundwater 31(5): 814–822.

Springer, A.E., Bair, E.S., 1992. Comparison of methods used to delineate capture zones of wells: 2. Stratified-drift buried-valley aquifer. Groundwater 30(6): 908–917.

Stewart, MK., 2012. A 40-year record of carbon-14 and tritium in the Christchurch groundwater system, New Zealand: Dating of young samples with carbon-14. Journal of Hydrology 430: 50–68.

Stoner, J.D., 1981. Horizontal anisotropy determined by pumping in Two Powder rivernbasin coal aquifers, Montana. Groundwater 19(1): 34–40.

Talma, A.S., Bredenkamp, D.B., 1985. Isotope work on the Transvaal Dolomites. Groundwater 1985. Pretoria. Geological Society of South Africa.

Talma, A.S., Vogel J.C., 2001. Isotopic and Chemical signatures of water in the Transvaal Dolomite springs. Pretoria. Water Research Commission, CSIR Report ENV-PC-2001/040.

Tamers, M.A., 1975. The validity of radiocarbon dates on groundwater. Geophys. Surv. 2: 217–239.

Tartakovsky, G.D., Neuman S.P., 2007. Three-dimensional saturated–unsaturated flow with an axial symmetry to a partially penetrating well in a compressible unconfined aquifer. Water Resources Research 43: W01410.

Theis, C.V., 1935. The relation between the lowering of the piezometric surface and the rate and duration of discharge of a well using ground-water storage. Transactions, American Geophysical Union 16: 519–524.

Van Rensburg H.J., 1995. Management of Southern African aquifers. Ph D. Thesis. University of the UOFS.

Van Tonder, G., Kunstmann, H., Xu, Y., Fourie, F., 2000. Estimation of the sustainable yield of a borehole including boundary information, drawdown derivatives and uncertainty propagation, Calibration and reliability in groundwater modeling. In Proceedings of ModelCARE 99 Conference held in Zurich, Switzerland. IAHS Publ. No 265, 2000.Verhagen, B.T., Smith, P.E., McGeorge, I. et al., 1979. Groundwater studies in the Gamagara catchment. Report to the Water Research Commission. Johannesburg. University of the Witwatersrand.

Verruijt, A., 1982. The Theory of Groundwater Flow, 2nd ed. MacMillan Press, Hong Kong.

Vogel, J.C., 1993. Variability of carbon isotope fractionation during photosynthesis. In Stable Isotopes and Plant Carbon-Water Relations. Academic Press, California.

Walton, W.C., 1964. Future water-level declines in deep sandstone wells in Chicago region. Groundwater 2(1): 13–20.

Wang, X.S., Zhan, H.B., 2009. A new solution of transient confined–unconfined flow driven by a pumping well. Advances in Water Resources 32(8): 1213-1222.

Warren, J.E., Root, P.J., 1963. The behavior of naturally fractured reservoirs. Society of Petroleum Engineers 3: 245–255.

Winde, P., Erasmus, E. P., 2011. Peatlands as Filters for Polluted Mine Water?—A Case Study from an Uranium-Contaminated Karst System in South Africa. Part I: Hydrogeological Setting and U Fluxes. Water 2011 3(1): 291-322.

Xiao, L., Xu, Y.X., 2014. Diagnostic Analysis of Pumping Tests Using Derivative of dlgs/dlgt with Case Study. Groundwater 52(S1): 208–217.

Zuber, A., 1986a. Mathematical models for the interpretation of environmental radioisotopes

in groundwater systems. In: Fritz, P., Fontes, J.Ch. (Eds.), Handbook of Environmental Isotope Geochemistry. Elsevier, Amsterdam: 1–59.

Zuber, A., 1986b. On the interpretation of tracer data in variable flow systems. Journal of Hydrology 86: 45–57.

Zuber, A., Maloszewski, P., 2000. Lumped parameter models. In: Mook, W.G. (Ed.), Environmental Isotopes in the Hydrological Cycle Principles and Applications. IAEA and UNESCO, Vienna: 5–35.

Appendix A Derivation processes of the analytical solution of the transient unconfined flow

Recall the mathematical model of the unconfined flow is as follow

$$\frac{\partial^2 s_1'}{\partial r^2} + \frac{1}{r}\frac{\partial s_1'}{\partial r} = \frac{S_y}{K_r h_0}\frac{\partial s_1'}{\partial t} \tag{A1a}$$

$$\lim_{r\to o} \pi K_r r \frac{\partial s_1'}{\partial r} = -Q \tag{A1b}$$

$$s_1'(R,t) = 0 \tag{A1c}$$

$$s_1'(r,0) = 0 \tag{A1d}$$

A similarity transform is introduced based on the principles of similarity solutions of Eq. (A1a) (see Eq. 8.11.12ab in Dehath (2004)) as follows,

$$v(\eta) = s_1' t^{-\frac{\gamma}{\beta}} \tag{A2a}$$

$$\eta = r t^{-\frac{\alpha}{\beta}} \tag{A2b}$$

where $v(\eta)$ is the similarity item of s_1' and t. η is the similarity item of r and t. α, β and γ are the fixed constants. Applying Eqs. (A2a) and (A2b), the three terms in Eq. (A1a) are rewritten with the independent variable η as follow,

$$\frac{\partial s_1'}{\partial r} = t^{\left(\frac{\gamma}{\beta}-\frac{1}{2}\right)}\frac{\partial v}{\partial \eta} \tag{A3a}$$

$$\frac{\partial^2 s_1'}{\partial r^2} = t^{\left(\frac{\gamma}{\beta}-1\right)}\frac{\partial^2 v}{\partial \eta^2} \tag{A3b}$$

$$\frac{\partial s_1'}{\partial t} = -\frac{\alpha}{\beta} r t^{\left(\frac{\gamma}{\beta}-\frac{\alpha}{\beta}-1\right)}\frac{\partial v}{\partial \eta} + \frac{\gamma}{\beta} v(\eta) t^{\left(\frac{\gamma}{\beta}-1\right)} \tag{A3c}$$

It is assumed that $\beta = 2\alpha$ and $\gamma = 0$ according to the Boltzmann transform (Debnath, 2004). Eqs. (A1a)-(A1c) are regenerated as

$$\frac{\partial^2 v}{\partial \eta^2} + \left(\frac{1}{\eta} + \frac{S_y}{2K_r h_0}\eta\right)\frac{\partial \mathrm{v}}{\partial \eta} = 0 \tag{A4a}$$

$$\lim_{\eta\to 0} \eta \frac{\partial v}{\partial \eta} = -\frac{Q}{\pi K_r} \tag{A4b}$$

$$v(\eta_R) = 0 \tag{A4c}$$

$$v(0) = 0 \tag{A4d}$$

where η_R is defined as $Rt^{-\frac{1}{2}}$. After separating variables and integrating Eq. (A4a), an expression of $\frac{\partial v}{\partial \eta}$ is given as

$$\frac{\partial v}{\partial \eta} = \frac{D}{\eta} \exp\left(-\frac{S_y \eta^2}{4K_r h_0}\right) \tag{A5}$$

where *D* is the integration constant. Applying Eq. (A4b), *D* is found as $-\frac{Q}{2\pi K_r}$. Hence, Eq. (A5) is captured as

$$\frac{\partial v}{\partial \eta} = -\frac{Q}{\pi K_r \eta} \exp\left(-\frac{S_y \eta^2}{4K_r h_0}\right) \tag{A6}$$

And integrating again, a general solution of $v(\eta)$ is given as

$$v(\eta) = -\int_0^{\eta} \frac{Q}{\pi K_r k} \exp\left(-\frac{S_y \eta^2}{4K_r h_0}\right) \mathrm{d}k + B \tag{A7}$$

where *k* is the variable of integration, *B* is the integration constant. Considering the boundary condition as Eq. (A4c), *B* is expressed as

$$B = \int_0^{\eta_R} \frac{Q}{\pi K_r k} \exp\left(-\frac{S_y \eta^2}{4K_r h_0}\right) \mathrm{d}k \tag{A8}$$

Combining Eq. (A7) with Eq. (A8) yields that

$$v(\eta) = -\int_0^{\eta} \frac{Q}{\pi K_r k} \exp\left(-\frac{S_y \eta^2}{4K_r h_0}\right) \mathrm{d}k + \int_0^{\eta_R} \frac{Q}{2\pi K_r k} \exp\left(-\frac{S_y \eta^2}{4K_r h_0}\right) \mathrm{d}k \tag{A9}$$

Letting $U = \frac{S_y k^2}{4K_r h_0}$, Eq. (A9) is given as

$$v(\eta) = \frac{Q}{2\pi K_r}\left[\int_{\frac{S_y \eta^2}{4K_r h_0}}^{\infty} \frac{\exp(-U)}{U} \mathrm{d}U - \int_{\frac{S_y \eta_R{}^2}{4K_r h_0}}^{\infty} \frac{\exp(-U)}{U} \mathrm{d}U\right] \tag{A10}$$

Considering Eqs. (A2a) and (A10), the final function of s_1' is given as

$$s_1'(r,t) = \frac{Q}{2\pi K_r}\left[W\left(\frac{S_y r^2}{4K_r h_0 t}\right) - W\left(\frac{S_y R^2}{4K_r h_0 t}\right)\right] \tag{A11}$$

Using the relationship $s_1'(r,t) = b^2 - h_1(r,t)^2$ to Eq. (A11) yields Eq. (4.6) as

$$h_1(r,t)^2 = b^2 - \frac{Q}{2\pi K_r}\left[W\left(\frac{S_y r^2}{4K_r h_0 t}\right) - W\left(\frac{S_y R^2}{4K_r h_0 t}\right)\right] \tag{A12}$$

Appendix B Derivation processes of the analytical solution of the transient confined flow

Recall Eqs. (4.7a)-(4.7c) are

$$\frac{\partial^2 s_2'}{\partial r^2} + \frac{1}{r}\frac{\partial s_2'}{\partial r} = \frac{S}{K_r b}\frac{\partial s_2'}{\partial t} \tag{B1a}$$

$$s_2'(r \to \infty, t) = 0 \tag{B1b}$$

$$s_2'(R, t) = h - b \tag{B1c}$$

A continuity of flow at the conversion interface in two- dimension is given as Eq. (4.3) as

$$\frac{\partial h_1'(r,t)}{\partial r}|_{r=R} = \frac{\partial h_2'(r,t)}{\partial r}|_{r=R} \tag{B2}$$

The solution of $\frac{\partial h_1'(r,t)}{\partial r}$ is given by using Eq. (A12) as

$$\frac{\partial h_1'(r,t)}{\partial r} = \frac{Q}{2\pi K_r h_1' r}\exp\left(-\frac{S_y r^2}{4K_r h_0 t}\right) \tag{B3}$$

Substituting Eqs. (B3), (4.1c) and the relationship $s_2'(r,t) = h - h_2(r,t)$ in Eq. (B2) yields that

$$r\frac{\partial s_2'(r,t)}{\partial r}|_{r\to R} = -\frac{Q}{2\pi K_r b}\exp\left(-\frac{S_y R^2}{4K_r h_0 t}\right) \tag{B4}$$

By using the same derivation process of Eqs. (A4a)-(A4c), the similar transform version of Eqs. (B1a)-(B1c) and (B4) are generated as

$$\frac{\partial^2 v}{\partial \eta^2} + \left(\frac{1}{\eta} + \frac{S}{2K_r b}\eta\right)\frac{\partial v}{\partial \eta} = 0 \tag{B5a}$$

$$v(\eta \to \infty) = 0 \tag{B5b}$$

$$v\left(\eta_R = Rt^{-\frac{1}{2}}\right) = h - b \tag{B5c}$$

$$\eta\frac{\partial v}{\partial \eta}|_{\eta\to\eta_R} = -\frac{Q}{2\pi K_r b}\exp\left(-\frac{S_y R^2}{4K_r h_0 t}\right) \tag{B5d}$$

Separating variables and integrating Eq. (B5a) produces an expression of $\frac{\partial v}{\partial \eta}$ as

$$\frac{\partial v}{\partial \eta} = \frac{D}{\eta}\exp\left(-\frac{S\eta^2}{4K_r b}\right) \tag{B6}$$

where *D* is the integration constant. Applying Eq. (B5d), *D* is found as

$$D = -\frac{Q}{2\pi K_r b}\frac{\exp\left(-\frac{S_y R^2}{4K_r h_0 t}\right)}{\exp\left(-\frac{S\eta_R{}^2}{4K_r b}\right)} \tag{B7}$$

Integrating Eq. (B6) yields a general solution as

$$v(\eta) = \int_0^{\eta} \frac{D}{k}\exp\left(-\frac{Sk^2}{4K_r b}\right)\mathrm{d}k + B \tag{B8}$$

where k is the variable of integration, B is the integration constant. Limiting Eq. (B8) to Eq. (B5b) obtains

$$0 = \int_0^{\infty} \frac{D}{k}\exp\left(-\frac{Sk^2}{4K_r b}\right)\mathrm{d}k + B \tag{B9}$$

$$B = -\int_0^{\infty} \frac{D}{k}\exp\left(-\frac{Sk^2}{4K_r b}\right)\mathrm{d}k \tag{B10}$$

Combining Eq. (B10) with Eq. (B8) gives that

$$v(\eta) = -\int_{\eta}^{\infty} \frac{D}{k}\exp\left(-\frac{Sk^2}{4K_r b}\right)\mathrm{d}k \tag{B11}$$

Substituting a new item defined as $U = \frac{Sk^2}{4K_r b}$ and Eq. (B7) in Eq. (B11) yields that

$$v(\eta) = \frac{Q}{4\pi K_r b}\frac{\exp\left(-\frac{S_y R^2}{4K_r h_0 t}\right)}{\exp\left(-\frac{S\eta_R{}^2}{4K_r b}\right)}\int_{\frac{S\eta^2}{4K_r b}}^{\infty}\frac{\exp(-U)}{U}\mathrm{d}U \tag{B12}$$

Application of Eq. (B5c) and Eqs. (A2a)-(A2b) to Eq. (B12) produces

$$s_2'(r,t) = \frac{Q}{4\pi K_r b}\frac{\exp\left(-\frac{S_y R^2}{4K_r h_0 t}\right)}{\exp\left(-\frac{SR^2}{4K_r bt}\right)}\int_{\frac{Sr^2}{4K_r bt}}^{\infty}\frac{\exp(-U)}{U}\mathrm{d}U \tag{B13}$$

Substituting the relationship $s_2'(r,t) = h - h_2(r,t)$ in Eq. (B13) produces Eq. (4.8)

$$h_2(r,t) = h - \frac{Q}{4\pi K_r b}\frac{\exp\left(-\frac{S_y R^2}{4K_r h_0 t}\right)}{\exp\left(-\frac{SR^2}{4K_r bt}\right)}W\left(\frac{Sr^2}{4K_r bt}\right) \tag{B14}$$

Appendix C Derivation processes of the MP model

Introducing a new item as $s_1'(r,t) = b - h_1(r,t)$, Eqs. (4.13a)-(4.13c) are rewritten as

$$\frac{\partial^2 s_1'}{\partial r^2} + \frac{1}{r}\frac{\partial s_1'}{\partial r} = \frac{S_y}{K_r b}\frac{\partial s_1'}{\partial t} \tag{C1a}$$

$$\lim_{r\to o} 2\pi K_r b r \frac{\partial s_1'}{\partial r} = -Q \tag{C1b}$$

$$s_1'(R,t) = 0 \tag{C1c}$$

$$s_1'(r,0) = 0 \tag{C1d}$$

A similarity transform is introduced based on the principles of similarity solutions of Eq. (C1a) (see Eq. 8.11.12ab in Dehath (2004)) as follows,

$$v(\eta) = s_1' t^{-\frac{\gamma}{\beta}} \tag{C2a}$$

$$\eta = r t^{-\frac{\alpha}{\beta}} \tag{C2b}$$

where $v(\eta)$ is the similarity function with s_1' and t. η is the similarity parameter of r and t. α, β and γ are the fixed constants. Applying Eqs. (C2a) and (C2b), the three terms in Eq. (C1a) are rewritten with the independent variable η as follow,

$$\frac{\partial s_1'}{\partial r} = t^{\left(\frac{\gamma}{\beta}-\frac{1}{2}\right)}\frac{\partial v}{\partial \eta} \tag{C3a}$$

$$\frac{\partial^2 s_1'}{\partial r^2} = t^{\left(\frac{\gamma}{\beta}-1\right)}\frac{\partial^2 v}{\partial \eta^2} \tag{C3b}$$

$$\frac{\partial s_1'}{\partial t} = -\frac{\alpha}{\beta} r t^{\left(\frac{\gamma}{\beta}-\frac{\alpha}{\beta}-1\right)}\frac{\partial v}{\partial \eta} + \frac{\gamma}{\beta} v(\eta) t^{\left(\frac{\gamma}{\beta}-1\right)} \tag{C3c}$$

It is assumed that $\beta = 2\alpha$ and $\gamma = 0$ according to the Boltzmann transform (Debnath, 2004). Eqs. (C1a)-(C1c) are regenerated as

$$\frac{\partial^2 v}{\partial \eta^2} + \left(\frac{1}{\eta} + \frac{S_y}{2K_r b}\eta\right)\frac{\partial \mathrm{v}}{\partial \eta} = 0 \tag{C4a}$$

$$\lim_{\eta\to 0} \eta \frac{\partial v}{\partial \eta} = -\frac{Q}{2\pi K_r b} \tag{C4b}$$

$$v(\eta_R) = 0 \text{ for } \eta_R = R t^{-\frac{1}{2}} \tag{C4c}$$

After separating variables and integrating Eq. (C4a), an expression of $\frac{\partial v}{\partial \eta}$ is given as

$$\frac{\partial v}{\partial \eta} = \frac{D}{\eta} \exp\left(-\frac{S_y \eta^2}{4K_r b}\right) \tag{C5}$$

where D is the integration constant. Applying Eq. (C4b), D is found as $-\frac{Q}{2\pi K_r}$. Hence, Eq. (C5) is captured as

$$\frac{\partial v}{\partial \eta} = -\frac{Q}{\pi K_r \eta} \exp\left(-\frac{S_y \eta^2}{4K_r b}\right) \tag{C6}$$

And integrating again, a general solution of $v(\eta)$ is given as

$$v(\eta) = -\int_0^{\eta} \frac{Q}{2\pi K_r b k} \exp\left(-\frac{S_y \eta^2}{4K_r b}\right) \mathrm{d}k + B \tag{C7}$$

where k is the variable of integration, B is the integration constant. Considering the boundary condition as Eq. (C4c), B is expressed as

$$B = \int_0^{\eta_R} \frac{Q}{2\pi K_r b k} \exp\left(-\frac{S_y \eta^2}{4K_r b}\right) \mathrm{d}k \tag{C8}$$

Combining Eq. (C7) with Eq. (C8) yields that

$$v(\eta) = -\int_0^{\eta} \frac{Q}{2\pi K_r b k} \exp\left(-\frac{S_y \eta^2}{4K_r b}\right) \mathrm{d}k + \int_0^{\eta_R} \frac{Q}{2\pi K_r b k} \exp\left(-\frac{S_y \eta^2}{4K_r b}\right) \mathrm{d}k \tag{C9}$$

Letting $U = \frac{S_y k^2}{4K_r b}$, Eq. (C9) is given as

$$v(\eta) = \frac{Q}{4\pi K_r b}\left[\int_{\frac{S_y \eta^2}{4K_r b}}^{\infty} \frac{\exp(-U)}{U} \mathrm{d}U - \int_{\frac{S_y \eta_R{}^2}{4K_r b}}^{\infty} \frac{\exp(-U)}{U} \mathrm{d}U\right] \tag{C10}$$

Considering Eqs. (C2a) and (C10), the final function of s_1' is given as

$$s_1'(r,t) = \frac{Q}{4\pi K_r b}\left[W\left(\frac{S_y r^2}{4K_r b t}\right) - W\left(\frac{S_y R^2}{4K_r b t}\right)\right] \tag{C11}$$

Using the relationship $s_1'(r,t) = b - h_1(r,t)$ to Eq. (C11) yields Eq. (4.16) as

$$h_1 = b - \frac{Q}{4\pi K_r b}\left[W\left(\frac{S_y r^2}{4Tt}\right) - W\left(\frac{S_y R^2}{4Tt}\right)\right] \tag{C12}$$

For the transient confined flow, introducing a new item as $s_2'(r,t) = h - h_2(r,t)$, Eqs. (4.15a)-(4.15c) and (4.17) are rewritten as

$$\frac{\partial^2 s_2'}{\partial r^2} + \frac{1}{r}\frac{\partial s_2'}{\partial r} = \frac{S}{K_r b}\frac{\partial s_2'}{\partial t} \tag{C13a}$$

$$s_2'(r \to \infty, t) = 0 \tag{C13b}$$

$$s_2'(R,t) = h - b \tag{C13c}$$

$$r\frac{\partial s_2'(r,t)}{\partial r}|_{r\to R} = -\frac{Q}{2\pi K_r b}\exp\left(-\frac{S_y R^2}{4Tt}\right) \tag{C13d}$$

By using the same derivation process of Eqs. (C4a)-(C4c), the similar transform version of Eqs. (C13a)-(C13d) are generated as

$$\frac{\partial^2 v}{\partial \eta^2} + \left(\frac{1}{\eta} + \frac{S}{2K_r b}\eta\right)\frac{\partial v}{\partial \eta} = 0 \tag{C14a}$$

$$v(\eta \to \infty) = 0 \tag{C14b}$$

$$v\left(\eta_R = Rt^{-\frac{1}{2}}\right) = h - b \tag{C14c}$$

$$\eta\frac{\partial v}{\partial \eta}|_{\eta\to\eta_R} = -\frac{Q}{2\pi K_r b}\exp\left(-\frac{S_y R^2}{4K_r bt}\right) \tag{C14d}$$

Separating variables and integrating Eq. (C14a) produces an expression of $\frac{\partial v}{\partial \eta}$ as

$$\frac{\partial v}{\partial \eta} = \frac{D}{\eta}\exp\left(-\frac{S\eta^2}{4K_r b}\right) \tag{C15}$$

where *D* is the integration constant. Applying Eq. (C14d), *D* is found as

$$D = -\frac{Q}{2\pi K_r b}\frac{\exp\left(-\frac{S_y R^2}{4K_r bt}\right)}{\exp\left(-\frac{S\eta_R^2}{4K_r b}\right)} \tag{C16}$$

Integrating Eq. (C15) yields a general solution as

$$v(\eta) = \int_0^\eta \frac{D}{k}\exp\left(-\frac{Sk^2}{4K_r b}\right)\mathrm{d}k + B \tag{C17}$$

where *k* is the variable of integration, *B* is the integration constant. Limiting Eq. (C17) to Eq. (C14b) obtains

$$0 = \int_0^\infty \frac{D}{k}\exp\left(-\frac{Sk^2}{4K_r b}\right)\mathrm{d}k + B \tag{C18}$$

$$B = -\int_0^\infty \frac{D}{k}\exp\left(-\frac{Sk^2}{4K_r b}\right)\mathrm{d}k \tag{C19}$$

Combining Eq. (C19) with Eq. (C17) gives that

$$v(\eta) = -\int_\eta^\infty \frac{D}{k}\exp\left(-\frac{Sk^2}{4K_r b}\right)\mathrm{d}k \tag{C20}$$

Substituting a new item defined as $U = \frac{Sk^2}{4K_r b}$ and Eq. (C16) in Eq. (C20) yields that

$$v(\eta) = \frac{Q}{4\pi K_r b} \frac{\exp\left(-\frac{S_y R^2}{4K_r bt}\right)}{\exp\left(-\frac{S\eta_R{}^2}{4K_r b}\right)} \int_{\frac{S\eta^2}{4K_r b}}^{\infty} \frac{\exp(-U)}{U} \mathrm{d}U \tag{C21}$$

Application of Eq. (C14c) and Eqs. (C2a)-(C2b) to Eq. (C21) produces

$$s_2'(r,t) = \frac{Q}{4\pi K_r b} \frac{\exp\left(-\frac{S_y R^2}{4K_r bt}\right)}{\exp\left(-\frac{SR^2}{4K_r bt}\right)} \int_{\frac{Sr^2}{4K_r bt}}^{\infty} \frac{\exp(-U)}{U} \mathrm{d}U \tag{C25}$$

Substituting the relationship $s_2'(r,t) = h - h_2(r,t)$ in Eq. (C25) produces Eq. (4.18) as

$$h_2(r,t) = h - \frac{Q}{4\pi K_r b} \frac{\exp\left(-\frac{S_y R^2}{4Tt}\right)}{\exp\left(-\frac{SR^2}{4Tt}\right)} W\left(\frac{Sr^2}{4Tt}\right) \tag{C26}$$

Appendix D Introduction of Excel program for diagnostic analysis of pumping tests

The Excel program is designed to automate the diagnostic analysis of pumping tests by use of combined derivative plots of dlgs/dlgt and ds/dlgt. The differentiation algorithms, Lagrange Interpolation Regression (LIR) and Least Square Regression (LSR), are implemented for numerical differentiation of drawdown data in the Excel program.

Interface

The Excel program includes two sheets: (1) adjusted time calculation and (2) derivative analysis. The sheet of adjusted time calculation is used to calculate the adjusted time of pumping tests.

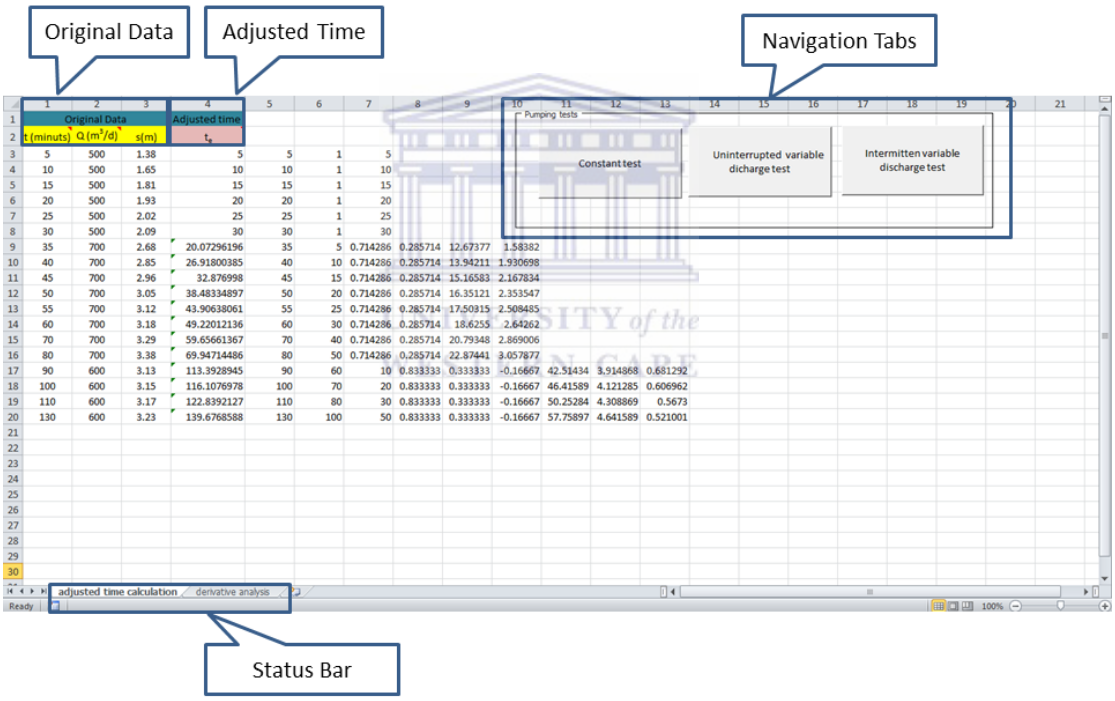

The interface of the sheet of adjusted time calculation is composed of three components:

1. Original Data: Data input of the pumping test; these data include the pumping time (t, *minutes*), pumping rate (Q, m^3/d) and drawdown data (s, *m*).
2. Navigation Tabs: Access to derivative analysis windows of different pumping tests; these pumping tests are constant test, uninterrupted variable discharge test and intermittent variable discharge test.
3. Adjusted Time: Data output of the calculation results of adjusted time.

The sheet of derivative analysis is applied to calculate numeric derivative values and determine the parameters of the pumping aquifer.

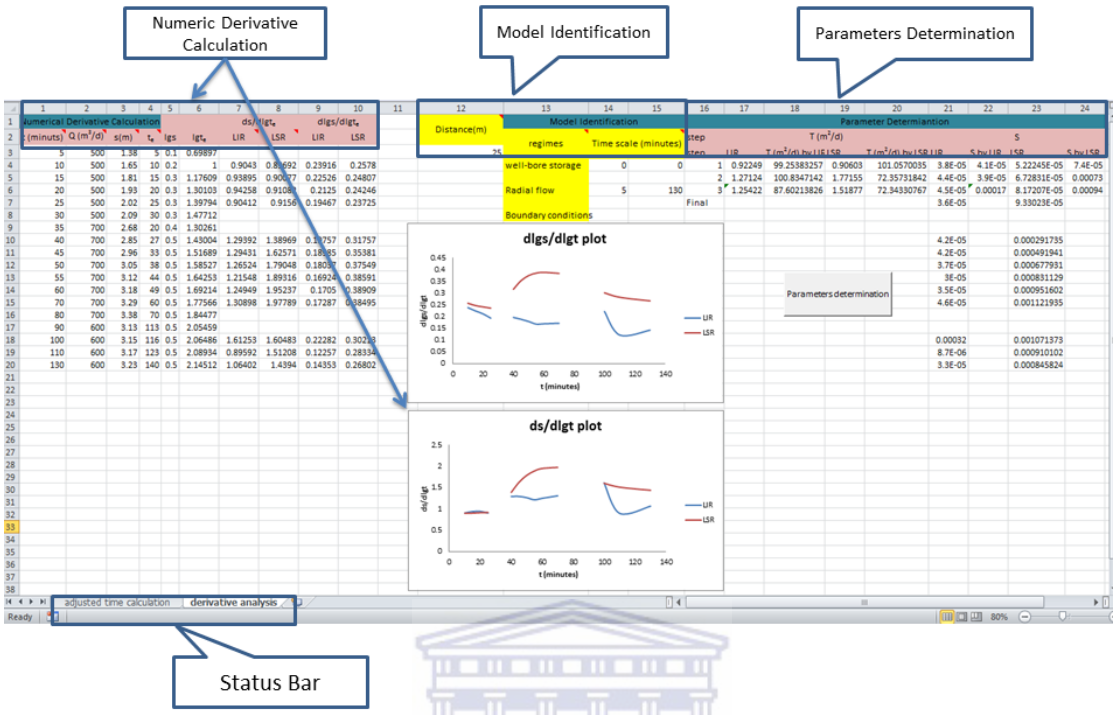

The interface of the sheet of derivative analysis consists of three components:

1. Numeric Derivative Calculation: Data output of the derivative patterns (dlgs/dlgt and ds/dlgt) by use of differentiation algorithms (LIR and LSR).
2. Model Identification: Identification of flow regimes by the user; the flow regimes include the wellbore storage, the radial flow and the boundary condition.
3. Parameters Determination: Calculation of the pumped aquifer parameters; the aquifer parameters are transmissivity (m^2/d) and storativity.

Procedures

To gain the diagnostic analyses of the pumping tests by means of the Excel program, the procedures are done as follows:

1. Data collection: Input the original data of a pumping test in the adjusted time calculation sheet.
2. Simulation process: Select and click an appropriate Navigation Tab for the pumping test.
3. Simulation results:

(1) Input the distance between the pumping and the observation wells.

(2) Identify the flow regimes and input the time scale of each flow regime by the user subjectively.

(3) Click “parameter determination” button to calculate the parameters (transmissivity and storativity) of the pumped aquifer.

Appendix E Geochemical compositions and isotopes of spring samples

Area	Spring name	Ca (mg/L)	Cl (mg/L)	DMS (mg/L)	EC (mS/m)	Mg (mg/L)	Na (mg/L)	pH (macro)	SO_4 (mg/L)	TAL ($mgCaCO_3/L$)	$\delta^{18}O$ (‰SMOW)	δD (‰SMOW)	$\delta^{13}C$ (‰PMB)	$\delta^{14}C$(Pmc) Before 2007	$\delta^{14}C$(Pmc) 2007	$^{87}Sr/^{86}Sr$	Tritium (TU)
Far East to Far West Rand	GMB	75.7	31	580	78.1	43.5	23.6	8	137	209	-2.95	-17.5	-9.9	73.48	76.6	0.72702	0 ±0.2
	TFI	82	49.7	671	89.5	44.7	42.6	8.2	163	228	-2.61	-16.6	-9.3	N/A	92.8	N/A	1.8±0.3
	TFU	80.9	40.3	650	84.7	41.9	39.3	8.1	152	233	-2.75	-16.5	-9.1	88.82	89.8	0.731785	1.4±0.2
North-West	BUF	56.9	5.4	435	51.2	32.8	4.8	8	11.8	264	-3.86	-24.4	-12.7	90.68	83.9	0.725464	0.8±0.2
	DKL	57.4	6.5	455	53.5	35.4	4.2	8.3	5.7	276	-4.64	-28.4	-11.7	N/A	96.9	0.730162	0.8±0.2
	DKU	46.6	4.9	382	44.8	28.5	4.5	8.1	6.5	233	-4.69	-28.8	-9.2	85.54	86.2	0.72926	1.3±0.2
	KLU	29.1	5.1	230	27.7	16.2	4	8.2	<4	141	-5.27	-33	-8.6	N/A	80.1	N/A	0.6±0.2
	MME	33.6	4.3	255	30.7	18.1	3	8.3	<4	157	-5.15	-31.9	-8.4	N/A	86.1	N/A	0.4±0.2
	MOL	45.2	4.7	357	41.1	24.6	4.3	8.4	6.2	220	-4.77	-28.3	-8.1	82.07	88.3	0.722284	1 ±0.2
	OLV	71.5	7.8	538	62	39.6	4.5	8.2	10.3	328	-3.36	-21.2	-8.4	107.9	102.4	0.722511	1.4±0.2
	RNF	50.6	12.1	396	48.3	27.8	7.4	8.2	10.6	230	-4.85	-31	-8.6	N/A	76.4	0.739861	0.6±0.2
	SBL	55.2	7.8	422	49.5	31	4.1	8.3	12.3	254	-3.76	-24.1	-10.5	91.06	95.4	0.727084	1 ±0.2
	TFL	53.6	5.5	404	46	29.2	4.6	8.4	4.8	249	-4.36	-28	-9.8	92.33	63.3	0.730805	1.7±0.2
	TWU	43.2	6.6	337	39.9	23.7	3.9	8.3	5.2	205	-4.57	-27.7	-8.1	87.02	102.7	0.726934	1.7±0.2
	WGD	60.9	7.1	470	53.4	34.3	5.1	8.4	9.3	288	-3.77	-23.4	-9.3	N/A	96.3	0.722834	1.2±0.2
	WGT	64.6	6.5	497	57.6	39.2	4.9	8.4	8.3	303	-2.76	-18.1	N/A	99.62	N/A	0.722667	2.4±0.4
	ELF	29	4.9	226	26.7	16	3.3	8	<4	134	-3.84	-23.1	-10.1	N/A	66.7	0.724354	0.4±0.2
	ERR	24.1	4.3	181	22.2	13.3	2.2	8	4.9	107	-4.16	-26	-7.8	53.95	65.1	0.724965	0.2±0.2
	GFR	24.2	<4	182	24.1	14	2.3	8.1	<4	110	-4.1	-25.1	-10	85.45	63.4	0.721806	0.9±0.2
	PFL	48.6	22.4	378	49	27.4	11	8.1	12.1	197	-3.2	-18.7	-10.9	80.2	80.7	0.726856	3.2±0.3
	PFU	43.5	8.3	346	41.4	25.4	5.6	8.1	6	205	-3.32	-20.8	-11.1	74.24	77.7	0.727444	2.2±0.3

	STF	43.2	11.6	365	46.7	28.4	6.2	8	18.9	193	-3.17	-19.9	-10.2	79.15	80.3	0.72739	2.2±0.3
	MAL	27.1	5.6	207	26.2	15.4	2.2	8.2	<4	125	-4.56	-27.3	-10	56.29	57.2	0.741761	0.5±0.2
	MRB	48.1	5.6	371	44.2	27	3.7	8.1	<4	228	-4.48	-28.2	-9.4	N/A	74.4	0.732865	0.1±0.2
	SSS	65.1	6.7	487	57	35.1	4.3	7.5	<4	293	-4.08	-27.5	-7	95.74	90.8	N/A	0.8±0.2
	BPO	41	8	256	31.8	11.2	6.6	8.2	9.1	145	-5.95	-38.2	-12.1	N/A	76.4	N/A	0.2±0.2
Ghaap Plateau	GKO	76.4	9.2	480	55.8	28.3	4.8	8.3	4.9	278	-5.89	-38.6	-11.1	N/A	98.9	0.719926	1.8±0.3
	KRF	20	6.4	141	19.4	8	4.5	8.1	10	72	-5.97	-38.9	-11.2	N/A	44.7	N/A	0.7±0.2
	KU1	53.7	6.3	326	38.2	17.6	6.1	8.3	5.4	189	-6.13	-38.9	-10.8	70.46	72.8	0.723462	0.5±0.2
	KU2	53.6	6.3	382	44.6	23.5	5.9	8.3	6.2	228	-5.94	-38	-8.8	81.3	83.8	0.722248	0.7±0.2
	MAY	68.8	10.2	487	56.7	36.5	4.7	8.4	5.2	288	-5.1	-35.2	-10	102.1	104.4	0.720427	1.7±0.3
	TBN	77.7	38.7	888	103.1	93.4	15	7.9	39	504	-2.42	-18.6	-11.6	N/A	110.3	N/A	2.4±0.3
	VKF	74.3	10	541	64.4	39.7	4.3	8.2	11.1	311	-4.54	-28.7	-10.6	N/A	99.8	0.720094	2.9±0.3

Appendix F Groundwater ^{14}C MRTs of spring samples using the EPM with *f=0.75*

Area		Spring name	Uncorrected MRT(years)	Pearson model			Tamer model				Former results*
				$\delta^{13}C$ (‰)	Dilution factor	Corrected MRT(years)	CO_2 (mmol/L)	HCO_3^{-1} (mmol/L)	Dilution factor	Corrected MRT(years)	MRT(years)
Far East to Far West Rand		Gerrit Minnebron	66.67	-7.63	0.58	16.9	0.43	4.18	0.55	12.0	22
		Turffontein Spring upper	51.67	-8.7	0.59	13.7	1.08	4.66	0.56	≤10	17.3
North-West	Western Region	Buffelshoekoog	50.08	-9.30	0.72	18.8	0.54	5.14	0.55	≤10	11.6
		Olievendraai spring	36.08	-8.05	0.62	≤10	1.71	6.81	0.60	≤10	8.6
		Molopo Spring	55.08	-6.68	0.51	≤10	0.22	4.43	0.52	≤10	21.9
		Stinkhoutboom Spring lower	51.33	-9.25	0.72	28.8	1.35	5.31	0.61	≤10	10.1
		Tweefontein lower	50.08	-9.02	0.69	17.5	N/A	5.11	N/A	N/A	N/A
		Tweefontein upper	55.33	-6.67	0.51	≤10	0.34	3.95	0.54	≤10	N/A
		Welgedachtoog	45.17	-9.03	0.69	≤10	N/A	5.81	N/A	N/A	N/A
		Dinokane upper eye	55.75	-7.80	0.60	≤10	0.27	4.85	0.53	≤10	12.5
		Schoonspruit southern eye	43	-6.32	0.49	≤10	0.43	5.86	0.53	≤10	12.2
	Eastern Region	Erasmus Rietvlei	83.25	-7.87	0.61	51.7	0.22	2.2	0.54	41.4	20.3
		Grootfontein Rietvlei	37.42	-9.95	0.78	25.6	0.11	2.46	0.52	≤10	12.7
		Pretoria Fountains lower eye	67.75	-8.88	0.66	33.0	0.54	3.77	0.56	15	16.8
		Pretoria Fountains upper eye	58.83	-8.91	0.70	31.0	0.54	3.73	0.58	11.6	18.3
		Sterkfontein Spring	61.33	-7.80	0.62	17.0	0.54	3.5	0.56	12	18.8
		Maloneys eye	82.75	-7.81	0.60	45.1	0.11	2.5	0.52	32.4	16.1
Ghaap Plateau		Kuruman Spring A	72.08	-8.78	0.68	40.4	1.71	3.78	0.66	37.4	22.4
		Kuruman Spring B	58.08	-9.23	0.70	27.1	0.22	4.30	0.52	≤10	27.3
		Manyeding Spring	41.67	-7.28	0.56	13.0	0.34	5.76	0.53	≤10	7.43

*the former results were presented in Bredenkamp (2007) and Bredenkamp et al. (2007).

Appendix G Introduction of Excel program for lumped-parameter models of groundwater dating

The Excel program is designed to automatically implement the lumped-parameter models. The Excel program includes two patterns: (1) Data input and (2) Lumped-parameter model.

Interface

The interface of the sheet of Data input is composed of four components:

1. Description of Box Model: Introduce the functions of the Excel program;
2. Input Data: The input data includes time series of the background values and the observation values of the tracer of groundwater samples.
3. Data Update: Copy the input data source automatically to the rest worksheets;
4. Navigation Tabs: Access to analysis windows of different lumped-parameter models; these lumped-parameter models are Piston flow model, Exponential flow model, Dispersion model and Exponential-piston flow model.

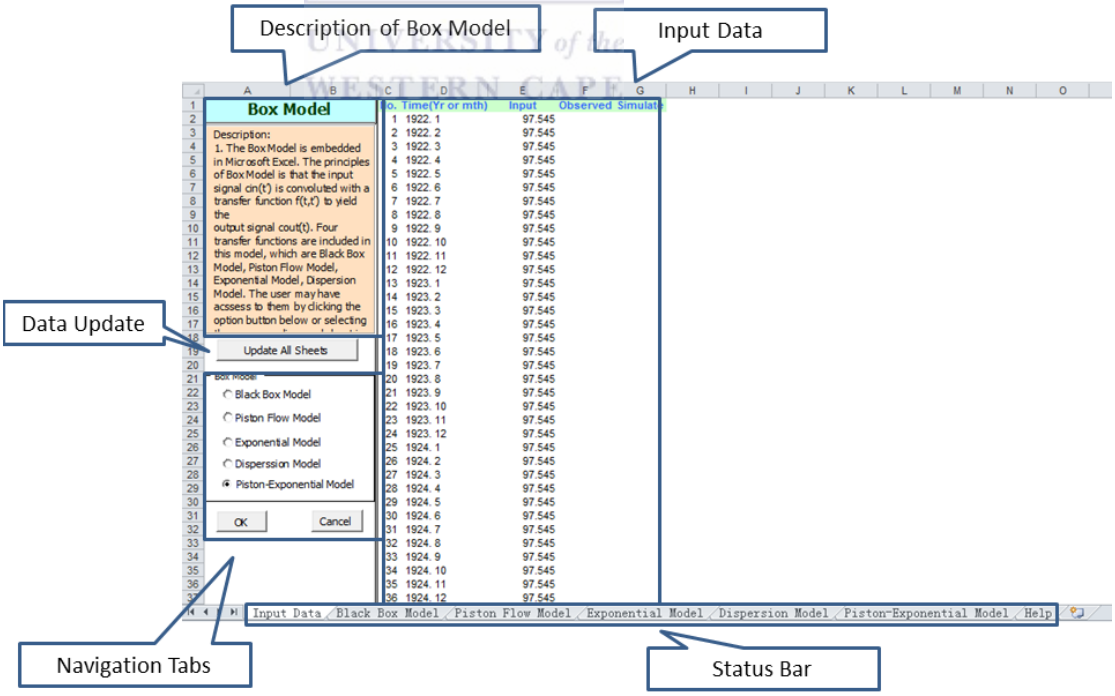

The interface of the sheet of Lumped-parameter model consists of four components:

1. Description of a selected Lumped-parameter Model.

2. Input Parameters: Parameters input by the user subjectively. The common parameters include the average transit time of the tracer (Tau), the start point of the simulation (Start No) and the decay coefficient of the tractor (Lamda). Two special parameters are the ratio of the total volume to the volume with the exponential distribution of transient time for the Exponential-piston flow model (*f*) and the dispersion coefficient for the Dispersion model (Delta).
3. Output Data: Output the simulation results of the tracer series and the mean square error of the observation values and the simulation results.
4. Function Buttons: These function buttons include
   (1) Calculation: Calculate the model simulation of the time series of the tracer according to the average transit time of the tracer (Tau) provided subjectively by the user;
   (2) Clear results: Delete the output of the simulation results;
   (3) Graph: Plot of the input data source versus the simulation results;
   (4) Optimize: Calculate the model simulation of the time series of the tracer automatically and provide an optimized average transit time of the tracer (Tau) based on the principle of minimal mean square error control.

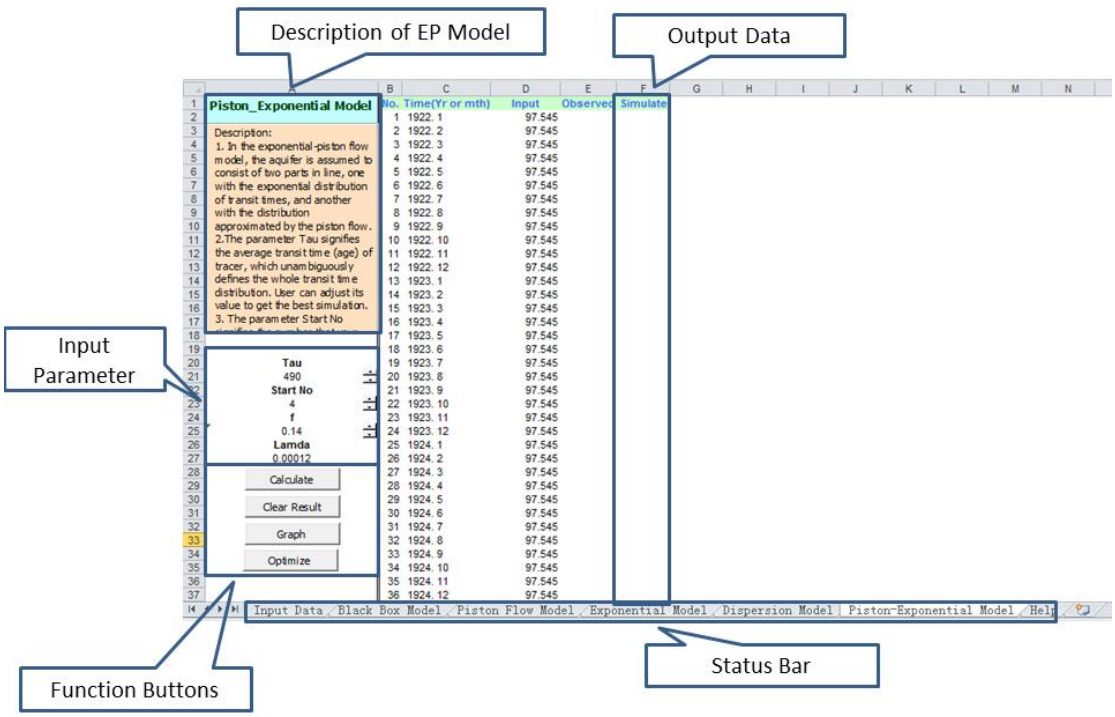

Procedures

To obtain an optimized simulation result of groundwater age by using the Excel program, the procedures are done as follows:

1. Data Collection: Input time series of tracer measurements of groundwater samples in the sheet of Data input.
2. Simulation Process:
   (1) Click ‘Update All Sheets’;
   (2) Select an appropriate lumped-parameter model in the Navigation Tabs. Click ‘OK’ button in the sheet of Data input;
   (3) Input required parameters in the sheet of the selected lumped-parameter model.
3. Simulation results:
   (1) Click ‘Optimize’ button to calculate simulation results of tracer series and optimized groundwater age (Tau);
   (2) Click ‘Graph’ button to produce plot of input data sources versus simulation results.

Appendix H Publication

Groundwater

Methods Note/

Diagnostic Analysis of Pumping Tests Using Derivative of dlg*s*/dlg*t* with Case Study

by Liang Xiao[1] and Yongxin Xu[2]

Abstract

Diagnostic derivative interpretation of drawdown data from pumping tests is discussed in this paper. An emphasis is placed on the conceptualization of derivative term of dlg*s*/dlg*t*. Use of a combined plot of dlg*s*/dlg*t* and d*s*/dlg*t* is made to identify various flow patterns from variable discharge tests with infinite conditions, constant rate tests in bounded aquifers, and tests involving double porosity, which can be used to further characterize the aquifer. Compared with the standard derivative method (d*s*/dlg*t*), the combined derivative analysis of dlg*s*/dlg*t* and d*s*/dlg*t* of drawdown behaviours possesses certain advantages identified as follows: (1) the plot of dlg*s*/dlg*t* is strikingly sensitive for use in unveiling differences between pumping and recovery periods in a variable discharge test; (2) storativity (S) of pumped aquifers can be accurately evaluated by the combined plot; and (3) a quantitative assessment of double porosity behaviour can also be achieved. Based on applied case studies, Lagrange Interpolation Regression (LIR) is recommended for numerical derivative calculation. Advantages and disadvantages of LIR and traditional methods are demonstrated via a selected case study. The result of the case study confirms that LIR is a preferred method for numerical derivative calculation as it can be used to effectively minimise noisy effect during derivative processes. The proposed derivative approach provides the hydrologists with an additional tool for characterizing pumped aquifers.

Introduction

Derivative interpretations of pressure data recorded during aquifer tests have been used to characterize pumped aquifers for many years. The conventional derivative analysis, d*s*/dlg*t*, is described by conceptual methodologies and computerized methods. Two types of applications of the derivative analysis were highlighted as (1) model identification and (2) parameter determination (Mattar and Zaoral 1992; Van Tonder et al. 2000; Renard 2005; Renard et al. 2009). The model identification is facilitated by diagnostic plot of the drawdown derivative. The drawdown derivative proved to be highly sensitive to changes in drawdown behaviours that are difficult to be observed on a drawdown curve alone. The drawdown derivative plot was first introduced as an aid for interpreting dynamic drawdown data from an artesian aquifer by Chow (1952). But Chow's method was limited to the interpretation of drawdown data with Theis' solution. Even since that, much useful work had been done, particularly in petroleum industry. This work employed pressure derivative analysis to improve an understanding of aquifer tests and to provide a description of different hydrogeological formations during constant rate and its following recovery tests (Djebbar and Kumar 1980; Bourdet et al. 1983, 1989; Beauheim and Pickens 1986; Ehlig-Economides 1988; McConnell 1993; Spane and Wurstner 1993; Horn 1995; Goode 1997; Renard 2005; Samani et al. 2006). These hydrogeological formations included inner boundaries (wellbore-storage), outer boundaries (inflow and no-flow), and various flow regimes (radial flow). The parameter determination was a specialized analysis of pumped aquifer properties during specific flow regimes. The derivative plot of d*s*/dlg*t* was used in place of the conventional semi-lg drawdown plot for the determination of transmissivity (Chow 1952; Bourdet

[1]Department of Earth Sciences, University of the Western Cape, Private Bag X17, Bellville, Cape Town, South Africa.
[2]Corresponding author: Department of Earth Sciences, University of the Western Cape, Private Bag X17, Bellville, Cape Town, South Africa; +27 82 7769612; fax: +27 21 9593118; yxu@uwc.ac.za

Received May 2013, accepted December 2013.

doi: 10.1111/gwat.12175

et al. 1989; Spane and Wurstner 1993) based on accurate identification of radial flows in a constant rate test.

An important aspect of performing derivative analysis is the selection of an appropriate calculation method to eliminate negative effects from "noise" data (Bourdet et al. 1983, 1989; Spane and Wurstner 1993). Bourdet (2002) recommended using adjacent points (nearest neighbours) for preliminary derivative analysis. To remove noise from the calculations, the Bourdet method used data points separated by a fixed distance measured in logarithmic time. Typically, the separation or differentiation interval required to remove noise ranges between 0.1 and 0.5 of a logarithm cycle. Spane and Wurstner (1993) presented an alternative method for computing derivatives. Like the Bourdet method, the Spane method used a logarithmic differentiation interval. However, instead of using three points in the derivative computation, the Spane method computed the left and right derivatives by applying linear regression to all the points falling within the differentiation interval. Based on these derivative algorithms, the software *AQTESOLV* (Duffield 2007) is used to perform simultaneous matching of any type-curve solution to both drawdown and derivative data.

In this paper, a lg-lg (lg stands for logarithm to the base 10) drawdown derivative, $\mathrm{dlg}s/\mathrm{dlg}t$, is proposed for diagnostic analysis of variable discharge tests with infinite conditions, constant rate tests in bounded aquifers, and tests involving double porosity. Transmissivity (T) and storativity (S) of a pumped aquifer and parameters for a double porosity system can be determined by a comprehensive derivative analysis. A new differentiation algorithm is introduced to prevent noisy data from being cumulative during the derivative calculation process. The advantages and disadvantages of the derivative techniques of this differentiation algorithm are also discussed.

Methodology

Derivative Plot for a Variable Discharge Test

Practically, aquifers are sometimes pumped at variable rates instead of a constant rate (Kruseman and Ridderna 1991). There are two general types of variable discharge tests: (1) uninterrupted variable discharge tests and (2) intermittent variable discharge tests. For uninterrupted variable discharge tests, an aquifer is continuously pumping at different discharge rates. For intermittent variable discharge tests, it involves a series of discharge and recovery phases. Adjusted time functions (t_e) based on deconvolution algorithms were introduced for drawdown expression of variable discharge tests by Birsoy and Summers (1980). The drawdown derivative is taken with respect to the logarithm of the adjusted time to the base 10, $\lg t_e$, in this paper.

A wellbore storage effect, defined as physical water storage in a well or borehole deviating from an ideal line sink, appears at early pumping time. This effect may last from a few seconds to many minutes, depending on the storage capacity of the well. According to the analytical solution presented by Spane and Wurstner (1993), drawdown and its logarithmic expression during the wellbore storage period can be written as

$$s = \frac{Q_1 t_e}{\pi r_c^2} \tag{1}$$

$$\lg s = lgt_e + \lg \frac{Q_1}{\pi r_c^2} \tag{2}$$

where s is the drawdown in the well, r_c is the stress well casing radius, and t_e is the adjusted time defined by Birsoy and Summers (1980).

A drawdown derivative of $\mathrm{dlg}s/\mathrm{dlg}t_e$ during the storage effect stage is found by noting that

$$\frac{\mathrm{dlg}s}{\mathrm{dlg}t_e} = 1 \tag{3}$$

After the wellbore storage effect is over, a radial flow will be expected for an ideal homogenous and isotropic aquifer. The drawdown expression proposed by Birsoy and Summers (1980) for the discharge and recovery period is as follows.

$$s_i = \frac{2.3Q_i}{4\pi T} \lg (ct_e) \tag{4}$$

where c is either $2.25T/r^2S$ for the discharge period or 1 for the recovery period (Cooper and Jacob 1946) and r is the distance from pumping well. Hence, logarithm of S_i with respect to logarithm of t_e is given as

$$\lg s_i = \lg \frac{2.3Q_i}{4\pi T} + \lg \left[\lg (ct_e)\right] \tag{5}$$

For a pumping period, the expressions of drawdown derivative, $\mathrm{d}s_i/\mathrm{dlg}t_e$ and $\mathrm{dlg}s_i/\mathrm{dlg}t_e$, for the radial flow can be written as

$$\frac{\mathrm{d}s_i}{\mathrm{dlg}t_e} = \frac{2.3Q_i}{4\pi T} \tag{6}$$

$$\frac{\mathrm{dlg}s_\mathrm{i}}{\mathrm{dlg}t_e} = \frac{1}{\ln\left(\frac{2.25T}{r^2S}t_e\right)} \tag{7}$$

The conventional application of derivative analysis during the radial flow is to evaluate properties of pumped aquifers, namely T (transmissivity) and S (storativity). Based on Equations 6 and 7, T and S are calculated as follows:

$$T = \frac{2.3Q_i}{4\pi \frac{\mathrm{d}s_i}{\mathrm{dlg}t_e}} \tag{8}$$

$$S = \frac{5.2Q_i t_e}{4\pi r^2 \frac{\mathrm{d}s_i}{\mathrm{dlg}t_e} * \exp\left(\frac{\mathrm{dlg}t_e}{\mathrm{dlg}s_\mathrm{i}}\right)} \tag{9}$$

In each pumping period, there is a T value generated based on a mean $\mathrm{d}s_i/\mathrm{dlg}t_e$ value using Equation 8. A mean value of the all T results over all pumping periods is

defined to be the T value of a pumped aquifer. For S value determination, an evaluated S value series in Equation 9 is given for points of interest in radial flows based on $ds_i/d\lg t_e$ and $d\lg s_i/d\lg t_e$ values; similarly, a mean value of the evaluated S series is assumed to be the S value of the pumped aquifer.

For a recovery period, the derivative formulas of $ds_i/d\lg t_e$ and $d\lg s_i/d\lg t_e$ can be assigned in a similar approach:

$$\frac{ds_i}{d\lg t_e} = \frac{2.3Q_i}{4\pi T} \tag{10}$$

$$\frac{d\lg s_i}{d\lg t_e} = \frac{1}{\ln t_e} \tag{11}$$

From Equation 10, T value can also be estimated in the recovery period as

$$T = \frac{2.3Q_i}{4\pi \frac{ds_i}{d\lg t_e}} \tag{12}$$

Figure 1 depicts the conceptual derivative plots of $d\lg s_i/d\lg t_e$ for both uninterrupted variable discharge and intermittent variable discharge tests. Characteristic behaviours can be identified in the derivative plots of $d\lg s_i/d\lg t_e$. Constant derivative plots of $d\lg s_i/d\lg t_e$ for wellbore storage effect are placed on straight lines with $d\lg s_i/d\lg t_e$ values equal to 1 in early time as pumping test starts. When the radial flow segments are attained, the derivative plots of $d\lg s_i/d\lg t_e$ are described as Equations 7 and 11 in discharge and recovery periods, respectively, while $ds_i/d\lg t_e$ values over a pumping and its following recovery periods lie along a same straight line as seen in Equations 6 and 10. It is indicated that the plot of $d\lg s_i/d\lg t_e$ is better fitted to distinguish pumping and recovery periods in an intermittent variable discharge test. Parameters (T and S values) of pumped aquifers can be evaluated during the radial flow segments by using Equations 8 and 9.

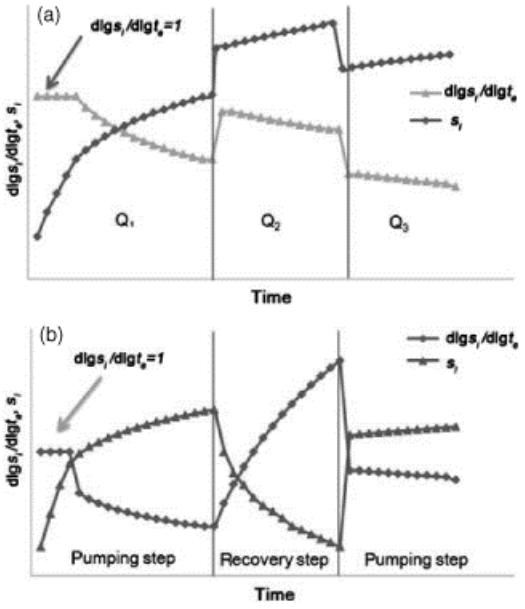

Figure 1. (a) Conceptual drawdown curve and $d\lg s_i/d\lg t_e$ plot of an uninterrupted variable discharge test; (b) conceptual drawdown curve and $d\lg s_i/d\lg t_e$ plot of an intermittent variable discharge test.

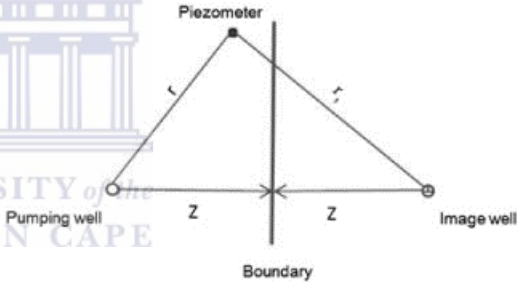

Figure 2. Conceptual image system under single boundary condition (after Ferris et al. 1962). The drawdown in piezometer is the discharging results from both pumping and image wells.

Derivative Plot for an Aquifer Boundary

In addition to obtaining aquifer parameters, another conventional application of drawdown derivative plots is to identify boundary conditions when a pumping test is conducted in a bounded aquifer. The boundary effects may occur at late time of the test as pumping proceeds. Stallman (Ferris et al. 1962) put forward a curve-fitting method of analyzing pumping tests in aquifers that has one or more straight boundaries. The real bounded system is replaced by an imaginary system including a pumping well, a piezometer, and a series of image wells. Drawdown, s, in a piezometer can be generalized according to Stallman method (Ferris et al. 1962) as

$$s = \frac{2.3Q}{4\pi T} W(u, r_{r1\to n}) \tag{13}$$

where $s_d = 2.3QW(u)/(4\pi T)$ is the drawdown from discharging well; $s_r = 2.3QW(r_{r1\to n})/(4\pi T)$ is the drawdown from image well; $r_{r1\to n}$ is a ratio equal to r_i/r; r is the distance between the piezometer and the real discharging well; r_i is the distance between the piezometer and ith image well.

Figure 2 shows an image system for a single boundary system. Under one recharge boundary condition, the drawdown in piezometer can be expressed as

$$s = \frac{2.3Q}{4\pi T}\left[\lg\left(\frac{2.25Tt}{r^2S}\right) - \lg\left(\frac{2.25Tt}{r_{r1}^2 r^2 S}\right)\right] \tag{14}$$

In this regime, the drawdown derivatives are characterized as

$$\frac{ds}{d\lg t} = 0 \tag{15}$$

$$\frac{d\lg s}{d\lg t} = 0 \tag{16}$$

For a single barrier boundary system, the drawdown in the piezometer is

$$s = \frac{2.3Q}{4\pi T}\left[\lg\left(\frac{2.25Tt}{r^2S}\right) + \lg\left(\frac{2.25Tt}{r_{r1}^2 r^2 S}\right)\right] \tag{17}$$

The derivatives of drawdown and logarithm drawdown are

$$\frac{ds}{d\lg t} = 2 * \frac{2.3Q}{4\pi T} \tag{18}$$

$$\frac{d\lg s}{d\lg t} = \frac{2 * 0.4343}{\lg\left(\frac{1}{r_{r1}^2}\right) + 2 * \lg\left(\frac{2.25Tt}{r^2 S}\right)} \tag{19}$$

Similar to the case of one boundary system, an image system for an aquifer with two boundaries at right angle to each other is assumed to have a pumping well and three image wells; an image system for an aquifer with two parallel boundaries is constructed by a pumping well and seven image wells (Ferris et al. 1962). The drawdown derivative patterns for a pumping test in an aquifer with two boundaries are described in Table 1.

As mentioned above, different drawdown derivative plots represent different boundary conditions. Under single- or two-barrier boundary condition, uses of both $ds/d\lg t$ and $d\lg s/d\lg t$ plots are adopted for barrier boundary identifications. For plots of $ds/d\lg t$, derivative patterns for different barrier boundary conditions can be simply explained as integer factors of that of radial flows immediately before boundary effect dominations, which are shown in Equation 20 and Table 1:

$$\frac{ds}{d\lg t} = n * \frac{2.3Q}{4\pi T} \tag{20}$$

For plots of $d\lg s/d\lg t$, derivative patterns for different barrier boundary systems can be given as follows:

$$\frac{d\lg s}{d\lg t} = \frac{n * 0.4343}{\lg\left(\frac{1}{\prod_{i=2}^{n} r_{r(i-1)}^2}\right) + n * \lg\left(\frac{2.25Tt}{r^2 S}\right)} \tag{21}$$

where n is the number of pumping and image wells in an image system in Equations 20 and 21.

The values of $ds/d\lg t$ and $d\lg s/d\lg t$ are both equal to 0 whenever recharge boundary is involved during pumping test (Table 1).

Table 1
Drawdown Derivative Patterns for Two Boundaries Condition Systems

Boundary Conditions System		$ds/d\lg t$	$d\lg s/d\lg t$
Two boundaries at right angle to each other	One barrier and one recharge boundary	0	0
	Two barrier boundaries	$4 * \frac{2.3Q}{4\pi T}$	$f(4)$[1]
	Two recharge boundaries	0	0
Two parallel boundaries	One barrier and one recharge boundary	0	0
	Two barrier boundaries	$8 * \frac{2.3Q}{4\pi T}$	$f(8)$[1]
	Two recharge boundaries	0	0

[1] $f(n) = \frac{n*0.4343}{\lg\left(\frac{1}{\prod_{i=2}^{n} r_{r(i-1)}^2}\right) + n*\lg\left(\frac{2.25Tt}{r^2 S}\right)}$, where n is the number of pumping and image wells in an image system.

Derivative Plot for a Dual Porosity Aquifer

One frequently encountered flow response of pumping tests in fractured rock is dual porosity behavior. In this case, a fractured reservoir consists of two media: the matrix and the fractures, which can be represented by an equivalent homogeneous dual porosity system (Warren and Root 1963). Kazemi et al. (1969) extended uses of the drawdown equations developed by Warren and Root (1963) for pumped wells to drawdown expression in observation wells. A semi-lg drawdown plot of a constant rate test in a double porosity aquifer, as shown in Figure 3, is revealed as two parallel straight lines connected by a transitional pattern.

Figure 3 also shows the conceptual derivative plot of $d\lg s/d\lg t$ for double porosity behavior. Two radial flow patterns, one of fracture system at early times ($t < t_1$) and one of fracture-matrix system at late times ($t > t_2$), are established in the plot of $d\lg s/d\lg t$. Recall

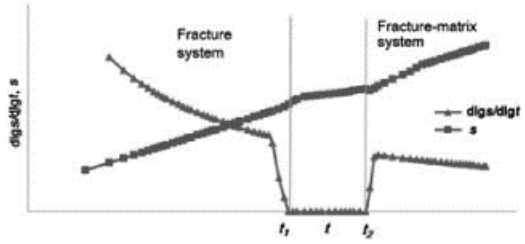

Figure 3. Conceptual drawdown and derivative curves of $d\lg s/d\lg t$ for double porosity behavior without wellbore storage on a semi-lg scale.

the expression of drawdown response (s) presented by Kazemi et al. (1969) for fracture system at early time is

$$s = \frac{2.3Q}{4\pi T_f} \lg \frac{2.25T_f t}{r^2 S_f} \tag{22}$$

$$\lg s = \lg \frac{2.3Q}{4\pi T_f} + \lg \left[\lg \left(\frac{2.25T_f t}{r^2 S_f} \right) \right] \tag{23}$$

where T_f is effective transmissivity of the fracture and S_f is storativity of the fracture. Based on Equations 22 and 23, the derivatives of drawdown for early times are written as

$$\frac{\mathrm{d}s}{\mathrm{dlg}t} = \frac{2.3Q}{4\pi T_f} \tag{24}$$

$$\frac{\mathrm{dlg}s}{\mathrm{dlg}t} = \frac{1}{\ln \left(\frac{2.25T_f t}{r^2 S_f} \right)} \tag{25}$$

According to Equations 24 and 25, the effective transmissivity of the fracture (T_f) and the storativity of the fracture (S_f) are expressed as

$$T_f = \frac{2.3Q}{4\pi \frac{\mathrm{d}s}{\mathrm{dlg}t}} \tag{26}$$

$$S_f = \frac{5.2Qt}{4\pi r^2 \frac{\mathrm{d}s}{\mathrm{dlg}t} * \exp \left(\frac{\mathrm{dlg}t}{\mathrm{dlg}s} \right)} \tag{27}$$

At late time, the drawdown expression can be given for a fracture-matrix system as

$$s = \frac{2.3Q}{4\pi T_f} \lg \frac{2.25T_f t}{r^2 \left(S_f + \beta S_m \right)} \tag{28}$$

$$\lg s = \lg \frac{2.3Q}{4\pi T_f} + \lg \left[\lg \frac{2.25T_f t}{r^2 \left(S_f + \beta S_m \right)} \right] \tag{29}$$

where β is a factor defined as 1/3 for orthogonal system or 1 for strata type by Warren and Root (1963) and S_m is the storativity of the matrix. Consequently, the drawdown derivative plots of the fracture-matrix system are

$$\frac{\mathrm{d}s}{\mathrm{dlg}t} = \frac{2.3Q}{4\pi T_f} \tag{30}$$

$$\frac{\mathrm{dlg}s}{\mathrm{dlg}t} = \frac{1}{\ln \left[\frac{2.25T_f t}{r^2 (S_f + \beta S_m)} \right]} \tag{31}$$

From Equations 30 and 31, a term of $S_f + \beta S_m$ can be shown that

$$S_f + \beta S_m = \frac{5.2Qt}{4\pi r^2 \frac{\mathrm{d}s}{\mathrm{dlg}t} * \exp \left(\frac{\mathrm{dlg}t}{\mathrm{dlg}s} \right)} \tag{32}$$

Utilizing Equations 27 and 32, the storativity of the matrix (S_m) and the storativity ratio (ω) are calculated as

$$S_m = \left[\frac{5.2Qt}{4\pi r^2 \frac{\mathrm{d}s}{\mathrm{dlg}t} * \exp \left(\frac{\mathrm{dlg}t}{\mathrm{dlg}s} \right)} - S_f \right] / \beta \tag{33}$$

$$\omega = \frac{S_f}{S_f + \beta S_m} \tag{34}$$

Bourdet and Gringarten (1980) also introduced that the drawdown of the transition curves is equal to $\left[2.3Q \lg \left(\frac{1.26}{\gamma} \right) \right] / \left(4\pi T_f \right)$, where γ is interporosity flow coefficient. Hence, the drawdown derivative values of $\mathrm{dlg}s/\mathrm{dlg}t$ and $\mathrm{d}s/\mathrm{dlg}t$ are both equal to 0 when transition occurs.

It is highlighted that this derivative analysis can also be applied to analyze the drawdown records in a pumped well if the distance from the observation well to the pumped well (r) can be replaced with an effective radius of the pumped well (r_w).

Differentiation and Algorithm

A "noise" component of numerical derivative could be generated due to incorrect field data, or the derivative calculation process itself. To remove this negative effect from "noise" data, the Lagrange Interpolation Regression (LIR) based on Lagrange polynomial (Meijering 2002) is introduced for the numeric derivative calculation of points of interest in this paper. The Lagrange polynomial was developed and published by Lagrange (Meijering 2002). For LIR, the corresponding slope of a point of interest is calculated based on data of adjacent three points in row. The weighted function of LIR is expressed as Equation 35.

$$\begin{aligned} \frac{\mathrm{d}y_i}{\mathrm{d}x_i} = {} & y_{i-1} \frac{x_i - x_{i-1}}{(x_{i-1} - x_i)(x_{i-1} - x_{i+1})} \\ & + y_i \frac{2x_i - x_{i-1} - x_{i+1}}{(x_i - x_{i-1})(x_i - x_{i+1})} \\ & + y_{i+1} \frac{x_i - x_{i-1}}{(x_{i+1} - x_{i-1})(x_{i+1} - x_i)} \end{aligned} \tag{35}$$

where i = point of interest, $i-1$ = point immediately before i, $i+1$ = point immediately after i, y = drawdown or logarithm of drawdown, and x = logarithm of time function.

The advantages and disadvantages of different derivative techniques of differentiation algorithms, including the LIR, standard methods from the software *AQTESOLV*, and Least Square Regression (LSR) (Spane and Wurstner 1993), are discussed and demonstrated via a following case study.

Case Study

Three case studies are investigated, including (1) a constant rate test "Oude Korendijk" (Wit 1963); (2) a pumping test from fractured rock aquifer in Tertiary volcanic rocks of the Nevada Test Site, USA (Kruseman

and Ridderna 1991); and (3) a variable discharge test in a hypothetical case (Kruseman and Ridderna 1991). The results of the case studies (1) and (2) give rise to a recommendation of use of LIR for derivative analyses of constant rate tests and double porosity tests. For purpose of simplicity, only case study (3) is described in detail to demonstrate the practical applications of purposed derivative analysis.

Drawdown data in case study (3) is taken from a hypothetical pumping test conducted in a fully penetrating confined aquifer (Kruseman and Ridderna 1991). Pertinent test information includes discharge rates of three pumping periods are 500 m^3/d, 700 m^3/d, and 600 m^3/d, respectively, distance from pumping well is 5 m, reported analysis results are $T = 102\ m^2/d$, $S = 9.6 \times 10^{-4}$. In this case study, LIR is used for calculation of $d\lg s_i/d\lg t_e$ values, while $ds_i/d\lg t_e$ values are calculated by uses of LIR, LSR, and standard methods available in the software *AQTESOLV*.

Values of $ds_i/d\lg t_e$ calculated using different derivative algorithms are plotted against normal time (Figure 4a). It is assumed that "noise" values of drawdown derivative calculations are transiently produced due to changes of pumping rates in the first and last points of each pumping period. The "noise" values are results out of limitations of the derivative algorithms themselves. According to Equation 6, a basic assumption is that the $ds_i/d\lg t_e$ value is calculated based on an unchanged pumping rate (Q). In reality, this rule cannot be achieved as numerical derivative calculations of the end points in each pumping period. As weighted function (Equation 35) of LIR, the $ds_i/d\lg t_e$ value of the first point of each pumping period at the discharge rate Q_n is determined based on the data of the last point of the preceding pumping period at the discharge rate Q_{n-1} and the data of second point of the pumping period at the discharge rate Q_n; the $ds_i/d\lg t_e$ value of the last point at the discharge rate Q_n is evaluated based on the second last point of the same pumping period and the first point of the next pumping period at the discharge rate Q_{n+1}. Due to the fact that the numeric derivative calculation of the end points requires the data from adjacent pumping periods, LIR is bound to introduce an error or "noise" during the derivative calculation. The same situations can be observed using the other derivative algorithms. In those cases, the "noise" derivative values of the end points in each pumping period are set up as null.

In Figure 4a, the plots of $ds_i/d\lg t_e$ are depicted as fairly straight lines over different pumping periods, suggesting that radial flows prevail. However, the plot of

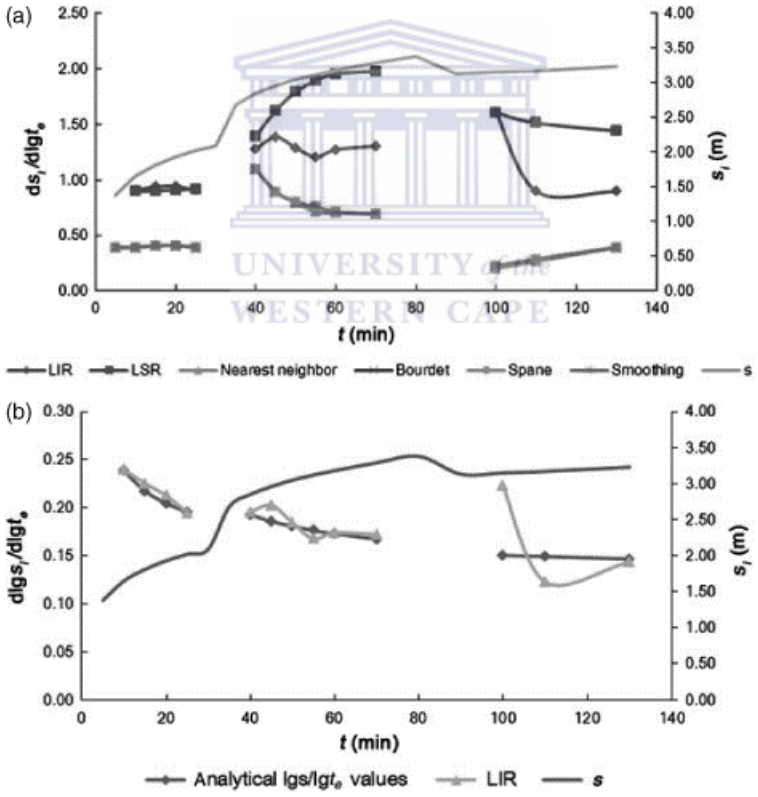

Figure 4. Derivative plots for the hypothetical pumping test: (a) $ds_i/d\lg t_e$ plots; (b) $d\lg s_i/d\lg t_e$ plots.

$ds_i/d\lg t_e$ from LIR shows an obvious curve over the third pumping period, suggesting that the "noise" is generated during derivative process in the third pumping period by the use of LIR. Analytical values of $ds_i/d\lg t_e$ in Equation 6 are also calculated for the first and second pumping periods as given in Table S1, Supporting Information. The results show that the $ds_i/d\lg t_e$ values using LIR (0.92) and LSR (0.90) are identical to analytical one (0.90) in the first pumping period; however, the $ds_i/d\lg t_e$ value using LSR (1.77) is greater than analytical one (1.25) in the second pumping period. This certifies that both LIR and LSR are recommended for $ds_i/d\lg t_e$ value calculations of points in first pumping periods without wellbore storage effects or "noise" data in the beginning of pumping tests. In the later pumping periods, LIR is better fitted for the $ds_i/d\lg t_e$ calculations, while use of LSR for $ds_i/d\lg t_e$ value calculations are negatively influenced by the changes of pumping rates (Q). For the other options provided by *AQTESOLV*, their $ds_i/d\lg t_e$ values of the radial flows are significantly smaller than analytical results.

In this case study, T values in Equation 8 are evaluated for both the first and second pumping periods using mean $ds_i/d\lg t_e$ results of the radial flows in the periods. As shown in Table S1, a mean value of evaluated T results in the first and second pumping periods using LIR is 99.46 m^2/d, which is close to the result (102 m^2/d) obtained from the Birsoy-Summers method. The mean evaluated T values obtained from other derivative methods, including LSR, nearest neighbor, Bourbet, Spane, and smoothing methods, are 86.60, 193.11, 197.39, 191.96, and 191.39 m^2/d, respectively, which are significantly different from analytical T value using Birsoy-Summers method. The discrepancies are attributed to the noisy calculations of $ds_i/d\lg t_e$ using LSR and differentiation algorithms from *AQTESOLV* (Table S1). Therefore, the use of LIR is recommended for the $ds_i/d\lg t_e$ calculations in variable discharge tests.

Numerical and analytical values of $d\lg s_i/d\lg t_e$ using LIR and Equation 7, respectively, are presented in Figure 4b and Table S2. The derivative plots of $d\lg s_i/d\lg t_e$ without straight lines as seen in Equation 3 imply that there is no effect of wellbore storage at the onset of the pumping test. The shape of the $d\lg s_i/d\lg t_e$ plot using LIR has a good match with analytical one using Equation 7 during the first and second pumping periods, indicating manifestation of the radial flows. "Noise" values cropped out in the third pumping period may be induced due to errors in the field work, and they cannot be used for determination of S values. Two series of evaluated S values in Equation 9 based on numerical and analytical derivative plots ($d\lg s_i/d\lg t_e$ and $ds_i/d\lg t_e$) are presented for points of radial flows in the first and second pumping periods (Table S2). A mean S value using LIR is estimated as 10.4×10^{-4}, which is almost identical with analytical one (9.3×10^{-4}).

Consequently, LIR is the preferred method for use in model identifications and parameter determinations for variable discharge tests. It is also of interest to notice that the use of LSR for derivative calculations is limited to the first pumping periods without the presence of wellbore storage effects or "noise" data before radial flows.

Discussion

The development of the pressure derivative method has noticeably improved the diagnostic and quantitative analysis of constant rate tests and slug tests (Karasaki et al. 1988; Ostrowski and Kloska 1989; Spane and Wurstner 1993) in confined aquifers. However, limitations of the use of the conventional derivative method ($ds/d\lg t$) and differentiation algorithms are observed in practices:

- A pumping period and its following recovery period in an intermittent variable discharge test cannot be revealed in a plot of $ds/d\lg t$.
- Storativity of a pumped aquifer cannot be evaluated by application of $ds/d\lg t$ alone.
- In a double porosity aquifer, the storativity of fracture system (S_f), the storativity of matrix (S_m), and storativity ratio (ω) cannot be determined by use of the plot of $ds/d\lg t$ alone.
- The noise effect could be not avoided in the derivative calculation process using conventional differentiation algorithms.

Compared with these conventional derivative methods, the advantages of derivative analysis based on the combined plot of $d\lg s/d\lg t$ and $ds/d\lg t$ and LIR are now discussed.

One of the two important aspects of the derivative analysis is model identification. For comparison purpose, a conceptual derivative plot of $d\lg s_i/d\lg t_e$ is presented against the standard derivative method ($ds_i/d\lg t_e$) for an intermittent variable discharge test in Figure 5. In early time of the pumping test, a plot of $d\lg s_i/d\lg t_e$ is done as a horizontal straight line with the value equal to 1 for wellbore storage effects, while the plot of $ds_i/d\lg t_e$ is made as a straight line with a fixed slope $2.3Q_1/(\pi r_c^2)$ (Renard et al. 2009). One advantage of $d\lg s_i/d\lg t_e$ is that it can be used to unveil differences between the pumping and its following recovery periods, which are otherwise not available from a conventional derivative plot of

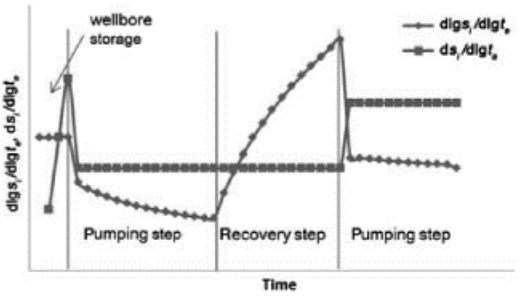

Figure 5. Conceptual derivative curves of $d\lg s_i/d\lg t_e$ and $ds_i/d\lg t_e$ for an intermittent variable discharge test.

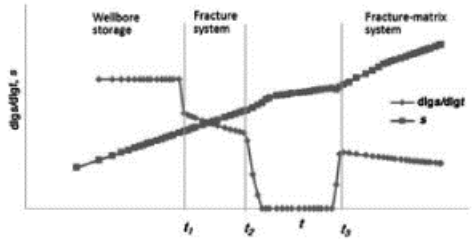

Figure 6. Conceptual time-drawdown and derivative plots of dlg$s$/dlg$t$ for double porosity behavior with wellbore storage using a semi-lg scale.

ds_i/dlgt_e. In the plot of ds_i/dlgt_e, the values of ds_i/dlgt_e from a pumping period and its following recovery period lie along same straight line as $2.3Q_i/(4\pi T)$. In plots of dlgs_i/dlgt_e, the derivative pattern of dlgs_i/dlgt_e for a pumping period is expressed as $1/\ln[2.25Tt_e/(r^2S)]$, while dlgs_i/dlgt_e of its following recovery period corresponds to $1/\ln t_e$. This makes it easy for the hydrologists to identify pumping and its following recovery periods in the derivative plots of dlgs_i/dlgt_e.

In double porosity aquifers, the fracture flow system is often masked by the wellbore storage in a semi-lg scale plot. Figure 6 shows conceptual plot of drawdown and derivative curves (dlg$s$/dlg$t$) for the double porosity behavior with wellbore storage effects. In this case, the wellbore storage region ($t < t_1$) is often misidentified as a radial flow in time-drawdown plots, which could lead to the wrong parameter estimates of pumped aquifers by Kazi et al.'s straight line method. The sensitivity of the dlg$s$/dlg$t$ makes it feasible to remove the negative effect of wellbore storage on fracture system identification in the derivative plot of dlg$s$/dlg$t$. In the plot of dlg$s$/dlg$t$, the wellbore storage effect is depicted as a straight line as Equation 3. The characteristic pattern ($t_1 < t < t_2$) for fracture flow systems is described as Equation 25 at early pumping time and another characteristic pattern ($t_3 < t$) is given as Equation 31 for fracture-matrix systems at late pumping time.

Another important aspect of the derivative analysis is parameter identification. The conventional derivative method (ds/dlg$t$) can only be applied to calculate the value of transmissivity (T) but not storativity (S) of a pumped aquifer. In this paper, a comprehensive quantitative analysis is presented for parameter determinations of pumping aquifers concerned. Based on the positive identification of the radial flows from the pumping phases in a variable discharge test, transmissivity (T) and storativity (S) of pumped aquifer are evaluated as Equations 8 and 9, respectively. In a double porosity aquifer, the derivative values of dlg$s$/dlg$t$ and ds/dlg$t$ from the fracture flow and matrix-fracture flow systems can be used to calculate the effective transmissivity of the fracture (T_f) (Equation 26), the storativity of fracture (S_f) (Equation 27), the storativity of matrix (S_m) (Equation 33), and storativity ratio (ω) (Equation 34) for a double porosity aquifer.

An appropriate differentiation approach should be adopted to prevent "noise" effects from being cumulative during numerical derivative calculation processes. Two derivative algorithms, LIR and LSR, are discussed in the case study. The results give rise to a recommendation that LIR is used for derivative analyses of aquifer tests (constant rate tests, variable discharge tests, and double porosity tests) without "noise" field data during radial flows.

With regard to LSR, it can be used for diagnostic analysis of aquifer tests with strict conditions. According to weighted function of LSR

$$\left(\mathrm{d}y_i/\mathrm{d}x_i = \left[n\sum_{j=1}^{i}(y_j x_j) - \left(\sum_{j=1}^{i} y_j \sum_{j=1}^{i} x_j\right)\right] / \left[n\sum_{j=1}^{i} x_j^2 - \left(\sum_{j=1}^{i} x_j\right)^2\right]\right),$$

the numerical derivative value of point of interest is affected by the data of all points before the point of interest. It is assumed that changes of flow segments (e.g., changes of flow segments from wellbore storage effects to radial flows, the changes of pumping rates in variable discharge tests, or changes of flow segments from radial flow in fracture system to transition period) or "noise" field data before each flow segment should have negative effects on accuracy of the derivative calculations using LSR. However, the negative effects would benefit from self-cancellation using LSR at late time of long radial flow segments. Hence, use of LSR is preferred for derivative analyses of constant rate tests with "noise" data during long radial flow segments.

Other derivative algorithms, including nearest neighbours method, Bourdet method, Spane method, and Smoothing method adopted in software *AQTESOLV*, cannot be used to effectively remove the noise from the derivative calculations as these methods tended to give smaller derivative values in the case study.

Conclusion

This paper discusses the possibility of use of dlg$s$/dlg$t$ for the derivative analysis and clarifies differences between LIR and conventional algorithms of use in numeric derivative calculation. Use of dlg$s$/dlg$t$ improves the applications (model identification and parameter determination) of derivative analysis of aquifer tests. Different characteristic flow segments, including wellbore storage, radial flow, boundary condition, and double porosity behavior, can be identified by defining curve patterns in derivative plots of dlg$s$/dlg$t$. By comparison with standard derivative method (ds/dlg$t$), derivative interpretation of drawdown data based on the plot of dlg$s$/dlg$t$ has advantages over the ds/dlg$t$ plot as mentioned in Discussion. A method is proposed for a composite understanding of pumped aquifer properties

based on combined derivative plots of dlg$s$/dlg$t$ and ds/dlg$t$. The main points are highlighted as follows.

1. Plots of dlg$s$/dlg$t$ are preferred for use in unveiling differences between pumping and recovery periods in intermittent variable discharge tests.
2. Storativity (S) of a pumped aquifer can be accurately evaluated using a comprehensive plot of dlg$s$/dlg$t$ and ds/dlg$t$.
3. Combined derivative plots of ds/dlg$t$ and dlg$s$/dlg$t$ has shown to be particularly powerful for diagnostic analysis of pumping tests involving double porosity. Negative effects of wellbore-storage on fracture system identifications are avoided using plots of dlg$s$/dlg$t$. Parameters of dual porosity aquifers are easy to be evaluated in aid of combined derivative plots of ds/dlg$t$ and dlg$s$/dlg$t$.
4. Use of LIR is recommended for derivative analysis of pumping tests, including constant rate tests, variable discharge tests, and tests involving double porosity, without "noise" data during radial flows, while use of LSR is preferred for derivative analysis of constant rate tests with "noise" data during long radial flows.

The paper provides the hydrogeologist with an additional method for use in characterization of the aquifer through combined derivative plots of ds/dlg$t$ and dlg$s$/dlg$t$. It is also pointed out that a caution must be exercised with use of numeric algorithms for derivative analysis during the interpretation of pumping tests.

Nomenclature

lg	logarithm to the base 10
ln	logarithm to the base e
Q	pumping rate
Q_i	pumping rate in ith pumping period
s	drawdown
s_d	drawdown from real discharging well
s_i	drawdown in ith pumping period
s_r	drawdown from image well
S	storativity
S_f	storativity of the fracture
S_m	storativity of the matrix
t	time
t_e	adjusted time
T	transmissivity
T_f	effective transmissivity of the fracture
r	distance between the piezometer and real discharging well
r_c	stress well casing radius
r_i	distance between the piezometer and ith image well
$r_{r1\to n}$	ratio equal to r_i/r
r_w	effective radius of the pumping well
u	argument of W function
W	Theis' well function
β	factor of pump test analysis in double porosity aquifer
ω	storativity ratio

Supporting Information

Additional Supporting Information may be found in the online version of this article:

Table S1. ds_i/dlgt_e and$T$ values from derivative methods and analytical method.
Table S2. dlgs_i/dlgt_e values and S values from LIR and analytical method.

References

Beauheim, R.L., and J.F. Pickens. 1986. Applicability of pressure derivative to hydraulic test analysis. Paper presented at poster session at the Annual Meeting of America Geophysical Union, Baltimore, Maryland.

Birsoy, Y.K., and W. Summers. 1980. Determination of aquifer parameters from step tests and intermittent pumping data. *Ground Water* 18, no. 2: 137–146.

Bourdet, D. 2002. *Well Test Analysis: The Use of Advanced Interpretation Models*. New York: Elsevier.

Bourdet, D., J. Ayoub, and Y. Pirard. 1989. Use of pressure derivative in well test interpretation. *SPE Formation Evaluation* 4, no. 2: 293–302.

Bourdet, D., T. Whittle, A.A. Douglas, and Y.M. Pirard. 1983. A new set of type curves simplifies well test analysis. *World Oil* 196, no. 6: 95–106.

Bourdet, D., and A.C. Gringarten. 1980. Determination of fissure volume and block size in fractured reservoirs by type-curve analysis. Paper SPE 9293 Presented at the SPE Annual Technical Conference and Exhibition, Dallas, September 21–24.

Chow, V.T. 1952. On the determination of transmissibility and storage coefficients from pumping test data. *Transactions, American Geophysical Union* 33, no. 3: 397–404.

Cooper, H.H., and C.E. Jacob. 1946. A generalized graphical method for evaluating formation constants and summarizing well field history. *Transactions, American Geophysical Union* 27, no. 4: 526–534.

Djebbar, T., and A. Kumar. 1980. Application of the p´D function to interference analysis. *Society of Petroleum Engineers* 32, no. 4: 1465–1470.

Duffield, G.M. 2007. *AQTESOLV for Windows Version 4.0 Professional*. Reston, Virginia: HydroSOLVE, Inc.

Ehlig-Economides, C. 1988. Use of the pressure derivative for diagnosing pressure-transient behavior. *Journal of Petroleum Technology* 40, no. 10: 1280–1282.

Ferris, J.G., D.B. Knowles, R.H. Brown, and R.W. Stallman. 1962. *Theory of Aquifer Tests*. Denver, Colorado: US Geological Survey.

Goode, D.J. 1997. Composite recovery type curves in normalized time from Theis' exact solution. *Ground Water* 35, no. 4: 672–677.

Horn, R.N. 1995. *Modern Well Test Analysis: A Computer Aided Approach*, 2nd ed. Palo Alto, California: Petroway Inc.

Karasaki, K.J., C.S. Long, and P.A. Witherspoon. 1988. Analytical models of slug tests. *Water Resources Research* 24, no. 1: 115–126.

Kazemi, H., M.S. Seth, and G.W. Thomas. 1969. The interpretation of interference tests in naturally fractured reservoirs with uniform fracture distribution. *Society of Petroleum Engineers* 9, no. 4: 463–472.

Kruseman, G.P., and D.E. Ridderna. 1991. *Analysis and Evaluation of Pumping Test Data*, 2nd ed. Wageningen, the Netherlands: International Institute for Land Reclamation and Improvement.

Mattar, L., and K. Zaoral. 1992. The primary pressure derivative (PPD) – A new diagnostic tool in well test interpretation. *Journal of Canadian Petroleum Technology* 4: 63–70.

McConnell, C.L. 1993. Double porosity well testing in the fractured carbonate rocks of the Ozarks. *Ground Water* 31, no. 1: 75–83.

Meijering, E. 2002. A chronology of interpolation: From ancient astronomy to modern signal and image processing. *Proceedings of the IEEE* 90, no. 3: 319–342.

Ostrowski, L.P., and M.B. Kloska. 1989. Use of pressure derivatives in analysis of slug test or DST flow period data. *Society of Petroleum Engineers* 18595: 13–23.

Renard, P. 2005. The future of hydraulic tests. *Hydrogeology Journal* 13, no. 1: 259–262.

Renard, P., D. Glenz, and M. Mejias. 2009. Understanding diagnostic plots for well-test interpretation. *Hydrogeology Journal* 17, no. 3: 1–12.

Samani, N., M. Pasandi, and D.A. Barry. 2006. Characterizing a heterogeneous aquifer by derivative analysis of pumping and recovery test data. *Journal of Geological Society of Iran* 1: 29–41.

Spane, J.F., and S. Wurstner. 1993. DERIV: A computer program for calculating pressure derivatives for use in hydraulic test analysis. *Ground Water* 31, no. 5: 814–822.

Van Tonder, G., H. Kunstmann, Y. Xu, and F. Fourie. 2000. Estimation of the sustainable yield of a borehole including boundary information, drawdown derivatives and uncertainty propagation, Calibration and reliability in groundwater modeling. In *Proceedings of ModelCARE 99 Conference held in Zurich, Switzerland*. IAHS Publ. No 265, 2000.

Warren, J.E., and P.J. Root. 1963. The behavior of naturally fractured reservoirs. *Society of Petroleum Engineers* 3: 245–255.

Wit, K.E. 1963. The hydraulic characteristics of the Oude Krorendijk polder, calculated from pumping test data and laboratory measurements of core samples (in Dutch), report No. 190:24. Wageningen, the Netherlands: Institute Land and Water Manager Research.